Ricardo Filipe Soares Serrão

Degree in Cell and Molecular Biology

Monitoring cell cultures in real time in a biochip

Dissertation to obtain master’s degree in Biotechnology

Supervisor: Professor Doctor João Pedro Conde,
Department of Bioengineering, Instituto Superior Técnico,
INESC-MN

FACULDADE DE CIÊNCIAS E TECNOLOGIA
UNIVERSIDADE NOVA DE LISBOA

September 2019

Ricardo Filipe Soares Serrão

Degree in Cell and Molecular Biology

Monitoring cell cultures in real time in a biochip

Dissertation to obtain master's degree in Biotechnology

Supervisor: Professor Doctor João Pedro Conde, Department of Bioengineering, Instituto Superior Técnico, INESC-MN

September 2019

“We’re all stories, in the end. Just make it a good one, eh?”

The Doctor

Acknowledgements

There are not enough words to thanks to every person who direct or indirectly supported me throughout this last year.

First, I have to express my gratitude o Prof. Dr. João Pedro Conde for his attention and availability during the whole year. It was a pleasure to work under his supervision and I'm thankful for the opportunity given to work in a motivational and challenging environment.

To Dr. Virginia Chu for all the support and advisory provided for the last year.

A special thanks must be also directed to Eduardo Brás for the mentorship given throughout the year, I'm very grateful for the things I have learned and the encouraging words in the hardest of times.

To André Faria, Andreia Jardim, Catarina Bombaça, Catarina Caneira, Cristiana Domingues, Inês Domingos, Katerina Nikolaidou and Pedro Monteiro for their friendship, their kindness and their availability when I needed it the most. To the other group members, Maria João, Tiago Pestana, Ricardo Fradique, Martim Costa, Michael, Angelina, Yasemin and Ronja, thank you for the free time conversations, advisement and for meeting you. Also, to all the people of Faculdade de Farmácia, especially Vanda Marques, Marta Afonso and Pedro Fontes that helped me through the cell culture experiments and gave me all the attention needed.

To my long-time friends, André Filipe, Gonçalo Ferraz and Simão Duarte, thank you for being with me since we were little and pardon me for my absence for one year. Without you figuring it out, you were very important to me during this journey.

To my college friends, João Diamantino, José Mendonça, Laura Custódio, Luís Bento, Luís Sousa, Pedro Augusto and Vicente Xavier, thank you for all the moments, all nights out, all trips for the country and for being real friends that never let me down.

To my little kids in CAPP, it is being an amazing experience to be in contact with you, your will to live and your growth as social beings. For sure you made me a better person.

To my family, for supporting me in their own way, always encouraging me to do better and better every single day. The person that I am today is because of you all.

To Filipa Ribeiro, my girlfriend and best friend, for the unconditional support, love, kindness, friendship that helped me for the past year to achieve so many things. Without you it would never be as easy as it was. Obrigado.

Abstract

Drug screening is a very important procedure in the approval of drugs for cancer treatment. This process is generally carried out using *in vitro* or *in vivo* models that aren't very efficient due to the non-reproducibility of the cellular and/or tissue microenvironment and ethical issues due to the use of animal models. Additionally, drug approval is a process that could last 10 to 15 years, too much time when therapy is required with urgency.

Microfluidic structures can address such issues, decreasing the time per assay, as well as decreasing the quantity of reagents used and the volume of waste generated, thus decreasing the costs. Also, due to the generation of concentration gradients inside a microfluidic device, it mimics the microenvironment characteristic of conventional cell culture.

In this work, a reproducible cell culture of HCT-116, a human colon cancer cell line, is successfully grown inside a microfluidic device for a posterior exposure to anti-cancer drugs. The cell viability, detected through staining the DNA with fluorophores, is on average 90%.

To monitor the cell death via exposure to drugs, a specific cell death biomarker, adenylate kinase (AK), is detected inside a microfluidic device using a photomultiplier and a fluorescence microscope in a chip-based immunoassay. AK concentrations near the concentrations of the enzyme released by dead cells were detected with the immunoassay by concentrating the AK in packed agarose beads inside de microfluidic structure.

Keywords: Microfluidics, Cell Culture, Cell Viability, Adenylate Kinase, Photomultiplier, Immunoassay.

Resumo

O processo de *drug screening* é muito importante na aprovação de fármacos para tratamento de cancro. Este processo é geralmente desenvolvido m plataformas *in vivo* ou *in vitro*, que não são muito eficientes devido ao facto não reproduzirem o microambiente celular e/ou tecidular e devido a problemas éticos levantados devido ao uso de modelos animais. O processo de aprovação de fármacos pode ainda durar cerca de 10 a 15 anos, o que revela ser muito tempo quando um tratamento é urgentemente necessário.

Estruturas de microfluídica apresentam características que podem ultrapassar estas barreiras, ao diminuírem o tempo por experiência, a quantidade de reagentes utilizados e de resíduos gerados, diminuindo assim também os custos associados a este processo. Como estas estruturas permitem ainda a criação de gradientes de concentração dentro do dispositivo, podem mimetizar o microambiente característico de uma cultura celular convencional.

Neste trabalho, foi cultivada com sucesso uma cultura celular reprodutível de células HCT-116, uma linhagem de cancro do cólon humano, dentro de um *chip* de microfluídica para posterior exposição a fármacos anti cancro. A viabilidade celular, detetada através da marcação do DNA com fluoróforos, é em média 90%.

De forma a monitorizar a morte celular por exposição a fármacos, um biomarcador específico de morte celular, a enzima adenilato cinase (AK), é detetado dentro uma estrutura de microfluídica utilizando primeiramente um fotomultiplicador e depois detetado por fluorescência num imunoensaio também dentro de um *chip*. Utilizando o método do imunoensaio e concentrando a enzima em *beads* empacotadas num microcanal, foram detetadas concentrações de AK perto das concentrações de AK libertado pela quantidade de células presente nas culturas celulares em chips.

Palavras-Chave: Microfluídica, Cultura Celular, Viabilidade Celular, Adenilato Cinase, Fotomultiplicador, Imunoensaio.

List of Contents

List of Figures

List of Tables

List of Abbreviations

Abbreviation	Full Form
AK	Adenylate Kinase
HO342	Hoechst 33342
7-AAD	7-Aminoactinomycin D
PMT	Photomultiplier
γ-norm	Gammanorm®
α-AK	AK-specific antibody
α-AK-430	AK-specific antibody labelled with Alexa 430
α-IgG-FITC	Anti-mouse anti-IgG antibody labelled with FITC
Ag – MMC	Agarose beads functionalized with Capto – MMC

1. Introduction

1.1 Motivation

Nowadays, cancer remains as the major cause of mortality in the world. In 2018, there was around 18.1 million new cases and 9.6 million deaths due to this disease (**Fig. 1.1**). This data shows very high values due to several factors, such as population growth and ageing. Human development may take part in increase of cancer cases in recent years, that is corroborated by the social and economic development, which can be verified in rapidly growing economies, regarding the existent shift between cancers related to poverty and infections and the ones connected to typical lifestyles of industrialized countries. Recent predictions estimate that by 2030, there will be approximately 22 million new cases per year, as well as nearly 13 million cancer-related deaths.[1,2]

Overall, lung and breast cancer are by far the most diagnosed and deadly both in men and women. Although, in more developed countries, prostate and lung cancer lead as the main cause of death cause amongst men and women, respectively. Around the world, other types of cancer such as the liver, stomach, cervix and colorectal are also frequently diagnosed.[23]

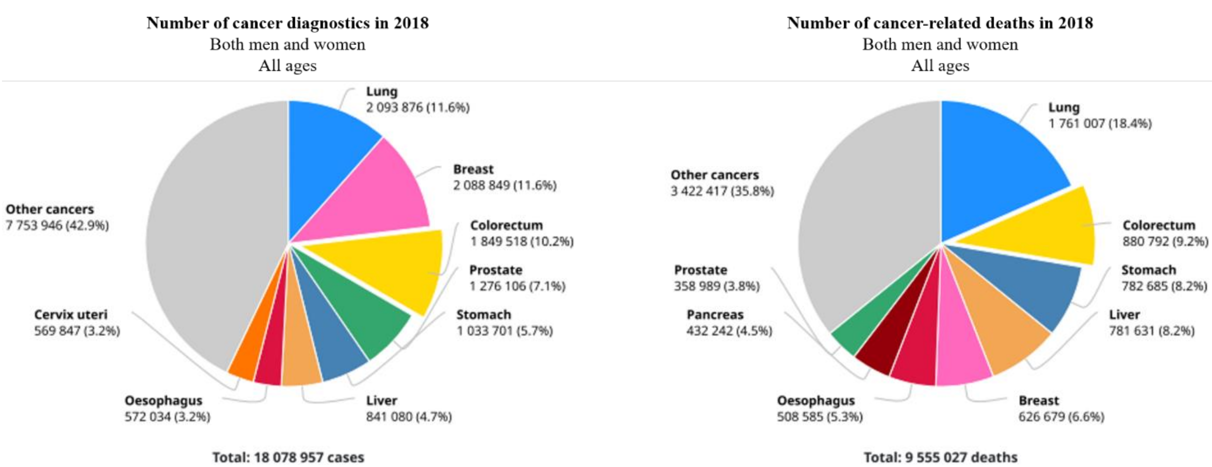

Figure 1.1 – Several types of cancer incidence for the year of 2018. Adapted from literature.[3]

In fact, after lung and female breast cancer, colorectal cancer is the third most diagnosed cancer. It is known to have reached in 2018 approximately 1.8 million diagnostics and to have caused near 881 000 deaths. The incidence of this type of cancer tend to be bigger in the regions of Australia/New Zealand, Europe and Northern America, being generally higher in men. Colorectal cancer shows a minor incidence rate in the regions of Africa and South and Central Asia. Such high mortality rates is due to the lack of efficient therapies, such as chemotherapy reducing the lethality rate from 51% to 40%.[4,5]

Current methods for drug screening of potential therapeutic agents for cancer treatment are generally carried out using two- and three-dimensional cell cultures, as well as animal models. The latter are very useful for providing information on *in vivo* tumour growth and drug response, however, costs of use are very high and some species used, such as mice or rats, have been shown to not be the most accurate models when translating treatments to humans. These reasons, amongst others, lead to the low success rate in finding new drugs demonstrated by pharmaceutical companies. Previously referred cell cultures are already used for cancer-specific drug screening in addition to cell signalling, proliferation and migration studies. Despite their low cost, ease handling and repeatability, cell cultures cannot mimic an organ or animal microenvironment, due to its complex spatial organisation and interactions.

These issues created a need for an economically friendly approach for the screening of potential drug candidates as well as, platforms capable of surpassing the biological limitations of standard 2D cultures and animal models. One field of study which is attempting to tackle these issues, on different fronts, is the area of **Microfluidics**. This technology can address cancer development and treatment, having the potential to increase current understandings in cancer biology, as soon as the process becomes faster and costs decrease.[6–8]

1.2 Microfluidics: main features and applications

For the last 20 to 30 years, following the invention of soft-lithography and its wide scale implementation, microfluidic devices had gained a major role in life scientific research[9], mostly in the areas of biological assays[10] and for biomedical use[11]. Consisting of microfabricated devices capable of liquid handling, with cross-section dimensions in the range of the micrometres (µm) and a volume capacity near the femtolitre (fL) and nanoliter (nL) range[12,13]. These characteristics, amongst others, allow researchers to decrease prototyping time and enhance the complexity and sophistication of the experiments to be realized in such devices[9].

There are many advantages in the use of microfluidic devices, such as small volumes of reagents needed, short reaction and analysis times, portability, low cost, low power consumption, little waste production and design versatility.[9,10] In addition to these, there is also high potential for instrumentation such as electrochemical and optical sensors, which can be connected to electronic equipment for automated result analysis[14,15]. In the case of biological experiments, due to the low number of cells necessary, it is possible to perform several experiments with small amounts of biological material such as tissues obtained from biopsies[16,17] or nucleic acids from bacterial swabs.[18,19]

There are a few parameters that allow the scientists to describe the flow nature inside a microfluidic device, though there is one that is of major importance: Reynolds number (*Re*). *Re* is defined as the ratio between inertial and viscous forces in a liquid and can be calculated using **Equation 1**:

$$Re = \frac{\rho v L}{\eta} \quad (\mathbf{1})$$

Where, ρ is the fluid's density (kg/m^3), ν is the mean velocity (m/s), L is the channel's characteristic dimension (m) and η is the fluid dynamic viscosity (kg/(m•s)). The Re is a direct indication of the nature of the flow regime in a system, whether it be laminar (up to Re=10) or turbulent (Re>2000). In a laminar flow, streamlines are parallel and the mass transport inside the microchamber is dominated by diffusion, unlike what happens in a turbulent-like flow, where streamlines are chaotic and the mixing happens mainly due to advection, however turbulent systems tend to be more difficult to control. In a microfluidic environment, due to such characteristic features, laminar flow is generally found, thus allowing high control over fluids, diffusion of reagents and reactions progression[20]. Additionally, heat transfer is yielded with these microfluidic devices. This is addressed to the temperature control over such devices, which leads to an homogeneous heat transfer through all microfluidic chamber.[21,22]

In recent years, microfluidic devices are being more sought to their portability and the possibility of point-of-care diagnostic devices.[9] Inside microfluidic channels, there are used small volumes, laminar flow is generally guaranteed and a surface-to-volume ratio is larger from the one presented in macroscopic assays, which ensure a very precise control over flow variables, fluid velocity, shear stress, temperature and reagent concentration.[11,13]

All the advantages inherent in microfluidic systems allows chemical and biological analysis, as well as some other measurements, enabling a consistent miniaturization, integration, automation and parallelization of both chemical and biochemical procedures, leading to the diversification of research directions.[9,12]

Besides the general geometry of the microfluidic systems, there is also a concern to introduce features such as columns, mixers and valves, these are used to introduce functions such as, mixing, pumping and storing fluids inside a microfluidic chamber. These functions are very useful for different assays within the fields of biology, analytical biochemistry, chemistry, engineering and biomedicine.[13,23]

The fact that microfluidics allows to perform a wide variety of assays without compromising portability scientific fields makes it a powerful tool to point-of-care (POC) diagnostics, as described by Nayak *et al* in her work the development of a multiplexed rapid lab-on-a-chip POC assay for the serologic diagnosis of human Lyme disease, inserting an ELISA screening experiment inside a microfluidic system (**Fig. 1.2 C**).[24] Another example of a POC microfluidics application was described by Smith *et al* in her work regarding the development of a microfluidic cartridge for blood cells counting, which was compared with accepted and conventional procedures including flow cytometry and cell counting using a haemocytometer with promising results.[25]

Additionally to its POC applications, microfluidics can be used for drug screening and development[26–28], cell analysis (**Fig 1.2 A and B**)[29–31] and biosensing (**Fig 1.2 D**).[32,33] These three main applications are often verified together, when reviewing the literature. Microchip-integrated sensors that Weltin *et al* developed in order to monitor cell culture conditions and carry out a drug screening assay on T98G (human brain cancer cells) is an example of the integration of these applications in one work.[34] Another drug screening assay was carried out by Wong *et al* on a PDMS-based droplet microfluidic device, internalizing a single cancer cell inside a droplet and treating it with potential anti-cancer drugs, obtaining the results after 24 hours of imaging.[35] In an attempt to monitor a cell culture during a long period of time, Zhang *et al* created a platform that operates in a continuous, dynamic and automated manner and managed to integrate real-time sensors that could monitor biochemical and biophysical parameters.[36] Microfluidic devices offer their users the capability to control almost all the parameters of the experiment. Lee *et al* were able to develop a device with integrated peristaltic pumps and valves that allow the control over culture medium inserted concentrations, as well as the possibility of carrying out several types of viable and non-contaminated cell cultures in both batch and fed-batch modes of operation.[37] Microfluidic systems can also be used to detect cell-secreted molecules using both optical and electromechanical measurements. The detection of hepatocyte growth factor (HGF) and transforming growth factor (TGF)-β1 was carried out by Son *et al* by developing a microfluidic device which has a hydrogel barrier-based separation between the cell culture region and the detection zone, in which HGF and TGF- β1 are detected by the use of fluorescent microbead-based sensors.[38] Not only biomarkers can be detected using microfluidic devices, oxygen content and pH are also two parameters that can be monitored. In the work developed by Yamagishi *et al*, microfluidic devices were coupled with Clarktype oxygen electrodes for the measurement of the bactericidal activity of neutrophil-like cells differentiated from the HL-60 cell line. The oxygen content was monitored by the observation of changes in the generated current.[39] The pH control is crucial not only in cell cultures, but also in enzymatic reactions assays. Gruber *et al* managed to integrate two different optical pH sensors that allowed them to monitor pH values in the range of 3.5 to 8.5, thus demonstrating for the first time pH monitoring in real-time of an enzymatic reaction progression inside a microfluidic device.[40]

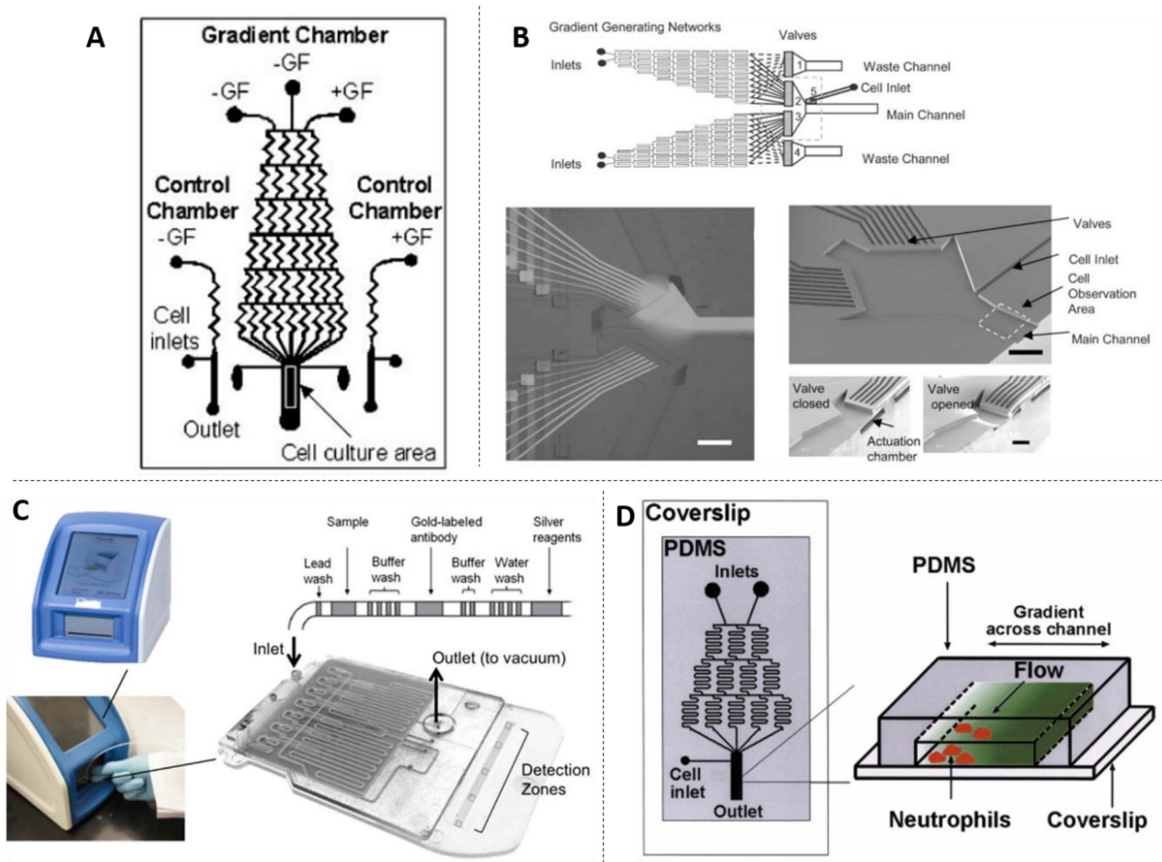

Figure 1.2 – Several works using microfluidic technology for point-of-care (POC) diagnostics, cell analysis and biosensing. (**A**) The design of a microfluidic structure designed by Chung *et al* and used as a gradient-generator for the microfluidic optimization of neural stem cells proliferation and differentiation in culture, in which there are two control chambers and a single gradient chamber.[29] (**B**) Irimia *et al* developed a microfluidic device comprising two gradient generator networks connected to two waste channel and a main channel through a system with valves (represented with numbers). This device is used to study the effect of different concentrations of chemokines in neutrophils migration and morphological depolarization.[30] (**C**) The system developed by Nayak *et al* for the serological diagnosis of uman Lyme disease in a multiplexed lab-on-a-chip POC assay. The microfluidic device is inserted inside a top-bench analyzer that is used to power the flow rate, control the temperature setpoints and detect the signals on the Detection Zone.[24] (**D**) Robust method to study the chemotaxis of neutrophils using simple and complex interleukin-8 (IL-8) is developed by Jeon *et al*. A top-view of the whole device, with the two inlets (IL-8), the gradient-generating structure and a cell inlet is represented with a three-dimensional schematic showing the device region where the chemotaxis is observed.[31] Adapted from literature.

1.3 Microfabrication

In the 1980's, with the arrival of micro-electro-mechanical systems (MEMS), used in electronics, and later in the 1990's, with the application in biological and biomedical fields, a new domain called BioMEMS derived from the initial. MEMS technology combined with fluidic channels allowed its application in cell biology due to such new advantages as high-throughput analysis or the *in vivo* environment mimicking. Owing to the gradient concentration creation and properties like electromagnetic fields and temperature, such areas as the drug screening and cell assays were benefited.[41]

Microfluidic structures are fabricated using the same microfabrication techniques as the semiconductor industry, usually used to produce integrated circuits due to its ability to construct objects with dimension from the micrometre to the millimetre range.[42] Much of these techniques are based in photo- and/or soft-lithography.[43] Lithography techniques are able to design a wide range of patterns in substrates surfaces and allow phenomena such as cell-extracellular matrix interactions and different and defined cell culture distributions to happen. Useful 3D scaffolds with an advanced surface chemistry for cells to adhere and to grow may be achieved through these same technologies, allowing to reliably reproduce cell environment at microscale.[44] Microfabrication techniques can be then used for the production of a wide set of miniature structures such as cantilevers and diaphragms, flow channels and wells, chemically sensitive surfaces and such electrical devices resistors and transistors.[42]

Photolithography is a microfabrication technique that requires three basic materials: light source, photo mask (later called hard mask) and photoresist.[45] This technology allow the transference of a certain pattern conceived by the designer to a certain surface. Designers draw such pattern in a computer-assisted design (CAD) program, which is then transferred to a hard-mask.[42] In this project, hard-mask were made of glass plates in which was deposited on top of it a layer of aluminium, but other chrome metals with the same purpose can be used. After the deposition of the aluminium layer, a positive photoresist is deposited for further exposure to radiation. This radiation belongs to a spectral range from around 300 to 450 nm (from UV to blue).[46] The positive photoresist, that becomes more soluble when exposed to radiation in the range previously referred, is scanned with a light beam with a precision in the order of the fraction of micrometre – around 500 nm[47] – is then developed, in a similar process as photography.[45,46]

After the mask development, the metal thin-layer right underneath the developed regions is then removed by a process called etching. Etchant selectivity should as high as possible, in order to decrease the etch made on the photoresist and on the substrate. Anisotropy is also a parameter to consider in this process. Generally, for wet chemical etching, the one carried out in this project, such processes are isotropic and can be done either by submerging the mask into an etch bath or by spray it with an etch solution.[48] After the etching process, the remaining photoresist on the top of the thin-metal layer is removed in a process called stripping.[49]

Then, using the previous produced hard mask, a master mold is fabricated. The process begins with a silicon substrate being spin-coated with a negative photoresist that, contrarily to the positive one, becomes more soluble after being exposed to light.[45] One of the most used negative photoresists is SU-8, which is a mix of SU-8 resin, an organic solvent and photo-initiator. The viscosity of the resist and thus the thickness of its layer after the spin coating process is dependent on the ratio of solvent to SU-8 resin. SU-8 molecule is composed by 8 epoxy groups (**Fig. 1.3**) and has become a product of general use in photolithography, primarily due to its high chemical and thermal resistance and suitable mechanical properties, that make it useful as a structural material.[50]

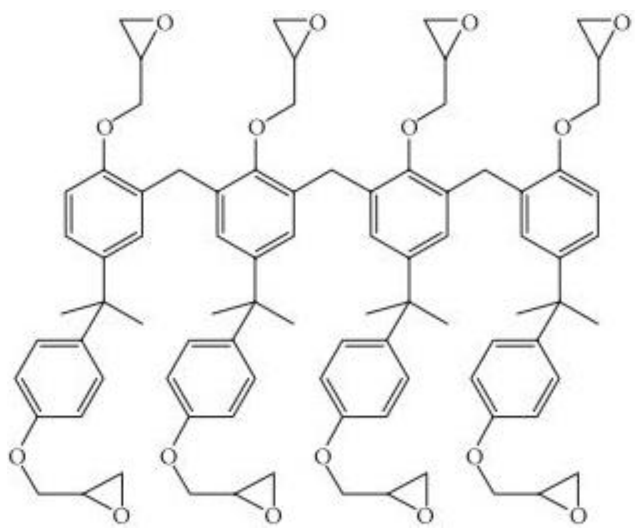

Figure 1.3 – Representation of the SU-8 resin molecule, composed by 8 epoxy groups. Adapted from literature.[50]

After the spin-coating step, the SU-8 film deposited above the silicon substrate presents similarities with a soft solid. At this step, almost all solvent evaporates from the resin, however, generally near 15% of this remaining layer still consists in solvent. If this solvent residue perpetuates on the resin, cracks and fissures on the resin may be caused when the reticulation step is completed. Therefore, a pre-exposure bake step is followed in order to enable the remaining solvent evaporation.

For the exposure step, the hard-mask previously fabricated and the substrate with the resist layer are aligned. The photoresist is then exposed to UV radiation. This radiation induces the formation of covalent bonds between principal and secondary resist chains, which allows these exposed areas to not be removed during the development step. After the exposure step, a post-exposure bake step is carried out to progressively complete the material rearrangement. After a pre-exposure bake, an exposure step and a post-exposure step, the resin may advance for the development step. At this phase three photoresist-inherent parameters must be considered: large solubility contrast between exposed and non-exposed areas, high photosensitivity and high resistance to certain classes of chemical reagents. The wafer is then submerged into a developing reagent and due to being a negative photoresist, non-exposed regions are removed, while the exposed motives stay attached (schematic of the process represented on **Fig. 1.4**). To finalize such process, generally a hard-baking step is followed to allow the hardening of the resin.[46]

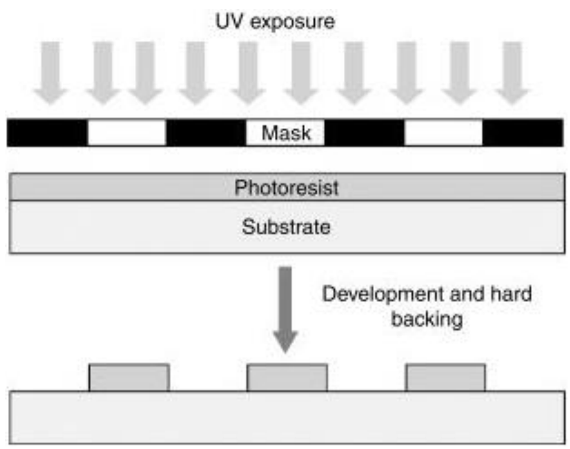

Figure 1.4 – Representation of the photolithography process using a negative photoresist. UV radiation passes through the transparent regions of the mask directly to the photoresist. After the development step, regions that were not exposed are removed from the substrate. Adapted from literature.[45]

In addition to photolithography technology, soft lithography resembles an approach to the rapid prototyping of several types of micro- and nanoscale structures and devices in several types of substrates, which gains more emphasis when are required lower costs. It is usual to assume the existence of four prime patterning techniques that can be performed: microcontact printing, replica molding, molding in capillaries and microtransfer molding. The base for this type of lithography are then are essentially composed by molding, embossing and printing techniques.[51,52]

Devices fabricated by soft lithography had an increased implementation in biomedical research mostly due to elastomeric materials used, such as PDMS, which is relatively easy to fabricate and remains as a compatible polymer with biological assays.[44] PDMS belongs to a group of polymeric organosilicon compounds, generally known as silicones and due to the presence of an inorganic siloxane backbone and organic methyl groups attached to silicon (**Fig. 1.5**), a unique combination of properties are conceded to it.

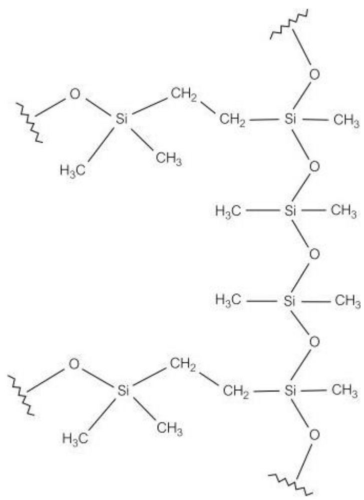

Figure 1.5 – Semi-structural formula of PDMS, with the organic methyl groups attached to the inorganic siloxane backbone. Adapted from literature.[46]

Such properties are the good chemical stability, its non-hygroscopic nature, the fact that it is chemical inertness, nontoxic and non-flammable, optically transparency down to wavelengths of nearly 300 nm, permeability to nonpolar gases like oxygen and good thermal stability, as well as mechanical flexibility, ease of manipulation and durability.[48,53] With this type of elastomer, structure's precision is very high, as it is possible to obtain submicrometric precision for PDMS-based microchannels, which is between 5 and 500 µm. To fabricate microchannels-like structures based in the replica molding technique (used in this project), three basic steps must be followed: mold fabrication, reticulation and separation from the mold.[46] The first step was already explained above and consists on the fabrication of the master mold. PDMS is liquid at room temperature, however by being mixed with a curing agent it can be converted in a solid elastomer through cross-linking reactions. These two compounds can be mixed in different ratios, that can give also different mechanical – e.g. Young modulus – and chemical properties to the resulting solid, depending on the type of assays that such structures are intended for.[48,53] In the curing step, the mixture of PDMS and curing is poured on the top of the master mold and baked at a relatively high temperature – around 70°C – which accelerates cross-linking reactions. Thus, PDMS polymerizes and reticulates, resulting in a solid structure that, after cooling down to room temperature[45], is then peeled off from the mold, which is favoured by its weak surface energy. Now, the PDMS mold-contact surface has the master mold's negative image represented (**Fig. 1.6**).[46,48]

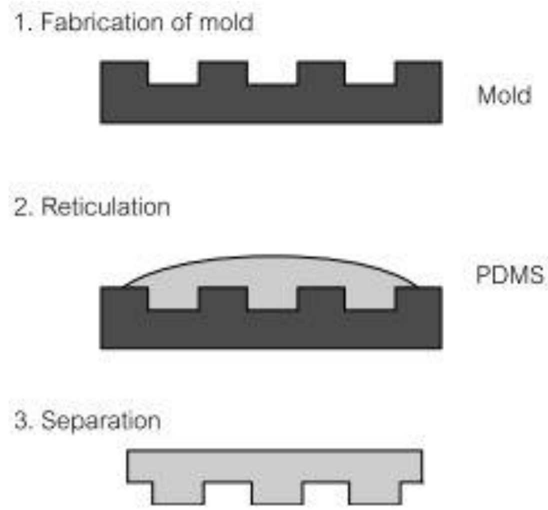

Figure 1.6 – Schematic of the three main steps of replica molding process. (1) Master mold fabrication by photolithography techniques. (2) The mixture of PDMS and curing agent in the desired ratio is poured on top of the mold and baked to enhance the reticulation step. (3) PDMS' peeling off from the mold, favoured by its low surface energy. Adapted from literature.[46]

After peeling off the PDMS structure from the mold, a microfluidic channel must be formed and that is achieved by sealing the PDMS structure against another thin layer of PDMS, glass or plastic. If the structure is put directly in contact with these other structures, the sealing between the two materials will be week and when liquid flows under pressure in microchannels, leaks will appear. At its surface, PDMS has exposed methyl (-CH_3) groups, exposure to oxygen plasma generates reactive silanol groups (SiOH), turning temporarily its surface from hydrophobic to hydrophilic. As soon as the other surface (PDMS, glass or plastic) has also been exposed to the plasma oxidation, when these two surfaces are put in contact, they form an irreversible-based covalent sealing, forming microchannels able to handle extremely high liquid pressures of around 350 kPa. These microfluidic devices are already prepared for the desired application.[46,54]

1.4 Cell-on-chip: miniaturizing a cell culture for clinical applications

It is fair to state that the miniaturization of top-bench technologies enabled scientific advances in many fields of biological sciences, such as molecular biology and pharmaceutical sciences.[55] Life science's introduction to microfluidics technology allows the science community to finally address crucial limitations in standard assays as temperature and gas control, nutrient supply, assay parallelization, cell culture automation, among others.[56]

Cancer migration, wound healing and stem cell development are cell biology fields of investigation that at some point, served as motivation to start new approaches in order to better understand cellular interaction phenoms.[56]

A cancer cell line microenvironment, amongst all others, can be classified into three categories regarding their self-renewal and differentiation: biochemical, physical and physicochemical. Additionally, cells are divided by size, components, activities, occurrence, a wide range of characteristics, among others. Another parameter that allow the categorization of cells is whether they are adherent or non-adherent, regarding their anchorage to a substrate. Adherent cells are anchorage-dependent and require a surface to attach in order to proliferate and in some cases to differentiate. Non-adherent type of cells can grow in suspension and doesn't require a surface to attach.[57]

In vitro and *in vivo* approaches for cell culture are very different from each other. The first lacks physiological functions and it becomes very difficult to maintain a viable and reproducible cell culture for a prolonged period.[43] While in the second one, cells are subject to cytokine gradients and secreted proteins, they interact biologically and mechanically with extracellular matrix and contact directly with other cells, they are exposed to a multitude of nutrients as soon as they are physically stimulated, allowing them to carry out all the physiological functions.[43,44] These differences between such cell culture techniques may be the reason for cellular failure when changing from the *in vivo* to the *in vitro* environment.[43] Due to the extracellular matrix, which has a fibrous nature and a complex molecular composition, another issue of mimicking cell cultures *in vitro*, when those come from animal organisms, is the inability to provide structural support, as they grow three-dimensionally.[56] Additionally, existent cell culture techniques can't always mimic living systems complexity, often leading to an incomplete cell maturation, preventing a cell culture to reach its full development, while hindering the extrapolation of predictions for an *in vivo* platform. In comparison, the high complexity of interconnected living tissues in vivo often leads to indistinct observations regarding the organism mode of action.[58]

Driven by a higher degree of control over the fluidic environment, the capability of cell adhesion by using biocompatible materials such as PDMS and mechanical stimuli to cells through the use of the aforementioned valves and pumps, in the early 2000's, researchers started to apply microfluidic devices for cell culturing and cell-cell interaction studies.[43,56]

As microfluidic platforms allow for a precise control of the cellular environment, these type of devices provides a major advance in the study of cell biology. Monitoring cell responses to controlled external perturbations represents a great achievement and supply an easier method to study biochemical pathways, cell-fate decisions and/or tissue morphogenesis. One of the most important external stimuli for cells, especially adherent (those who need a surface to proliferate), is the type of fluid flow through the microfluidic system. In addition to the nutrient transport, fluid also represents a source of mechanical shear stress. Also, one of the major benefits that a microfluidic environment provides is the origin of a concentration gradient, due to the properties of the diffusive mixing of the laminar flow, allowing the simultaneous probation of several conditions and mimicking *in vivo* conditions.[44]

When researchers must an experimental approach, there is always advantages and challenges in both macroscopic (*in vivo* and *in vitro* assays previously compared) and microfluidic approaches for the desired application. Overall, microfluidic technologies seem to offer a more profitable advantages-challenges ratio comparing to macroscopic approaches for cell culturing (**Fig. 1.7**).[12]

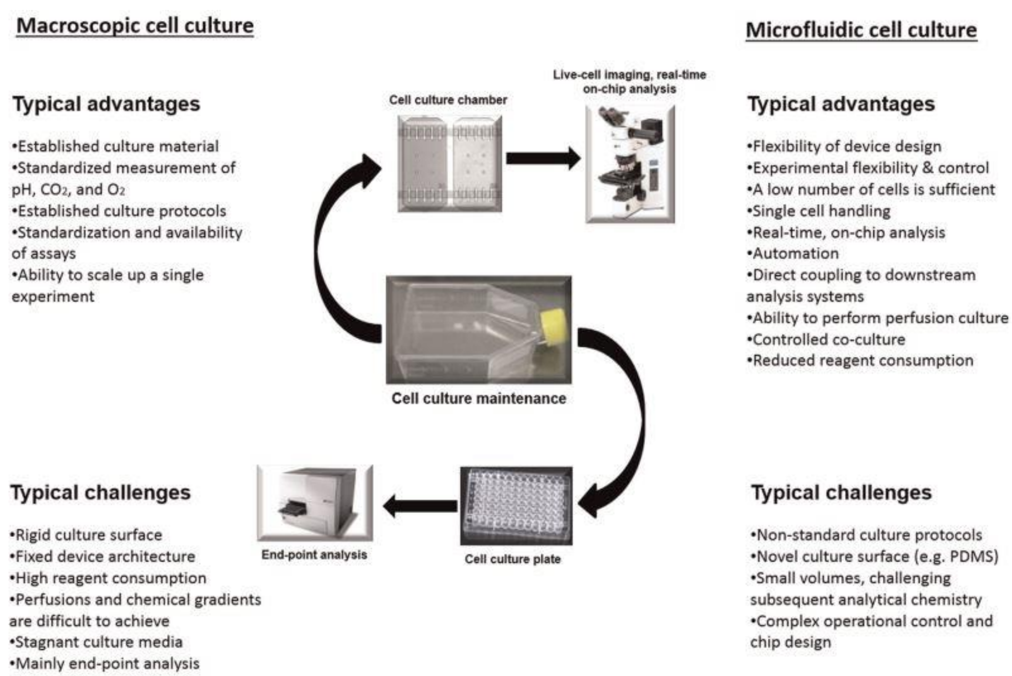

Figure 1.7 – Main advantages and challenges comparison regarding macroscopic and microfluidic approaches for cell culture. Adapted from literature.[12]

1.5 Drug screening

The drug screening process, which must be carried out before the release of a certain drug into the market, is longstanding and expensive, with yearly expenses, according to data of 2013, of approximately 135 billion dollars. Each new compound needs to be approved by the FDA, regarding the United States of America, which is a process that takes around 15 years in preclinical and clinical trials alone, requiring approximately 1 and 1.5 billion dollars, respectively.

The main steps to be followed for a new drug to be approved, from its initial testing to the commercialization, in addition to the approximate process costs are schematized in **Fig. 1.8 (a)**. Generally, it initiates with initial testing, followed by the preclinical stage, in which tests regarding activity, drug-response, toxicity and ADME features are carried out. Then, *in vivo* tests in animals or well plate tests are realized to prove whether a drug can be or cannot be used in humans. Such expensive and time consuming steps could be replaced by microfluidic-based assays, shown in **Fig. 1.8 (b)**. The ability to reduce analysis time and chemicals used would help the pharmaceutical industry to reduce its expenses. There are still no defined processes for drugs approval based on assays carried out on microfluidic devices. However, for a drug candidate it will be easier to be commercialized if its benefits outweighs its risks, its safe and effective are assured and its production methods are appropriate.[59]

Since its first use, microfluidic technology for cell-based experiments have been applied in such assays as cell sampling, trapping, sorting, drug administration, among others.[56] Regarding drug screening and administration fields, the science community has been trying to test new approaches in order to generate reliable predictions of drugs efficacy and safety in humans, in order to anticipate possible side effects ate the clinical trial phase with one of these approaches being the development of microfluidic systems. These devices may fulfil such needs by creating micro-engineered cell culture models that, by integrating both assay miniaturization and automation will increase its resolution and precision.[58]

Until this day in the drug-screening field, there has been many issues regarding standard methods, involving Petri dishes and animal organisms use. Such issues as the long time for the complete evaluation of a drug candidate, more than 10 years, high costs, excessive labour and in addition the ethical issue raised by the use of animals for such experiments produce complications regarding the transformation of drug candidates in real clinical medication.[60] This ability to predict a drug's effect even decreases if it is tested in patients, due to the increase of complexity introduced by the human body. Such restrictions demand more information as genomic data and new approaches are quite necessary, primarily if the use of different drug combinations is required. Such difficulties could be overtaken if drug tests were made directly on patient's samples. However, these drug screening technologies are limited to the large number of cells needed for this type of assays, being blood tumours still one of the few that can be used for large-scale drug screening. Patient-derived cell lines could also become an alternative, although this type of cell cultures take too much time to grow, which therefore could change cell's phenotype.[61]

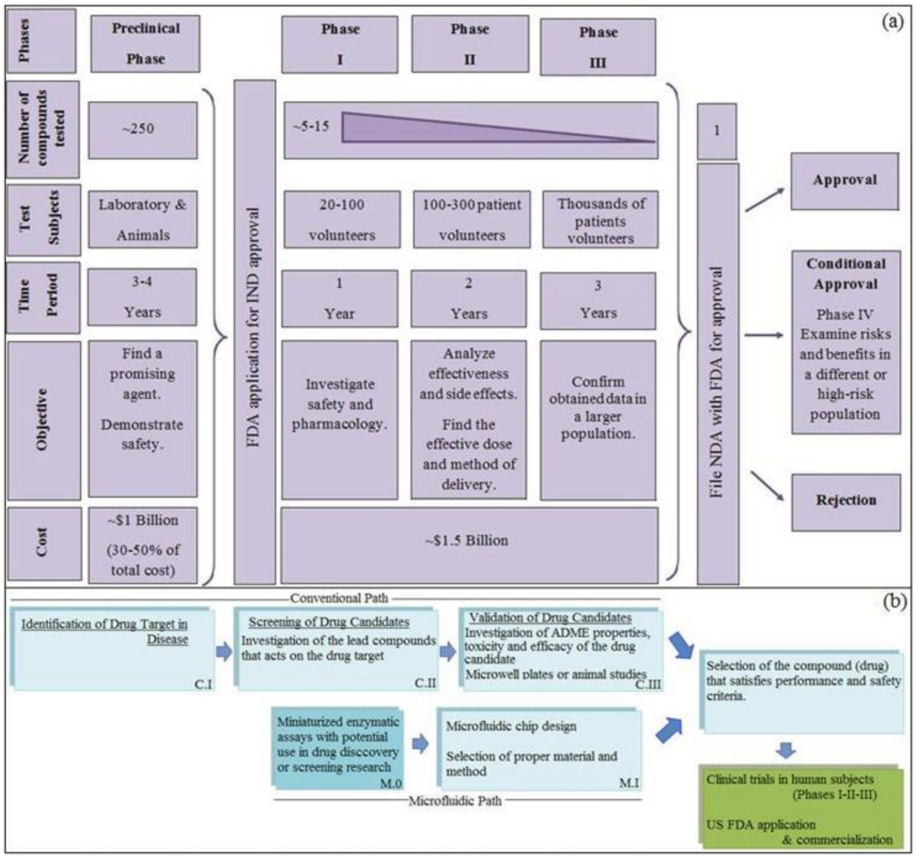

Figure 1.8 – Drug discovery, research, development and market implementation steps. (**a**) Costs, time spent, subjects tested, objectives and number of compounds tested for different phases of a new drug approval process. (**b**) Steps in the conventional path that can be replaced by microfluidic approaches. Adapted from literature.[59]

The use of conventional drug screening platforms presents many disadvantages that lead for the failure of more than 80% of drug candidates in phase 2 and 3 of clinical trials. Drug screening assays requires a wide number of drug candidates that must be checked for their cytotoxicity and side effects in patients. Two-dimensional culture systems and i*n vivo* animal models used for chemotherapy efficacy studies are being less used due to non-reproducibility of the tumour physiology, as in the human body, ethical issues regarding the latter and other previously mentioned problems, creating a need for research methods that mimic the *in vivo* environment of living organisms.[4,59,60]

Since an efficient method for drug screening is highly anticipated, there has been a great use of microfluidics devices in order to meet the needs not met by commonly used platforms.[59,60] This emerged as a platform to carry out pre-clinical assays drug-screening assays before drugs commercialization and revealed to be more efficient than high-density well plates, also used in cell viability assays, IC50 values determination or certain enzymes inhibitors finding.[59] Revolutionization of drug screening methods can be achieved by the microfluidic technologies from the bottom to the top of the process. Besides the reduction of high-cost compound volumes, such devices can save the costs of the drug discovery process. Large-scale drug toxicity and optimal concentration values evaluation can be addressed by the concentration gradient generator ability of such microstructures. Regarding in vitro platforms for drug screening assays, if a comparison between Petri dishes and microfluidic devices is to be made, the latter can better mimic physiological conditions, as it can be used to create an environment that resembles the in vivo conditions of different cells interactions in an organism.[60]

Such microfluidic systems may have different configurations depending on the application the user is addressing. There are several types of device designs and fabrication techniques that microfluidic researchers can explore.[59]

1.6 Cell death detection in a microfluidic device

In order to perform a drug screening assay, there is a need to track such drugs effects. In this type of assay, after cells' exposure to drugs, cell death is then monitored. There are several biomarkers, not produced by the cells, that could be used for the detection and monitoring of cell death by producing an optical response.

Some biomarkers are DNA-specific dyes that binds to such nucleic acids differently whether the cell is alive or dead. Hoechst 33342 (HO342) and 7-amino-actinomycin D (7-AAD) are both DNA intercalating agents used in cell viability assays. HO342 can penetrate the membrane of both live and dead cells, while 7-AAD can only stain the cell when the membrane is already compromised, which happens after cell death. However, there are some drawbacks regarding the use of these dyes. Many DNA probes are known to present cytotoxicity effects on cells by detrimentally interacting with cellular constituents and by affecting functional pathways. Thus, these probes are generally used only for end-point assays.[62–65]

A biomarker can also be produced and/or released by the cell and represents a certain characteristic that is measured and describes a biological state, these can be used to track cell viability as well as which metabolic pathways are being activated. Such measurement is made by analysing biomolecules such as nucleic acids or proteins and even biomolecules modifications via a specific cellular process. The World Health Organization define that a biomarker as substance, structure or process that can be measured and predict the incidence of the desired cell response.[66] In such assays, whether it implies the detection of an over- or sub-expression of a specific gene or to evaluate the release of a protein after cell death, it is critical to identify and validate biomarker's robustness in order to predict a the sensitivity or resistance of cells to a specific modification or drug exposure.[67] In drug screening assays it is then important to make some efforts in order to identify biomarkers that can give researchers the required information regarding drugs-anticancer efficacy.[68]

Adenylate kinase is a family of ubiquitous phosphotransferases, composed by various isoenzymes, that is present in a wide range of organisms, including animals. Its main role remains in the cellular nucleotide synthetic machinery, catalysing the interconversion of adenine nucleotides between each other. Important to refer that nucleotides, not only adenine's, are the monomers in nucleic acids, which are important in cell metabolism, not only as energy sources but also as activated intermediates in biosynthetic pathways, cell signalling and as components in coenzymes. It performs a crucial buffering part by maintaining the equilibrium between such nucleotides by catalysing the reversible reaction ATP + AMP $\leftrightarrow$ 2 ADP, transferring one of the phosphate groups, gamma or beta, between two adenine nucleotides (**Fig. 1.9**). Thus, it is responsible for the maintenance of the energy balance, also favouring the storage and the use of adenine nucleotides-descendant energy. It participates in several adenine nucleotides-containing enzymatic reactions as a regulatory factor. Additionally to these functions inside a cell, it is also involved in the synthesis of nucleic acids. Regarding its applications, it is used in cancer treatment and viral infections due to its nucleoside analogues phosphorylation ability. Due to all functions and the range of applications, it is used in studies in areas such as enzymology, human genetics and protein chemistry.[69–71]

This phosphotransferase family includes nine major isoforms, AK1 to AK9, and some sub-forms differing on their subcellular localization, tissue-specific distribution and kinetic properties. Beyond their role previously explained at a cellular scale, they are also involved in such processes as muscle contraction, cellular electrical activity, cell motility and the response to unfolded proteins. Due to the fact of these isoforms being in various cell compartments such as the cell membrane, cytosol, mitochondria and nucleus, an efficient phosphotransfer network is composed.[72,73]

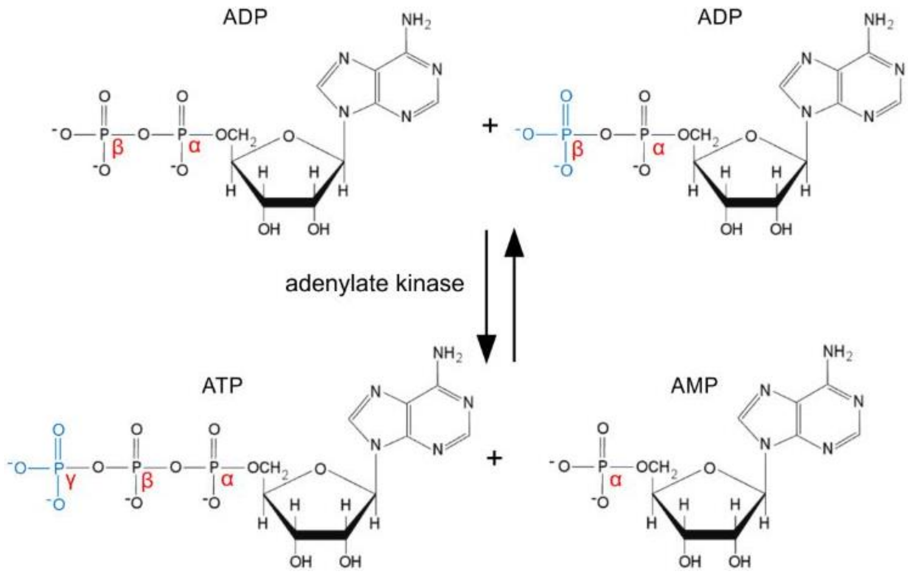

Figure 1.9 – Reaction mechanism of the major role of adenylate kinase inside the cell. It is responsible for the interconversion and balance of the adenine nucleotides (ATP, ADP and AMP). Adapted from literature.[71]

From all nine isoenzymes, in mammalian cells AK1, -2, -3 and -4 are the most important ones. AK1 is the major AK isoform and is mainly present in tissues with a high energy demand such as brain, skeletal muscle, heart and in cell as erythrocytes, being localized in the cytosol. In such tissues, this isoform shows the highest expression levels when compared to other isoenzymes in this family. One specific characteristic is that AK1 can use various nucleoside triphosphates to phosphorylate AMP. The other three important isoforms are localized in the mitochondria. While AK2 is localized in the mitochondrial intermembrane space, AK3 and -4 are localized in the mitochondrial matrix. AK2 plays an important role in the regulation of transferred energy between mitochondria and cytosol because of its interface localization. As well, it is also involved in the regulation of the overall energy homeostasis of cells. Unlike other isoforms, AK3 uses guanosine triphosphate instead of ATP and is not expressed in erythrocytes. Regarding the last of the four main isoforms, AK4 is expressed in almost all vital organs, however, its function as a kinase is still unknow. The expression of AK1, -2 and -4 is regulated and is specific of several organs, as opposed to AK3 that is ubiquitously expressed and is seen as a housekeeping enzyme.[70,72–74]

During cell death process, proteins and enzymes are released from the cell, whether if it is by apoptosis or necrosis.[75] When treated with anti-cancer drugs, the human colon cancer cell line used for this work, HCT-116, releases adenylate kinase to the supernatant due to the drug cytotoxic effect engaged on plasma membrane, causing its disruption.[76] Therefore, adenylate kinase detection represents a way to monitor cell culture viability. Such detection occurs via chemi- and/or bioluminescent and fluorescent methods. On mammalian cells, luminescence methods rely on the detection of light produced by an enzymatic oxidation of a substrate outside the cell. This method is known for its sensitivity due to usual non-production of luminescent substrates by mammalian cells, resulting in a very low background luminescence. On the fluorescent imaging method, a fluorescent material such as a dye, a probe or a reporter transgene product is excited by a light energy with a specific wavelength, releasing light on a longer wavelength and consequently with less energy.[77]

1.7 Project Goals

In this project, a human colon cancer cell line, HCT-116, is cultured using a microfluidic device. For the past decades until nowadays, cell lines derived from human tumour have been used as one of the pillars in cancer research, being a target in molecular and cell biology studies, helping the scientific community to better understand the genetic and epigenetic variations that cause the cancer development. Such cell lines are also usually used in fields of investigation as drug screening and biomarker discovery.[78]

HCT-116 is a colon cancer cell line commonly used to study cancer biology. It is a growth factor-independent line and is highly invasive and motile, in what concerns to *in vitro* studies.[79]

As HCT-116 is an adherent type cell, a microfluidic device must be projected in order to fulfil such needs. Generally, an in vitro system must be designed with the focus on cell interactions with their attachment substrate, as soon as the ability to influence and control the cell culture. Growth rate of both adherent and non-adherent cells is greatly influenced by their proliferation in a stationary environment, in which they can maintain a constant size distribution with time. Thus, the characteristics of the chosen substrate determines the quality of the cell attachment to the referred surface. Regarding a microfluidic platform, its design and substrate choice is projected considering cells dependence on surface attachment, whether if they are adherent or non-adherent. In the case of adherent cells, substrate's hydrophobicity remains as a critical factor for the proliferation and growth uniformity. Hydrophobic surfaces are known to inhibit substrate's attachment by adherent cells. Hydrophilic surfaces, contrarily to hydrophobic ones, don't show any influence in the adhesion of cells to a substrate, usually causing the formation of small aggregates.

It is frequent to functionalize such surfaces with biomolecules, as sugars or proteins in order to stimulate substrate's interaction with cells.[57] Collagen is the most abundant protein in humans, a major component of ligaments, skin, bones and in the structural network of other tissues. It also has a high structural integrity, a feature conceded by its fibrous nature, collagen is used in biomedical studies as a biomaterial to be applied in tissue engineered scaffolds.[80] This protein is implicated in several biological functions as tissue structuring and processes of biorecognition, being considered as a vital molecule to understand cells adsorption phenomena to surfaces.[81] Having a highly biomedical relevance, collagen is a major protein in cells' extracellular matrix (ECM) in various tissues, having a known vital role in the improvement of cellular adhesion and proliferation.[80,82]

As collagen is present in the ECM, it will bind to the chosen substrate, which is in this case the microfluidic device material: PDMS. Without any surface coating-treatment, collagen binds at the substrate via weak forces such as electrostatic, hydrophobic or van der Waals. After surface treatment, collagen binds to the surface, more precisely to the chemical groups used for the surface coating. This bond is now covalent, a stronger chemical connection than previous ones, and will enhance both cell adhesion and proliferation.[83] In this project, collagen will be used for this purpose.

In this work, a drug screening platform is developed by growing a reproducible and viable HCT-116 cell culture inside a microfluidic device, which is then exposed to several anti-cancer drugs, releasing an amount of AK that is monitored via luminescent and fluorescent approaches. In order to accomplish this there are crucial milestones to be achieved: maintain a viable cell culture of this cell line in a microfluidic device over a large period of time (i); establish a correlation between the amount of AK released per cell in order to correctly determine cell death rates in the microfluidic device (ii); optimize a biochemical detection method for on-chip detection of AK (iii); successfully perform drug screening assays on chip and confirmation via standard methods (iv).

2. Materials and Methods

This segment begins by clarifying methodologies used for the microfabrication part of the devices, from the cleanroom to the PDMS chip sealing. Then, the pre-inoculum and generation of a specific cell culture inside the microfluidic chamber will be explained. Finally, methods followed for the detection of the specific biomarker will also be clarified.

2.1 Microfabrication

2.1.1 Hard mask fabrication

This step is the one that requires more precision and cares regarding the amount of dust and possible contaminations. Thus, the fabrication of the hard mask is carried out inside a class 100 cleanroom (100 000 particles over 1 µm per m^2). In the photolithography step regarding the fabrication of the hard mask, the process was carried out inside a class 10 (10 000 over 1 µm per m^2). **Table 2.1** listss the materials, equipment and reagents necessary for the hard mask fabrication step.

Table 2.1 – Summary of the hard mask fabrication necessary materials, equipment and reagents

Materials	• Glass Substrate, Corning Inc. (Corning, NY/USA) • Silicon Wafer (150 mm diameter), University Wafer (South Boston, MA/USA)
Equipment	• AutoCAD software (Autodesk Inc., Mill Valley, CA/USA) • Automatic dicing SAW DAD-321, Disco Corporation (Tokyo, JP) • DWL Lithograph, Heidelberg Instruments (Heidelberg, DE) • Kerry Ultrasonic Bath (Skipton, North Yorkshire, USA) • Nordiko 7000 Magnetron Sputtering System, Nordiko Technical Services, Ltd (Havant, Hampshire, UK) • SVG Resist Coater and Developer Track, Silicon Valley Group Inc. (San Jose, CA/USA)
Reagents	• Acetone (99.6%), LabChem Inc. (Zelienople, PA/USA) • Alconox™ Solution, Alconox Inc. (White Plains, NY/USA) • Aluminum Etchant TechniEtch A180, Microchemicals (Ulm, DE) • Deionized (DI) water • Isopropanol (99.9%), LabChem Inc. (Zelienople, PA/USA) • Photoresist PFR 7790G, JSR (Sunnyvale, CA/USA)

The hard mask fabrication step begins with the design of a two-dimension Computer Aided Design (CAD) structure using AutoCAD™ software (**Fig. 2.1**) followed by the file saving as dxf format. Using this software, microfluidic structures' dimensions are defined, except for the height, that is only defined in the master mold fabrication step. However, if for the same structure two or more heights are required, the same number of hard masks must be fabricated according to the number of different heights existent for each structure. As two microfluidic structures are used in this project and one of them presents two different heights, three hard masks were fabricated.

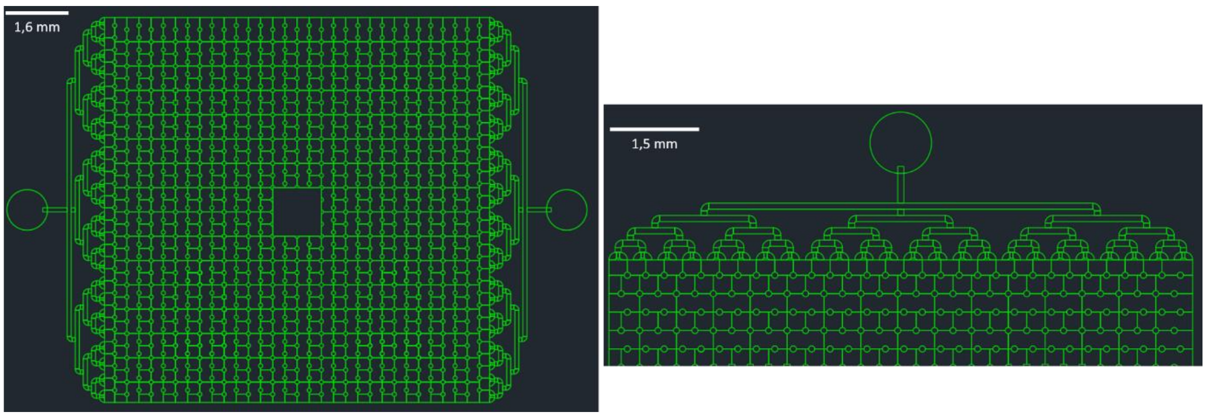

Figure 2.1 – Representation of the CAD design of the cell culture microfluidic structure. On the left image, the entire design is represented, presenting similarities with a square (approximately 1 cm side). On the right image, a zoomed detail of the structure, showing the entrances to the microchamber and the posts inside to make sure the structure doesn't collapse.

After the structure designing step, 5x5 cm glass substrates were cut using the Automatic Dicing SAW DAD-321. Then, such substrates were washed with acetone, isopropanol, DI water, following this order, and finally immersed into an Alconox™ solution for 40 minutes at 65°C inside the ultrasonic bath. Then, a 2000 Å aluminium layer was deposited by sputtering on the top of the substrate using a Nordiko 7000 Magnetron Sputtering System.

Afterward, the metal-coated substrate is taped to a silicon wafer and inserted into the SVG track for the positive photoresist coating and development. Coating step resulted in a 1.5 μm layer of photoresist that was then baked at 85°C for 60 seconds. The previously designed CAD is inserted into the DWL Lithograph machine. In this way, the design is transferred for the photoresist layer through a photolithography process using a direct write laser (405 nm, blue). After the exposure, the photoresist was baked at 110°C for 60 seconds, cooled for 30 seconds and finally developed for 60 seconds. As the aluminium is exposed on the developed areas, such spots are etched with a standard aluminium etchant until such regions are dissolved. To finalize the process, the remaining photoresist on the top is removed with acetone and isopropanol. A schematic summary of this process is represented on **Figure 2.2**.

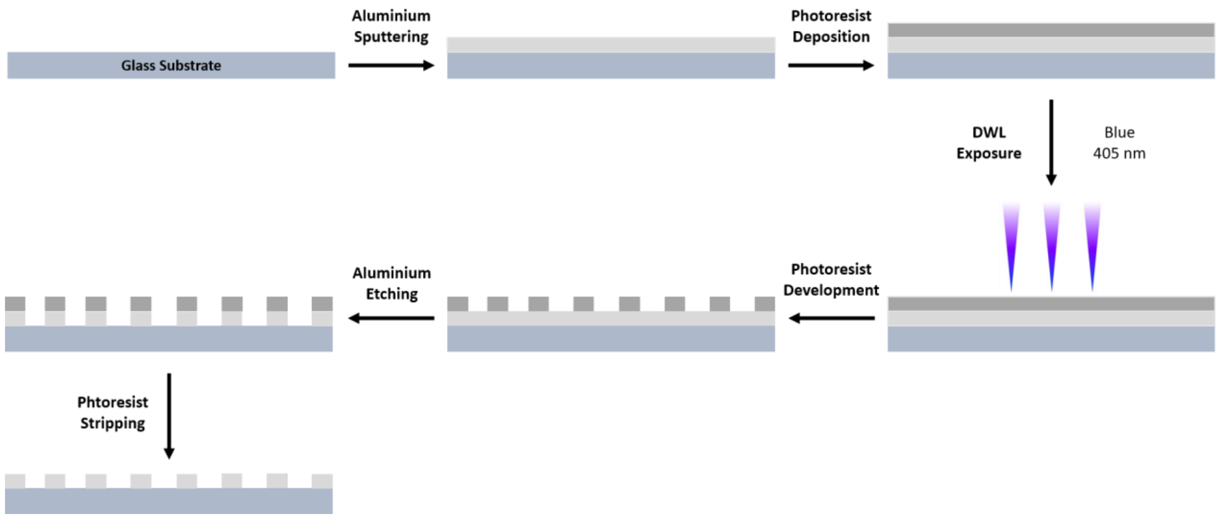

Figure 2.2 – Step-by-step schematic representation of the hard mask fabrication process.

2.1.2 Master mold fabrication

For each of the two required microfluidic structures, a master mold is fabricated. Hard masks fabricated through the process described in the previous section will be used in this process. The structure used for cell culture has a 100 µm height chamber, while the structure used for the biomarker detection has a chamber with 100 µm and another with 20 µm. The master mold fabrication is carried out inside a laminar flow hood, to minimize the appearance of dust in the fabricated structure. **Table 2.2** lists the materials, equipment and reagents necessary for the master mold fabrication.

Table 2.2 – Summary of the master mold fabrication necessary materials, equipment and reagents

Materials	• Silicon Wafer (150 mm diameter), University Wafer (South Boston, MA/USA) • Hard masks fabricated in previous section
Equipment	• Hotplate, Stuart (Stafforshine, UK) • Spinner, Laurel Corp. (North Wales, PA/USA) • Stereo Microscope, AmScope (Irvine, CA/USA) • UV Light (254 nm, 400 W), UV Light Technology Limited (Birmingham, UK)

	• Vertical Laminar Airflow Cabinet, FASTER-BSC-EN (Cornaredo, IT) • Kerry Ultrasonic Bath (Skipton, North Yorkshire, USA)
Reagents	• Acetone (99.6%), LabChem Inc. (Zelienople, PA/USA) • Alconox™ Solution, Alconox Inc. (White Plains, NY/USA) • DI water • Isopropanol (99.9%), LabChem Inc. (Zelienople, PA/USA) • Propylene glycol methyl ether acetate (PGMEA) (99.5%), Sigma-Aldrich (St. Louis, MO/USA) • SU-8 2015 Photoresist, MicroChem Corp. (Newton, MA/USA) • SU-8 50 Photoresist, MicroChem Corp. (Newton, MA/USA)

The master mold fabrication process begins with the cut of 5x5 cm squares of a silicon substrate, followed by the cleaning with isopropanol and DI water for residues removal and finally immersed into an Alconox™ solution for 25 minutes at 65°C inside the ultrasonic bath. After the Alconox immersion, it is washed with DI water and carefully dried using compressed air. In the end, the substrate is washed again with DI water and carefully dried using compressed air.

In order to fabricate the master mold used for the biomarker detection, which has two different heights, two different hard masks were used. The process followed the steps already described in the literature.[84]

After washing the substrate, the process continues with the 20 µm layer fabrication. The negative photoresist SU-8 2015 is spin-coated on top of the silicon substrate, beginning with 30 seconds at 500 rpm and 100 rpm/s, being followed by 34 seconds at 1700 rpm and 300 rpm/s. After the photoresist spin-coat, the substrate is put on a hot plate for a pre-exposure bake for 4 minutes at 95°C, being followed for a cooling step for 1 minute. Afterwards, the first hard mask is put on top of the photoresist, with the aluminium layer in contact with the photoresist, and it is exposed to UV light for 30 seconds. The substrate is then baked at 95°C for 5 minutes, followed by another cooling down step of 2 minutes. The development step is carried out with the immersion of the substrate in a PGMEA solution with manual agitation for around 2 minutes. At the development step, the patterned design starts to be observed and then the substrate is taken out of the bath and rinsed with isopropanol and carefully dried with compressed air.

After the development of the 20 µm layer, the 100 µm layer can be fabricated. The negative photoresist SU-8 50 is spin-coated on top of the silicon substrate, beginning with 10 seconds at 500 rpm and 100 rpm/s, being followed by 30 seconds at 1000 rpm and 300 rpm/s. After the photoresist spin-coat, the substrate is put on a hot plate for a two different temperature pre-exposure bake: beginning with 10 minutes at 65°C and then increasing the temperature to 95°C, remaining at that temperature for 30 minutes. Pre-exposure bake is followed by a cooling step for 1 minute at room temperature. Afterwards, the second hard mask, that is manually aligned with the alignment marks designed in the 20 µm layer, is put on top of the photoresist, with the thin aluminium layer in contact with the photoresist, and it is exposed to UV light for 30 seconds. The substrate is then baked at 95°C for 10 minutes, followed by another cooling down step of 2 minutes. The development step is carried out with the immersion of the substrate in a PGMEA solution with manual agitation for around 10 minutes. At the development step, the patterned design starts to be observed and then the substrate is taken out of the bath and rinsed with isopropanol and carefully dried with compressed air.

Due to the fact that the patterned photoresist is going to be part of the final device and is going to be subject to thermal processing in regular operation, a hard bake step is carried out to ensure that the photoresist properties do not change by use.[85] After the deposition of both photoresist layers, the hard bake step consists in the substrate bake at 150°C for 45 minutes.

Cell culture's device's master mold fabrication uses a third hard mask fabricated and since its height is 20 µm, the process is the same as the last part of the AK detection master mold. In this process, after the substrate washing step, the SU-8 50 negative photoresist is spin-coated and the same process is followed. A scheme presenting summarily the process explained is represented in the figure below (**Fig. 2.3**).

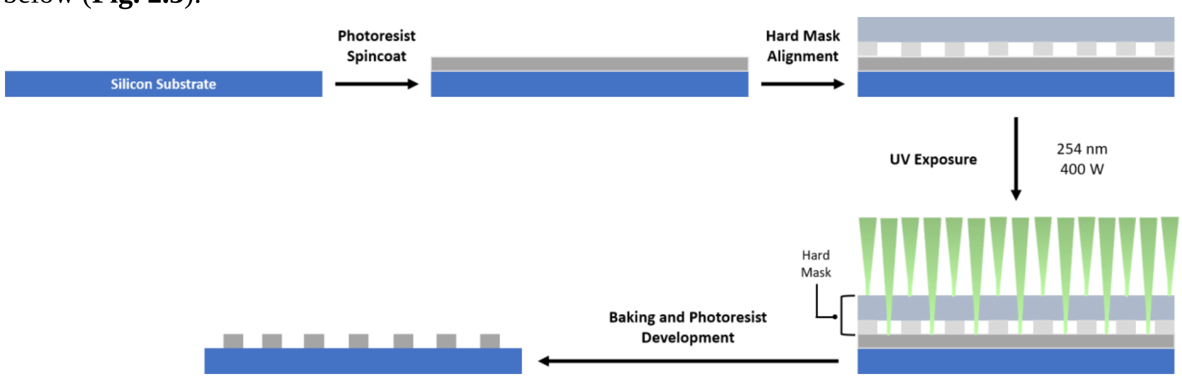

Figure 2.3 – Step-by-step schematic representation of the hard mask fabrication process.

2.1.3 PDMS device fabrication

The two master molds that were fabricated following the process explained previously are used for the casting of PDMS in order to fabricate the structures. Despite the two master molds fabricated being different between each other, the process for the PDMS casting is the same for both. **Table 2.3** lists shows the materials, equipment and reagents necessary for the PDMS devices fabrication.

Table 2.3 – Summary of the PDMS devices fabrication necessary materials, equipment and reagents

Materials	• Silicon Wafer (150 mm diameter), University Wafer (South Boston, MA/USA) • Coverslip 0.8 mm, Assistant (Sondheim, DE) • Rounded Syringes tips (20 Gauge), Instech Laboratories (Plymouth Meeting, PA/USA) • Polystyrene Promed ® Petri Dish, FL MEDICAL (Torreglia, IT) • Master molds fabricated in previous section
Equipment	• Analytical Scale d=0.0001 g, ScienTech (Boulder, CO/USA) • Spinner, Laurel Corp. (North Wales, PA/USA) • Expanded Oxygen Plasma Cleaner PDC-002-CE, Harrick Plasma (Ithaca, NY/USA) • Oven Loading Model 100-800, Memmert (Schwabach, DE) • Vertical Laminar Airflow Cabinet, FASTER-BSC-EN (Cornaredo, IT) • Vaccum Desiccator, Bel-Art Products (South Wayre, NJ/USA)
Reagents	• DI water • Sylgard 184 PDMS and Curing Agent – Silicon Elastomer Kit, Dow Corning (Midland, MI/USA) • 3-Aminopropyltriethoxysilane (APTES) 99%, AcroSeal ®, Thermo Fisher Scientific (Geel, BE)

PDMS device fabrication process begins with the preparation of a 1:10 mixture of PDMS and curing agent. PDMS mixture is thoroughly mixed with a spatula and placed inside a desiccator for 45 minutes for degasification. The master mold is fixed inside a Petri dish with Kapton tape in the substrate corners and after the degasification process, the 1:10 PDMS + curing agent mixture is poured inside the Petri dish until it reaches a height between 0.5 and 1 cm. Afterwards, the Petri dish containing the mixture is taken the oven for 90 minutes at 70°C for curing. After the curing step, the hardened PDMS is cut from the Petri dish using a scalpel and peeled off from the master mold using a tweezers. Afterwards, the inlet and outlet holes are pierced using a rounded 20 Gauge luer stub to allow the connection of the microfluidic chamber to the outer space, ready for the final sealing step.

In the case of the cell culture device, the microfluidic chamber is sealed against a polystyrene Petri dish. Cell culture microfluidic device sealing begins with the Petri dish receiving an oxygen plasma treatment for 5 minutes at high intensity. Afterwards, the Petri dish receives a surface silane functionalization, following a process described in the literature[86] (**Fig. 2.4**), by pouring into the Petri dish a 1:100 APTES solution in DI water, followed by a 20 minutes incubation at room temperature. After the incubation, the PDMS structure is washed with isopropanol, DI water and dried with compressed air, while the Petri dish is washed with DI water and dried with compressed air. Then, the PDMS structure receives an oxygen plasma treatment for 5 minutes at high intensity. Finally, both Petri dish and PDMS oxidized surfaces are put against each other, generating a covalently bonded device.

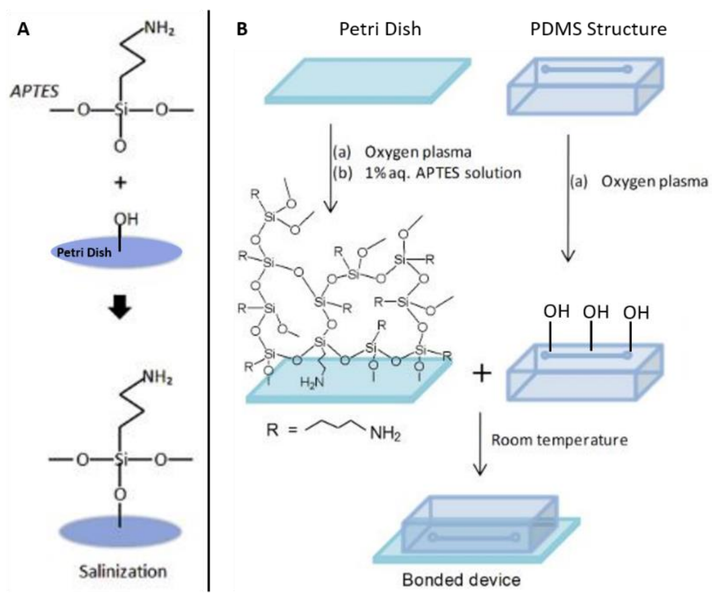

Figure 2.4 – Silanization process summary. (A) Silanization reaction with APTES reacting with the -OH group, which resulted from a previous oxygen plasma treatment, on the Petri dish surface. (B) Scheme of the cell culture microfluidic chamber using a silane functionalization of the Petri dish surface. Adapted from the literature.[83,86]

Regarding the biomarker detection chamber sealing, the microfluidic chamber is sealed either against a 500 µm PDMS layer or a coverslip. PDMS membranes are produced by spin coating the degasified polymer on top of a silicon wafer for 25 seconds at 250 rpm and 100 rpm/s. The PDMS layer is then cured for 90 minutes at 70°C. Afterwards, the PDMS membrane is cut with a scalpel and peeled off from the silicon substrate. After the curing step, both PDMS membrane/coverslip and the PDMS structures were washed with isopropanol, DI water and dried with compressed air. Finally, both PDMS membrane/coverslip and the PDMS structure receive an oxygen plasma treatment for 5 minutes at high intensity, being put against each other, generating a covalently bonded device (**Fig. 2.5**).

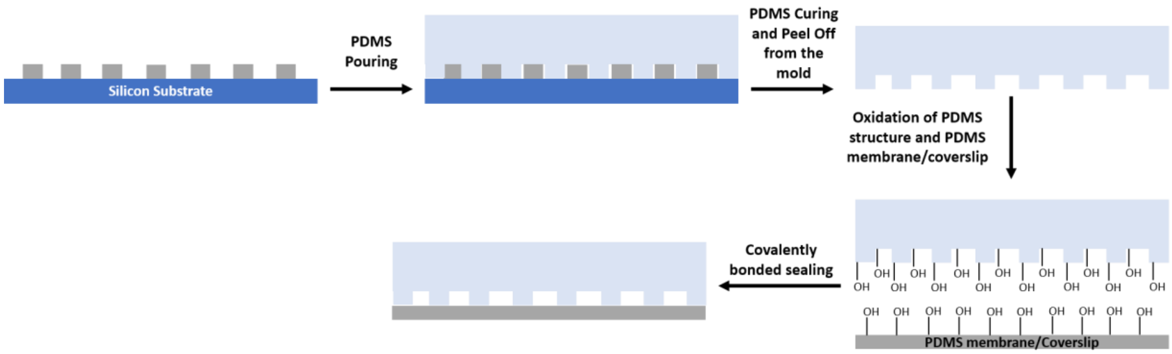

Figure 2.5 – Step-by-step schematic representation of the PDMS microfluidic device fabrication process.

2.2 HCT-116 Microfluidic Cell Culture

The microfluidic cell culture process of the HCT-116 cell line is carried out in Faculdade de Farmácia – UL facilities. This step involves the growth of the cell culture inside a t-flask and the following injection of the cells inside of the sealed microfluidic device, followed by cell culture growth and proliferation inside the microfluidic chamber. **Table 2.4** shows the materials, equipment and reagents necessary for the HCT-116 microfluidic cell culture process.

Table 2.4 – Summary of the required materials, equipment and reagents for the growth of the HCT-116 cell line inside a microfluidic device

Materials	• PE-90 Tubing (0.034 x 0.050 in), Instech Laboratories (Plymouth Meeting, PA/USA) • Stainless Steel Catheter Coupler (20 Gauge x 15 mm), Instech Laboratories (Plymouth Meeting, PA/USA) • Rounded Syringe Luer Stub (20 Gauge), Instech Laboratories (Plymouth Meeting, PA/USA) • 1 mL Single-use Syringe, CODAN PORTUGAL Instrumentos Médicos (Odivelas, PT)

	• dicoNEX 3 mL luer lock, Zarys (Zabrze, PL) • Parafilm ® M Plastin Paraffin Film, Bemis NA (Neenah, WI/USA) • Neubauer Chamber, BRAND GmbH + CO KG (Wertheim, DE) • Adhesive PCR Plate Seal, Thermo Fisher Scientific (Geel, BE) • Sealed microfluidic cell culture devices fabricated in previous section
Equipment	• Labculture ® Class II (Low Noise) Biosafety Cabinet, Esco Technologies, Inc. (Horsham, PA/USA) • Heracell™ 150i CO_2 Incubator with Stainless-Steel Chambers, Thermo Fisher Scientific (Geel, BE) • Inverted Microscope PrimoVert coupled with AxioCam 105 Color, Zeiss (Oberkochen, DE) • Zen 2012 (blue edition) Software, Zeiss (Oberkochen, DE) • NE-1200 Twelve Channel Programmable Syringe Pump, New Era Pump Systems, Inc. (Farmingdale, NY/USA) • NE-1000 Programmable Single Syringe Pump, New Era Pump Systems, Inc. (Farmingdale, NY/USA)
Reagents	• Gibco™ McCoy’s 5A (Modified) Medium Supplemented with FBS (Fetal Bovine Serum), Thermo Fisher Scientific (Geel, BE) • Ethanol Absolute, Honeywell | Research Chemicals (Mexico City, MX) • Gibco™ PBS (Phosphate Buffer Saline) 10x pH7.4, Thermo Fisher Scientific (Geel, BE) • HCT-116 Cell Line, Public Health England (Salisbury, UK) • Gibco™ TrypLE™ Express Enzyme (1x), Thermo Fisher Scientific (Geel, BE) • Trypan Blue Solution, Sigma-Aldrich (St. Louis, MO/USA) • Collagen Type I, Sigma-Aldrich (St. Louis, MO/USA)

2.2.1 Liquid Phase Cell Culture Handling

Cells are grown inside a T-flask with McCoy’s culture medium at 37°C and a 5% CO_2 atmosphere for 3 days.

For the preparation of an aliquot of suspended HCT-116 cells in culture medium the supernatant inside the t-flask is discarded in a first instance and cells suffer a trypsinization process at 37°C for 5 minutes through the addition of 1 mL of trypsin to the t-flask in order to put them into suspension. Then, to inactivate the trypsin, the same volume of culture medium is added to the t-flask. Afterwards, the suspended cell solution is pipetted to a Falcon tube and centrifuged for 5 minutes at 500 RCF. After the centrifugation step, the supernatant containing rests of trypsin is discarded and cells are resuspended with culture medium. Then, an aliquot of 1:10 cells in Trypan Blue is prepared and 10 µL are pipetted into a Neubauer chamber and live cells counting is proceeded. Finally, cell solution is diluted to obtain a cell concentration of 4×10^6 cells/mL.

2.2.2 Microfluidic Cell Culture Growth

The process begins with the sterilization of the material that is going to be in contact with the cells, including the cell culture devices, luer stubs and metallic couplers, by UV exposition for 20 minutes. After the sterilization step, the microchambers are filled with ethanol and then sterile DI water through manual injection. Afterwards, a collagen solution of 0.3 mg/mL in PBS is prepared and flowed into the channel for 2 minutes at a flow rate 4 µL/min for the adsorption to the microfluidic chamber's walls. The microchamber is then washed in culture medium.

After the preparation of the cell suspension with the desired concentration, cells must be inserted into the microfluidic chamber with the adsorbed collagen. First, a syringe is filled with water and connected with a luer stub, tube and a metallic coupler, in this order. The syringe apparatus is then assembled on a single channel syringe pump. After setting up the apparatus, the tube is filled with water until it flows out to ensure the absence of air bubbles. After this step, an air gap is created at the tip of the tube and then filled in the cell solution. The metallic coupler is then inserted in the microfluidic chamber and the cell solution is flowed for 2 minutes at 4 µL/min. Finally, the microdevices containing the cells are incubated for 4 hours at 37°C to allow the cell attachment to the inner structure of the microfluidic device (**Fig. 2.6**). After 4 hours, micrographs of the cells' are taken in order to visually inspect the cells.

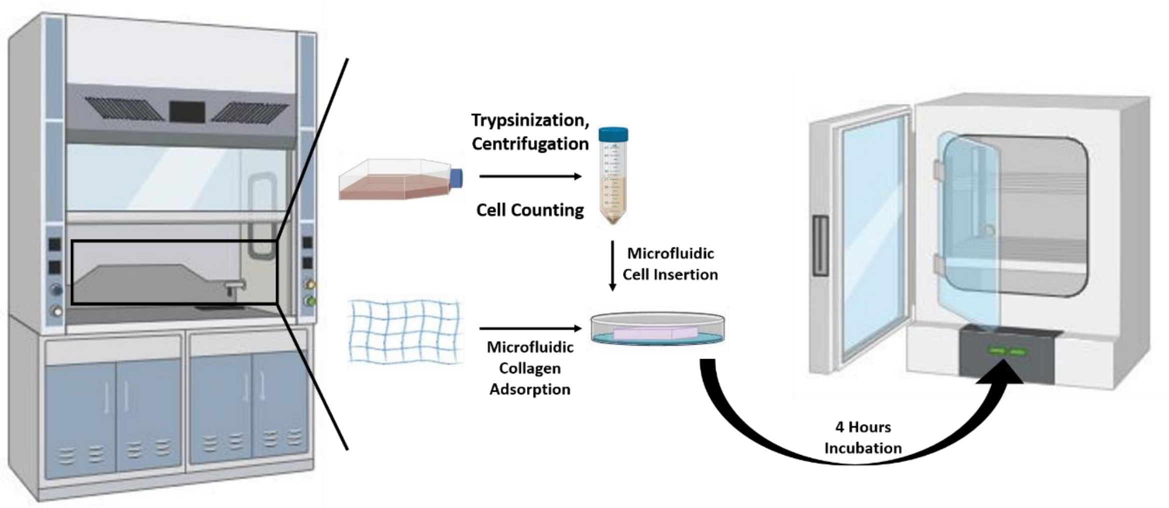

Figure 2.6 – Schematic representation of the cell culture process. Inside the laminar flow hood, both the liquid phase cell handling, comprising the trypsinization and the preparation of an aliquot with a cell suspension with the desired concentration, and the microfluidic handling, comprising the collagen adsorption process as well as the insertion of cells into the microfluidic device by perfusion, are carried out. The microfluidic cell culture is then put inside an incubator at 37°C for 4 hours for the incubation step.

The microfluidic chips are supplied with culture medium using 3mL syringes mounted on a multi-channel syringe pump. The tube that is going to be used is sterilized with ethanol 70% and washed with PBS. Fill the tube with culture medium and assemble the syringes used in a 12 channels syringe pump. After setting the apparatus, insert the tubes with the metallic adaptors in the inlets of the microfluidic devices. On the outlet, a metallic adaptor with a small tube connected to an empty Eppendorf tube is assembled to discard the medium that flows out of the chamber. Afterwards, a small piece of PCR tape is cut to seal the centre hole in the microfluidic device. Finally, the culture medium flows through the microfluidic chamber for 48 hours at 0.1 µL/min and 37°C (**Fig. 2.7**).

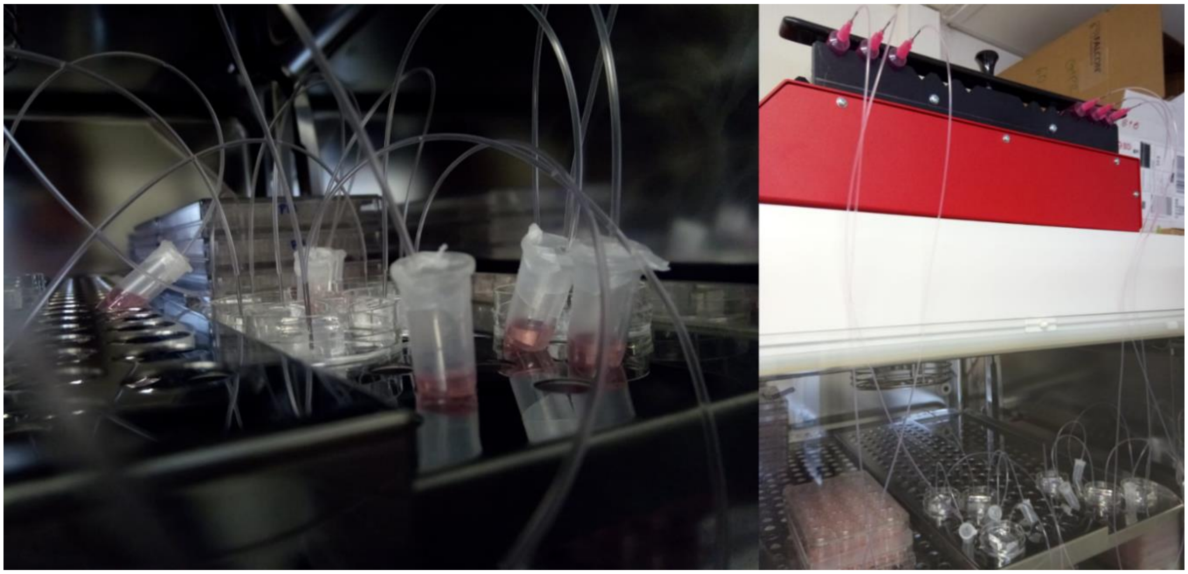

Figure 2.7 – Photography showing the microfluidic cell culture apparatus. In the left image is shown the small Petri dishes with the sealed microfluidic devices and the Eppendorf tubes being used to collect the outflow liquid. On the right image, the representation of the syringes assembled to the syringe pump, which stays on top of the incubator. Syringes containing the culture medium are connected to the culture chambers through polyethylene tubing.

2.3 Cell viability assays

2.3.1 DNA fluorescent dyes

After the growth and proliferation of a cell culture inside a microfluidic chamber, there is a need to verify its cell viability. One way to check on the cell culture viability is through nucleic acid labelling with fluorescent dyes that intercalate the DNA differentially in live or dead cells. **Table 2.5** shows the materials, equipment and reagents required for this cell viability assay.

Table 2.5 – Summary of the required materials, equipment and reagents for the monitoring of cell viability through the detection of DNA-specific fluorescent dyes

Materials	• PE-90 Tubing (0.034 x 0.050 in), Instech Laboratories (Plymouth Meeting, PA/USA) • Stainless Steel Catheter Coupler (20 Gauge x 15 mm), Instech Laboratories (Plymouth Meeting, PA/USA) • Rounded Syringe Luer Stub (20 Gauge), Instech Laboratories (Plymouth Meeting, PA/USA) • 1 mL Single-use Syringe, CODAN PORTUGAL Instrumentos Médicos (Odivelas, PT)

	• dicoNEX 3 mL luer lock, Zarys (Zabrze, PL) • Parafilm ® M Plastin Paraffin Film, Bemis NA (Neenah, WI/USA) • Microfluidic cell cultures grown in previous section
Equipment	• Labculture ® Class II (Low Noise) Biosafety Cabinet, Esco Technologies, Inc. (Horsham, PA/USA) • Fluorescence Microscope Axio Scope A. 1 coupled with AxioCam HRm, Zeiss (Oberkochen, DE) • Fluorescence Filter Set DAPI Shift Free (E), Zeiss (Oberkochen, DE) • Fluorescence Filter Set Rhodamin Shift Free (F), Zeiss (Oberkochen, DE) • Zen 2012 (blue edition) Software, Zeiss (Oberkochen, DE) • NE-1000 Programmable Single Syringe Pump, New Era Pump Systems, Inc. (Farmingdale, NY/USA)
Reagents	• Gibco™ McCoy's 5A (Modified) Medium Supplemented with FBS (Fetal Bovine Serum), Thermo Fisher Scientific (Geel, BE) • Gibco™ PBS (Phosphate Buffer Saline) 10x pH7.4, Thermo Fisher Scientific (Geel, BE) • Thermo Scientific™ Hoechst 33342 Solution (20 mM), Thermo Fisher Scientific (Geel, BE) • Invitrogen 7-AAD (7-Aminoactinomycin D), Thermo Fisher Scientific (Geel, BE)

After the 48 hours of the growth and proliferation step of the cell culture inside a microfluidic device, a single solution of DNA-specific fluorescent dyes is prepared. First, both 1 mg/mL aliquots of HO342 and 7-AAD are taken out from the fridge and the freezer, respectively, letting them thaw and heat up to room temperature. Afterwards, HO342 and 7-AAD are diluted in culture medium in a same solution for a final concentration of 2 µg/mL and 1 µg/mL. A syringe is filled with the dye's solution, coupled with the luer stub, tube and the metallic adaptor and assembled on a syringe pump. The metallic adaptor is inserted in the inlet hole of the microfluidic device and flow the double-dye solution for 15 minutes at a flow rate of 2 µL/min. While the solution is being flowed, the apparatus is put in the dark. After flowing the dyes through the cell culture, the apparatus is disassembled, and cells' labelling degree is observed under a fluorescent microscope. Considering the excitation/emission wavelengths of HO342 and 7-AAD, 361/486 nm and 546/647 nm respectively, and setting the DAPI Fluorescence Filter Set for HO342 and the Rhodamin Fluorescence Filter set for 7-AAD, micrographs are taken with a total magnification of 100x using the Zen 2012 Software to set the exposure time at 1 second for each dye, eliminate the background signal and save the micrographs with merged and separate dyes.

2.4 Adenylate Kinase Detection

2.4.1 Luminescent Detection

2.4.1.1 Macroscale Calibration between Adenylate Kinase Solutions and Cell Supernatants

The detection of adenylate kinase was carried in a first instance on a macroscale assay before the transition to a microfluidic device. The table (**Table 2.6**) below shows the material, equipment and reagents required for the macroscale detection of adenylate kinase in solution and adenylate kinase present in cell's supernatants.

Table 2.6 – Summary of the required materials, equipment and reagents for the calibration between Adenylate Kinase and Live and Dead Cells Supernatant.

Materials	• 96-Well Plate • Multi-channel Micropipette
Equipment	• Microplate Reader Glomax Multi+ Detection System, Promega (Madison, WI/USA) • Refrigerated Centrifuge 5804 R, Eppendorf (Hamburg, DE)
Reagents	• AK1 Human Recombinant, Sigma-Aldrich (St. Louis, MO/USA) • RIPA buffer • Gibco™ McCoy's 5A (Modified) Medium Supplemented with FBS (Fetal Bovine Serum), Thermo Fisher Scientific (Geel, BE) • Gibco™ PBS (Phosphate Buffer Saline) 10x pH7.4, Thermo Fisher Scientific (Geel, BE) • ToxiLight™ bioassay kit, Lonza (Basel, CH) • HCT-116 Solution in culture medium

First, 5 solutions of HCT-116 live cells with a range of concentrations from 3×10^4 cells/mL to 6.8×10^5 cells/mL were obtained, following the procedure explained in **Section 2.2**. Afterwards, cell suspensions' supernatants are transferred to new tubes and stored while the remaining precipitated cells in the initial tube are made up with the same volume to maintain the concentration.

After the solution's split in two, the solutions containing the cells are treated with RIPA buffer to induce cell death through lysis.

RIPA buffer is added to each cell solution and it is left to incubate on ice for 30 minutes with manual agitation at t = 10, 20 and 30 minutes. After the 30 minutes' incubation step, cell solutions are centrifuged for 30 minutes at 4°C at 16 000 g. In the end of the centrifugation step, cells are resuspended in culture medium. The 5 solutions of both live and lysed cells, with the same cell concentration, are diluted to a final concentration of 1 cell/mL.

Regarding the pure AK solutions, a stock aliquot with 1 mg/mL of adenylate kinase I from human is diluted in PBS in six concentrations from 0.2 µg/mL to 1×10^{-3} µg/mL.

Finally, for the luminescent detection of adenylate kinase, a commercial ToxiLight™ bioassay kit is used following the specifications of the fabricant. Pure AK dilutions, live cells supernatant and dead cells solutions are mixed with the ToxiLight™ kit in a 96-well plate and the 562 nm emission light is detected inside a GloMax-Multi+ Detection System, which is programmed to an agitation step of 30 seconds, an incubation step of 5 minutes and an integration time of 0.5 seconds for each well.

2.4.1.2 Chemiluminescent Detection of Adenylate Kinase using a Photomultiplier

After the assay following a standard luminescent detection mode, another macroscale approach using a photomultiplier (PMT) module was carried out. Due to the sensitivity of the photomultiplier, this type of assays is carried out inside a dark room. The table (**Table 2.7**) below shows the material, equipment and reagents required for the macroscale detection of adenylate kinase using a photomultiplier.

Table 2.7 – Summary of the required materials, equipment and reagents for the macroscale detection of adenylate kinase using a photmultiplier.

Materials	• Coverslip 0.8 mm, Assistant (Sondheim, DE) • Micropipette • Rounded Syringe Luer Stub (20 Gauge), Instech Laboratories (Plymouth Meeting, PA/USA)

Equipment	• 1 mL Single-use Syringe, CODAN PORTUGAL Instrumentos Médicos (Odivelas, PT) • PE-90 Tubing (0.034 x 0.050 in), Instech Laboratories (Plymouth Meeting, PA/USA) • Glass-Sealed Microfluidic Device with Two Entrances
	• 2 Agilent/HP E3612A DC Power Supplies, Agilent (Santa Clara, CA/USA) • Agilent/HP 6209B DC Power Supply, Agilent (Santa Clara, CA/USA) • Agilent InfiniiVision MSO7054A Oscilloscope, Agilent (Santa Clara, CA/USA) • ISO-TECH IDM 71 Multimeter • H5784-01 Photosensor Module, Hamamatsu Photonics (Hamamatsu City, JP) • 2 NE-1000 Programmable Single Syringe Pump, New Era Pump Systems, Inc. (Farmingdale, NY/USA) • Spyder Software
Reagents	• AK1 Human Recombinant, Sigma-Aldrich (St. Louis, MO/USA) • Gibco™ PBS (Phosphate Buffer Saline) 10x pH7.4, Thermo Fisher Scientific (Geel, BE) • ToxiLight™ bioassay kit, Lonza (Basel, CH)

This assay begins by the construction of a black box with connection to exterior, where the PMT will be put, due to the high sensitivity of the PMT, that is able to detect the background signal. As the PMT needs power voltage to work out, the connection of the PMT to two different power supplies, one with +15 V and another with -15 V, is carried out through co-axial cables. However, the PMT requires a control voltage. Before connecting the third power supply to the PMT, a handheld multimeter is used to measure its output voltage, in order to not apply a higher voltage to the one specified in the PMT datasheet. After this monitoring step, the last power supply need is connected to the PMT. Afterwards the PMT is connected to an Agilent oscilloscope for data output. The time per window and the voltage per square in the oscilloscope were set before data acquiring (**Fig. 2.8**). For data saving, an USB Pen drive is connected to the oscilloscope.

Regarding the data output, instead of the oscilloscope, the PMT can also be connected to an Agilent multimeter. In this case, data acquisition can be carried out manually, by writing values between certain periods of time or it can be carried out automatically using a Python-language script written on Spyder Software (script on **Appendix A**). Spyder script is programmed with the acquisition time, defining also the intervals of time in which it acquires the data, as well as the mode of signal integration and the time of integration.

Beyond being connected to the PMT, the data acquisition device must be also connected to a computer for the automatic data acquisition.

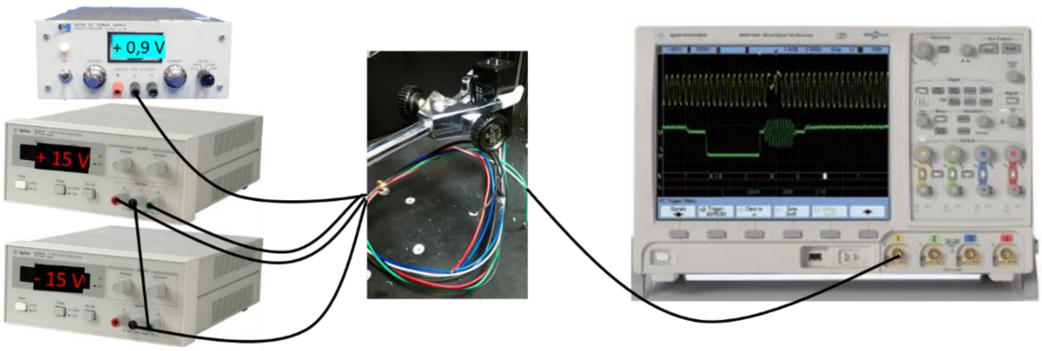

Figure 2.8 – Macroscale detection setup representing the connection between the power supplies to the PMT and the PMT to the data output device, the oscilloscope.

Several dilutions of adenylate kinase in PBS were prepared. Following the specifications of the fabricant, ToxiLight™ kit was used for the optical detection of AK. Then, on the top of a coverslip is poured a droplet containing a mixture of AK with ToxiLight™. As the mixture is set, the reaction begins and quickly the coverslip is put on top of the reading region of the PMT. The output signal was saved in the pen drive at each 4 minutes.

AK chemiluminescent detection using a photomultiplier was also carried out inside a microfluidic device with two entrances. In a first instance, two syringe pumps, one with an assembled syringe filled with an AK solution diluted in PBS and another with an assembled syringe filled with the ToxiLight™ kit. Following the specifications of the fabricant, the syringe pump containing the syring filled with the AK solution works with a lower flow rate than the other. After coupling the metallic adaptors to each entrance of the microfluidic device used, it is put inside the black box and pumps are turned on. After 5 minutes, ToxiLight™ syringe pump is turned off and after 2 minutes the other is also turned on. After 2 minutes both pumps are turned on and turned off after 5 minutes.

2.4.2 Immunoassay Detection

2.4.2.1 Immunoassay using Protein G Sepharose Beads

A different approach of the detection of adenylate kinase is based on the fluorescent detection. An immunoassay using Protein G Sepharose beads is carried out for the fluorescent detection of adenylate kinase. In this section the detection antibody is the AK-specific antibody (α-AK) itself that was labelled with the fluorophore Alexa 430. The table (**Table 2.8**) below shows the material, equipment and reagents required for the fluorescent detection of AK through the AK-specific binding of a labelled AK antibody (α-AK-430).

Table 2.8 – Summary of the required materials, equipment and reagents for the fluorescent detection of adenylate kinase (AK) inside a microfluidic channel using Sepharose beads functionalized with Protein G as adsorption matrix for AK.

Materials	• 1 mL Single-use Syringe, CODAN PORTUGAL Instrumentos Médicos (Odivelas, PT) • PE-90 Tubing (0.034 x 0.050 in), Instech Laboratories (Plymouth Meeting, PA/USA) • Rounded Syringe Luer Stub (20 Gauge), Instech Laboratories (Plymouth Meeting, PA/USA) • Stainless Steel Catheter Coupler (20 Gauge x 15 mm), Instech Laboratories (Plymouth Meeting, PA/USA) • Amicon® Ultra 0.5mL Centrifugal Filters, Sigma-Aldrich (St. Louis, MO/USA) • AK Detection Microfluidic Device sealed against a thin PDMS membrane
Equipment	• NE-4000 Programmable 2 Channel Syringe Pump, New Era Pump Systems, Inc. (Farmingdale, NY/USA) • Leica DMLM Microscope, Leica Microsystems (Wetzlar, DE) • Digital Color Camera DFC300FX, Leica Microsystems (Wetzlar, DE) • mySpin™ 12 Mini Centrifuge, Thermo Fisher Scientific (Geel, BE)
Reagents	• AK1 Human Recombinant, Sigma-Aldrich (St. Louis, MO/USA) • Invitrogen Adenylate Kinase 1 Monoclonal Antibody (OTI19D1), Thermo Fisher Scientific (Geel, BE) • Gibco™ PBS (Phosphate Buffer Saline) 10x pH7.4, Thermo Fisher Scientific (Geel, BE) • Alexa Fluor™ 430 NHS Ester (Succinimidyl Ester), Thermo Fisher Scientific (Geel, BE) • Bovine Serum Albumin (BSA), Sigma-Aldrich (St. Louis, MO/USA) • Protein G Sepharose 4 Fast Flow, GE Healthcare Bio-Sciences (Pittsburgh, PA/USA)

- Polyethylene glycol (PEG), Sigma-Aldrich (St. Louis, MO/USA)
- DI water

For the labelling of the AK-specific antibody with the Alexa 430 dye, the procedure is followed as described in the literature.[84] The antibody buffer was changed from sodium azide to sodium bicarbonate through a double-centrifugation step at 9800 g for 10 minutes. For the collection of the remaining antibodies adsorbed on the Amicon membrane, the tube containg the membrane was turned upside down, inserted again in the collection tube and centrifuged for 5 minutes at 9800 g. A mix containing a volume ratio of 4:1 of antibody to the dye is incubated under continuous agitation in the dark for 1 hour. Then, a series of 9 diafiltration steps using an Amicon ultracentrifugal unit at 9800 g for 10 minutes is carried out to remove the non-conjugated dye.

The fluorescent detection of adenylate kinase inside a microfluidic channel begins by turning on the fluorescent lamp that is coupled to the microscope since it needs at least 20 minutes to reach its maximum potency. Then, several solutions of non-labelled α-AK, BSA and α-AK-430 are prepared in PBS with the desired concentrations (**Table 2.9**).

Table 2.9 – Work concentrations of the non-labelled AK-specific antibody, BSA and the AK-specific antibody labelled with Alexa 430 for the adenylate kinase fluorescent detection using Protein G Sepharose beads.

Non-labelled α-AK	10 µg/mL
BSA	1% ($^{m}/_{m}$) in PBS
α-AK-430	100 µg/mL

For the beginning of the assay, an air gap is created in the tube and the metallic adaptor is inserted in the outlet of the microchannel. From this moment until the end of the experiment, the metallic adaptor remains connected to the outlet hole of the microfluidic channel. In this experiment, the syringe pump function "Withdraw" is used in all steps, thus, the only material that keeps being changed is the tip inserted in the inlet hole, which is quickly changed by another filled with another solution.

A micropipette tip is filled with 20 µL of microbeads solution, which was diluted in a ratio of 1:10 in PEG and inserted in the inlet. The flow rate is set to 7 µL/min and the pump is turned on. Using tweezers, soft movements underneath the microfluidic channels are made to ensure the beads are flowing out from the tip and being packed in the column. When the column is half-filled with beads, the syringe is turned off. Another tip is filled with 40 µL of PBS and inserted in the microfluidic device. For this step, the level of the liquid in the tip is observed and the washing step is carried out at 7 µL/min until the liquid reaches a certain level. Afterwards, another tip is filled with 7 µL of the non-labelled α-AK solution, inserted in the inlet and is pulled through the microchannel at 1 µL/min for 5 minutes. Then, a tip is filled with 15 µL of BSA 1% ($^m/_m$) in PBS, the blocking agent for the blocking of non-specific binding regions, inserted in the chip inlet and flowed in the column at 1 µL/min for 10 minutes. Afterwards, another tip is filled with the 7 µL of the desired AK dilution, inserted in the inlet hole of the microfluidic device and flowed through the microfluidic channel for 5 min at 1 µL/min. Then, a tip is filled with 7 µL of α-AK-430, inserted in the device and flowed at 1 µL/min for 5 minutes (**Fig. 2.10**). After the last step, a microchannel micrograph is taken using the a Digital Color Camera DFC300FX coupled to a Leica microscope. Finally, a last tip is filled with 10 µL of PBS and a washing step at 5 µL/min for 1 minute is carried out and a final micrograph of the same region of the microfluidic channel is taken. A total magnification of 100x is used to acquire the micrographs.

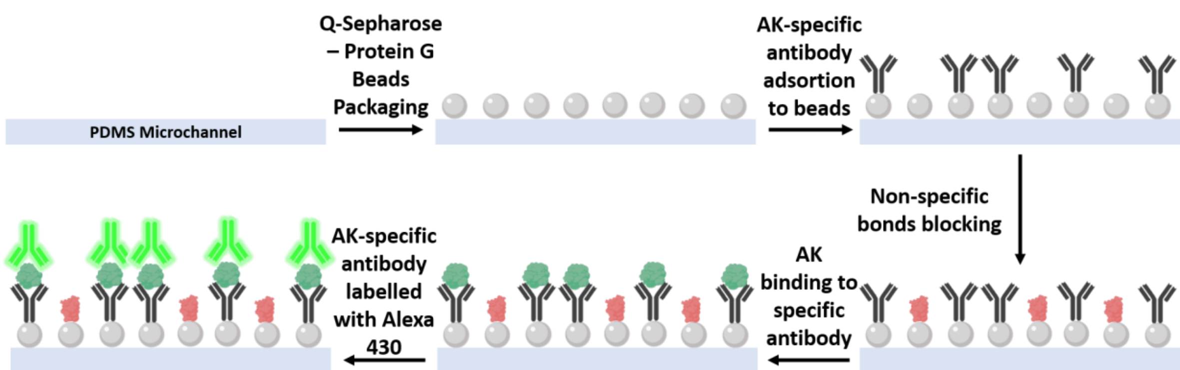

Figure 2.9 – Step-by-step schematic representation of the fluorescent detection of adenylate kinase using Protein G Sepharose beads packed inside a microfluidic channel.

Immunoassay using Agarose Beads functionalized with Capto-MMC groups

This assay is based on the standard macroscale ELISA carried out inside on a well plate. As well as in the previous section, this assay is carried out inside a microfluidic device, using agarose beads to adsorb AK. The table (**Table 2.11**) below shows the material, equipment and reagents required for the fluorescent detection of AK when it is adsorbed to packed beads inside a microfluidic channel.

Table 2.10 – Summary of the required materials, equipment and reagents for the fluorescent detection of adenylate kinase (AK) inside a microfluidic channel using agarose beads functionalized with Capto-MMC groups as adsorption matrix for AK.

Materials	• 1 mL Single-use Syringe, CODAN PORTUGAL Instrumentos Médicos (Odivelas, PT) • PE-90 Tubing (0.034 x 0.050 in), Instech Laboratories (Plymouth Meeting, PA/USA) • Rounded Syringe Luer Stub (20 Gauge), Instech Laboratories (Plymouth Meeting, PA/USA) • Stainless Steel Catheter Coupler (20 Gauge x 15 mm), Instech Laboratories (Plymouth Meeting, PA/USA) • AK Detection Microfluidic Device sealed against a thin PDMS membrane
Equipment	• NE-4000 Programmable 2 Channel Syringe Pump, New Era Pump Systems, Inc. (Farmingdale, NY/USA) • Leica DMLM Microscope, Leica Microsystems (Wetzlar, DE) • Digital Color Camera DFC300FX, Leica Microsystems (Wetzlar, DE)
Reagents	• AK1 Human Recombinant, Sigma-Aldrich (St. Louis, MO/USA) • Invitrogen Adenylate Kinase 1 Monoclonal Antibody (OTI19D1), Thermo Fisher Scientific (Geel, BE) • Gibco™ PBS (Phosphate Buffer Saline) 10x pH7.4, Thermo Fisher Scientific (Geel, BE) • Capto-MMC Multimodal Cation Exchanger Microbeads, GE Healthcare Bio-Sciences (Pittsburgh, PA/USA)

- Anti-Mouse IgG (whole molecule)-FITC antibody produced in goat, Sigma-Aldrich (St. Louis, MO/USA)
- Human normal immunoglobulin Gammanorm®, Octapharma AG (Lachen, CH)
- DI water

Several solutions of AK-specific antibody, Gammanorm® (γ-norm) and anti-mouse anti-IgG labelled with FITC (α-IgG-FITC), with maximum excitation/emission wavelengths of 490/525, are prepared in PBS with the desired concentrations (**Table 2.12**).

Table 2.11 – Work concentrations of the AK-specific antibody, γ-norm and the α-IgG-FITC for the adenylate kinase fluorescent detection using agarose beads.

α-AK	10 µg/mL
γ-norm	5 µg/mL
Anti-mouse IgG-FITC	10 µg/mL

For the beginning of the assay, the tube is filled with 20 µL of PBS and the metallic adaptor is inserted in the outlet of the microchannel. The flow rate is set to 10 µL/min and the pump is turned on in the "Pumping" function until PBS flows out through the inlet hole. Before taking off the metallic adaptor from the outlet, PBS is poured in the region around the adaptor to ensure that no air enters in the microchannel (this step is made right after each solution flows through the microchannel and right before taking off the metallic adaptor from the chip). Afterwards, an air gap is created on the tip of the tube and inserted again in the outlet hole. A micropipette tip is filled with 5 µL of microbeads solution (used as it comes from its fabricant) and inserted in the inlet. The flow rate is set to 15 µL/min and the pump is turned on in the "Withdraw" function. Using a tweezers, soft movements underneath the microfluidic channels are made to ensure the beads are flowing out from the tip and being packed in the column. When the column is half-filled with beads, the syringe is turned off. A washing step is carried out with PBS at 5 µL/min for 1 minute. Afterwards, the AK solution with the desired concentration is flowed inside the microchannel for 5min at 1 µL/min. Then, γ-norm, the blocking agent for the blocking of non-specific binding regions, is flowed in the column at 1 µL/min for 10 minutes. Afterwards, the α-AK is flowed at 1 µL/min for 5 minutes. Then, the solution of α-IgG-FITC is flowed at 1 µL/min for 5 minutes (**Fig. 2.9**). After the last step, a microchannel micrograph is taken using the a Digital Color Camera DFC300FX coupled to a Leica microscope. Finally, a washing step with PBS at 5 µL/min for 2 minutes is carried out and a final micrograph of the same region of the microfluidic channel is taken. A total magnification of 100x is used to acquire the micrographs.

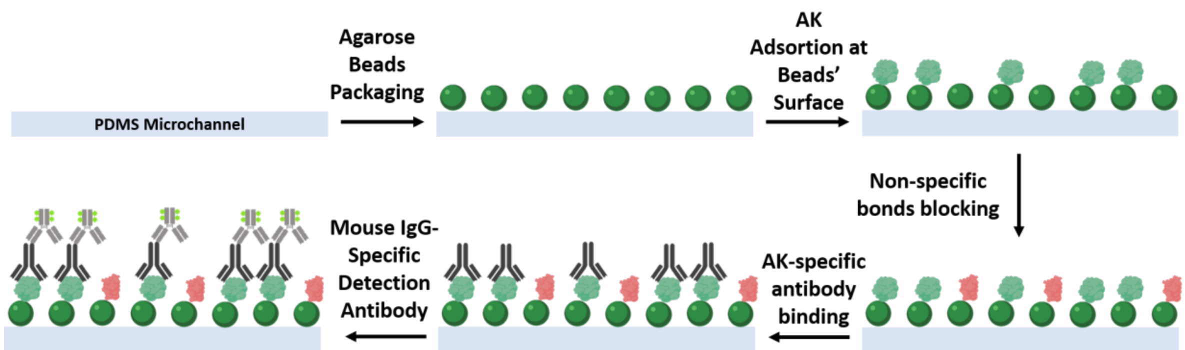

Figure 2.10 – Step-by-step schematic representation of the fluorescent detection of adenylate kinase using agarose beads packed inside a microfluidic channel.

3. Results and Discussion

3.1 Optimization of cell culture conditions[1]

In this section, the optimization of the parameters of the microfluidic cell culture is addressed. It will be focused the optimization of the collagen concentration, the cell concentration perfused inside the microfluidic device, the incubation time after cell perfusion, the method of collagen adsorption to the microfluidic inner walls and the flow rate for the proliferation step.

3.1.1 Collagen Concentration

Whether if an adherent cell culture grows in a Petri dish or inside a microfluidic device, it needs a physical matrix in which it can create a support to proliferate. The extracellular matrix (ECM) is the microenvironment of most cells in living tissues, thus a need to mimic and control the in vivo conditions inside a microfluidic device is crucial.[56] In various cell types, collagen promotes the adhesion to a substrate as well as the survival and proliferation.[87] To test the importance of collagen on cell cultures' viability (**Fig. 3.1**), microfluidic devices were perfused with HCT-116 cells with different concentrations of collagen.

Collagen concentrations of 0, 0.01, 0.1 and 0.3 mg/mL (**Fig. 3.1 A**, **B**, **C** and **D**, respectively) were tested. Amongst all the concentrations used for this set of experiments, the condition with collagen concentration of 0.3 mg/mL showed a higher rate of cell adhesion after 4 hours of incubation at 37°C, as it can be observed by cells' stretched phenotype, its adhered phenotype, in conformation with photomicrographs of this type of cells in plaque.[88]

[1] The author of this project was involved in the design of the experimental work, the development of the experimental work and in the analysis of the results regarding the experiments described in this section and his contributions are included in the accepted µTAS Conference Abstract and Extended Abstract presented in **Appendix B**

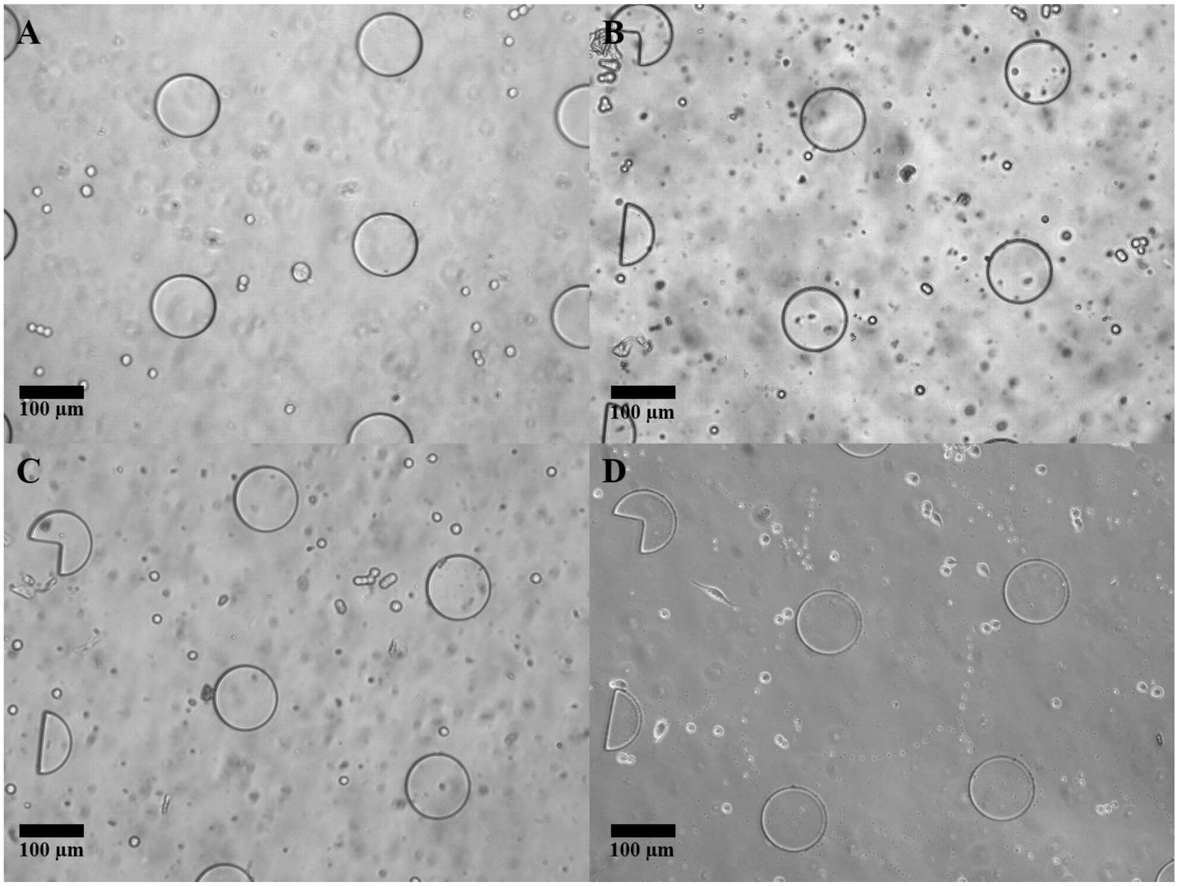

Figure 3.1 – Micrographs taken right after the incubation time of 4 hours focusing collagen concentration conditions. Collagen concentrations of (**A**) 0, (**B**) 0.01, (**C**) 0.1 and (**D**) 0.3 mg/mL were tested. The condition with 0.3 mg/mL of collagen showed a better effect on cells, as some are already in their stretched phenotype, being adhered to the microstructure.

After cell culture proliferation during 48h at 37°C, micrographs were taken (**Fig. 3.2**), and the previous observations are corroborated.

After 48 hours of medium flowing through the microchannel, the condition with a collagen concentration of 0.3 mg/mL (**Fig. 3.2 D**) presents a higher number of adhered cells, as well as a higher number of cells that have already divided or are in the cell division process.

The fact that the collagen concentration influences the adhesion and cell proliferation inside a microfluidic device is confirmed through the observation of the figures above. For concentrations below 0.1 mg/mL (**Fig. 3.2 C**), there is a little number of cells observed in the observerd region of the microchamber after the 48h cell proliferation step. This is due to the lack of physical support for the cells to bind and when the medium flow arrives, cells are detached from the substrate. As collagen is one of the major constituents of the ECM, a matrix that provides physical scaffolding to cells,[89] a higher concentration of collagen provides the cells a more efficient scaffold matrix to handle the medium flow, being the collagen concentration of 0.3 mg/mL the optimal concentration.

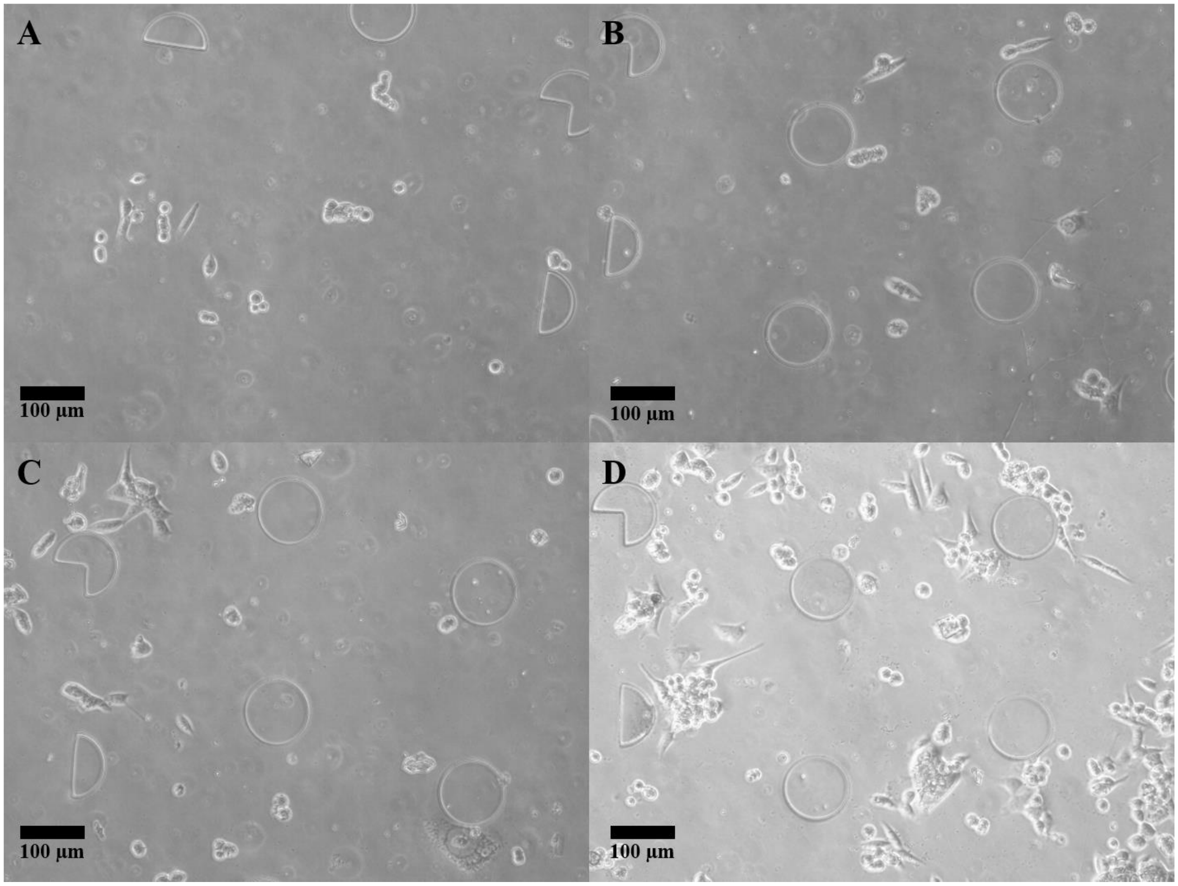

Figure 3.2 – Micrographs taken at t = 48 h, focusing collagen concentration conditions. Collagen concentrations of (**A**) 0, (**B**) 0.01, (**C**) 0.1 and (**D**) 0.3 mg/mL mg/mL were tested. The condition with 0.3 mg/mL of collagen presents a better support scaffold to cells, as they managed to divide and proliferate with the culture medium flow for 48 hours.

In summary, with these collagen concentration experiments and comparing both **Figs. 3.1** and **3.2**, using the concentration of collagen of 0.3 mg/mL not only increases cell adhesion during the time of incubation but also enables cells to handle the medium flow for 48 hours due to a more efficient cell adhesion to the support scaffold. However, a optimized collagen concentration by its own doesn't assure the amount of cells required after the time of proliferation for the desired applications. Cell concentration was then optimized.

3.1.2 Cell Concentration

Inside a bioreactor, cell concentration is also a crucial a parameter that needs to be monitored and optimized, in order to fulfil the requirement of the culture medium containing the nutrients to keep a viable cell culture.[90] There are several applications such as imaging and the determination of cell viability that are affected by the cell concentration inside a microfluidic device.[91] After the proliferation step, cell viability is measured through fluorescent imaging and several cell concentrations perfused into the microfluidic device are tested (**Fig. 3.3**).

Cell concentrations of 1×10^6, 2×10^6 and 4×10^6 cells/mL (**Fig. 3.3 A**, **B** and **C**, respectively) were perfused into the microfluidic chamber. After 4 hours of incubation right after cell insertion and the 48 hours of medium flowing through the microchannel, the condition with a cell concentration of 4×10^6 cells/mL shows a higher cell confluence and disposition throughout the chip.

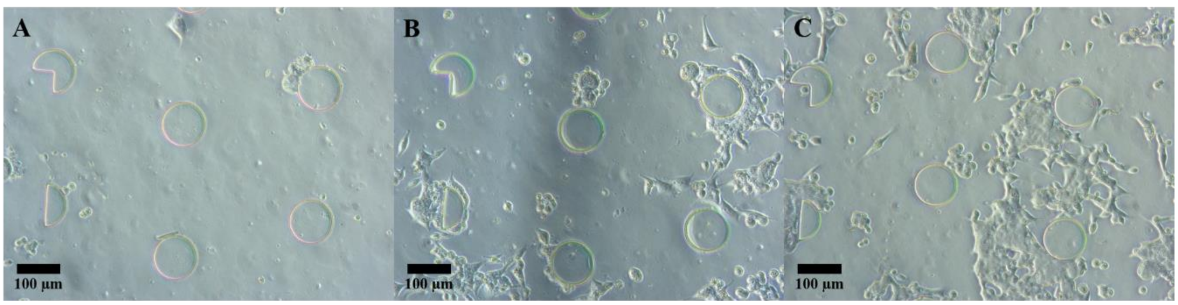

Figure 3.3 – Micrograph taken at t = 48 h regarding cell concentrations optimization experiments. Cell concentrations of (**A**) 1×10^6, (**B**) 2×10^6 and (**C**) 4×10^6 cells/mL were used. The cell concentration of 4×10^6 cells/mL resulted in an increased cell confluence, as observed in the right side of the micrograph and was chosen as the optimal cell concentration to be perfused inside a microfluidic device for imaging and cell viability assays applications.

For different cell lines, there are different cell confluence percentages that are appropriate.[92] To measure cell viability with DNA-specific fluorescent dyes and for possible experiments regarding the capture of drugs, an appropriate cell concentration must be used.[93] In these experiments, the cell concentration of 1×10^6 cells/mL showed almost no cells inside the microfluidic device. Between the conditions of 2×10^6 and 4×10^6 cells/mL, the latter showed a higher cell confluence, as it is observed in the right side of the micrograph, that was found suitable for the following imaging and cell viability applications.

In summary, after cell concentration optimization, the cell concentration of 4×10^6 cells/mL was found to be the most appropriate for the cell viability assays, as it is necessary a big enough number of cells inside a microfluidic device for such type of assays. Although, time of incubation also plays an important role in the cell adhesion to the support scaffold to ensure stable cell-substrate bonds and was then optimized.

3.1.3 Incubation time

Not only the collagen concentration and the cell concentration contribute for the cell proliferation after cell perfusion inside the microfluidic device. The time of incubation at 37°C is also a crucial parameter to be optimized in order to increase the cell attachment to the microfluidic chamber, in order to handle the fluid flow with culture medium.[57] For the optimization of the period of incubation, different microfluidic devices were perfused with the same optimized concentrations of cells and collagen, and incubated for different periods of time, at 37°C. **Fig. 3.4** shows the aspect of cells perfused inside the microfluidic device right after the incubation times of 4, 6 and 8 hours (**Fig. 3.4 A, B and C, respectively**).

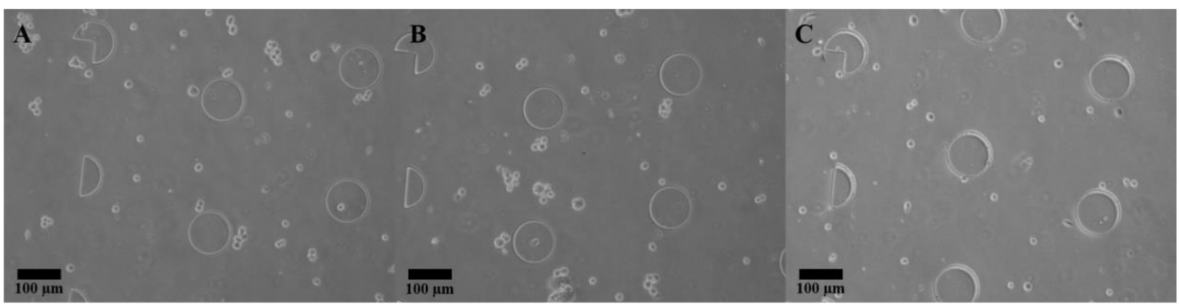

Figure 3.4 – Micrographs taken after (**A**) 4, (**B**) 6 and (**C**) 8 hours in different microfluidic devices. Different incubation times were tested and only in the chip incubated for 8 hours at 37°C cells are observed as having a rounded phenotype, that may indicate that 8 hours is excessive for the incubation step.

After perfusion, cells were put at 37°C for incubation for 4, 6 and 8 hours in different microfluidic devices. Through the observation of the micrographs shown in Fig. 3.4, there are no big differences between the 4 and 6 hours of incubation conditions. However, the 8 hours incubation time condition shows almost all cells with a perfectly rounded phenotype, indicating that 8 hours might be too long for incubation, as cells can’t handle that much time without fresh culture medium being perfused into the microfluidic device.

Fig. 3.5 shows the micrographs taken of the same structures in same regions, after 48 hours of medium flowing for each incubation time tested, Δt = 4, 6 and 8 hours (**Fig. 3.5 A, B and C**, respectively).

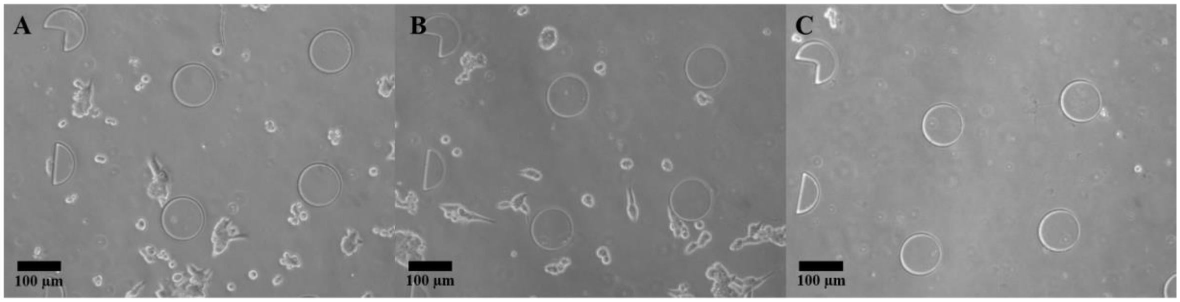

Figure 3.5 – Micrographs taken after 48 hours in different microfluidic devices incubated for (**A**) 4, (**B**) 6 and (**C**) 8 hours right after cell insertion. In the chip incubated for 8 hours at 37°C cells are observed as having a rounded phenotype, that may indicate that 8 hours is excessive for the incubation step. Regarding the conditions of 4 and 6 hours of incubation, cells' phenotype observed is very similar, indicating that the seeding between 4 and 6 hours of incubation.

Cell seeding is a critical step in a microfluidic cell culture. It is important to guarantee a good cell attachment to the scaffolding surface to ensure they are not washed away when culture medium is perfused. As shown in the literature, different cell lines have their own optimal cell seeding time that also depend on the cell concentration perfused, as well as the scaffolding substrate properties and the composition of the culture medium used.[94]

After 48 hours of proliferation, cells that were incubated for 4 and 6 hours showed a stretched phenotype, indicating that they managed to adhere to the microfluidic inner surface and handled well the culture medium flow rate. On the opposite, the microchip containing cells that was incubated for 8 hours shows almost no cells in the same region after 48 hours of media being perfused inside the microchamber. In the case of the cell culture incubated for 8 hours, cells attached to the surface but after 6 hours of incubation, if cells aren't fed with culture medium, they start to disattach and when medium flow starts, cells are washed away.

Cell cultures incubated for 4 and 6 hours were not washed away during media perfusion, indicating a good cell attachment thanks to adequate incubation times. As results regarding these two incubation times are so similar, the time chosen was 4 hours for time saving reasons.

With the incubation time experiments, cell adhesion during the incubation step was optimized and the period selected as the optimized one (Δt = 4 h) revealed to have a more efficient cell adhesion/time ratio. To finish the optimizations regarding the incubation step before medium flow through the chip, the type of collagen coating to the chip was tested.

3.1.4 Microfluidic Collagen-Coating

After establishing collagen and cell concentrations and the incubation time, it was questioned if the collagen should be inserted at the same time of the cells or before cells' insertion in order to coat the microfluidic chamber surface. In order to cells attach to substrate materials, adhesive proteins or peptides existent in the culture medium or pre-immobilized cell-attachment proteins must adsorb at the substrate's surface.[94] Some microfluidic cell cultures are developed with a previously collagen-coated chamber and higher proliferation rates are verified.[95]

Fig. 3.6 shows the difference in cells' phenotype after 4 hours of incubation at 37°C resulting from different collagen insertion inside the device.

In **Fig.3.6 A**, collagen was inserted into the chip before cells' perfusion, while in **Fig. 3.6 B**, collagen was diluted in the same suspension as cells and perfused at the same time as cells were. In the first, almost all cells observed show a stretched phenotype, indicating a good attachment to the microfluidic structure, while in the latter, besides cells didn't show a complete rounded phenotype, are not as attached as in the previous one.

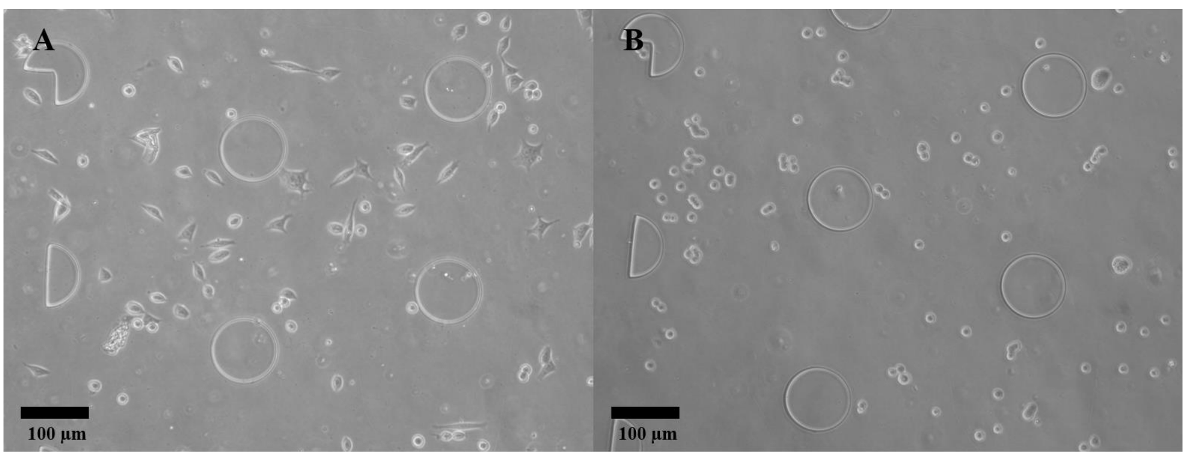

Figure 3.6 – Phenotype comparison between cell cultures incubated in different microfluidic devices with different methods of collagen perfusion. Cells showed a stretched phenotype when incubated for 4 hours inside a device pre-coated with collagen (**A**) and show a rounded phenotype when incubated in the same conditions inside a microchamber in which collagen was perfused at the same time as cells (**B**), showing a better cell seeding in the pre-coated device.

Fig. 3.7 shows the difference in cells' phenotype after 48 hours of proliferation at 37°C resulting from different collagen insertion inside the device.

In **Fig. 3.7 A**, collagen was inserted into the chip before cells' perfusion, while in **Fig. 3.7 B**, collagen was diluted in the same suspension as cells and perfused at the same time as cells were. Cells phenotypes after 48 hours of medium flowing through the chip corroborate the observations made in **Fig. 3.6** after incubation.

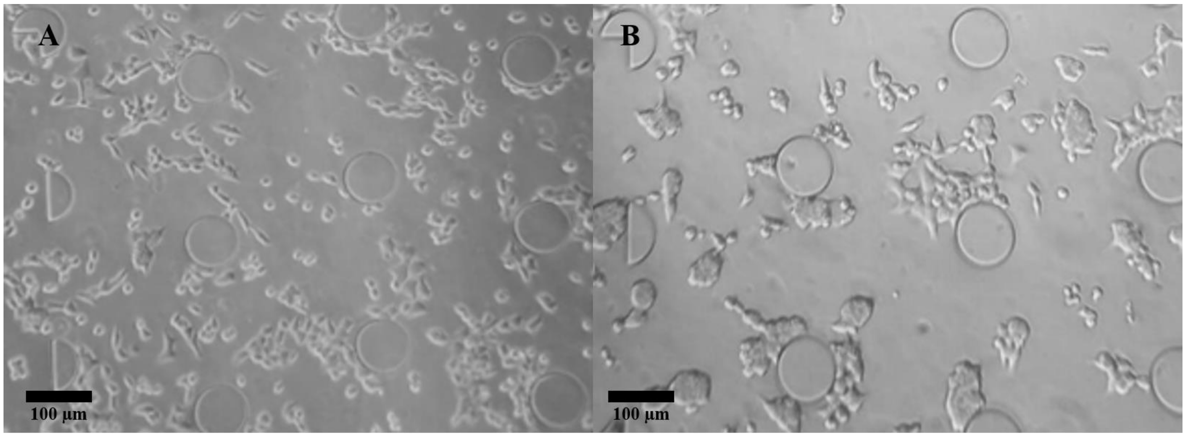

Figure 3.7 – Phenotype comparison between cell cultures incubated and grown in different microfluidic devices with different methods of collagen perfusion. Almost all cells showed a stretched phenotype as well as a cell number increase when grown for 48 hours inside a device pre-coated with collagen (**A**) and show a rounded phenotype, with a cell number increase also, when grown in the same conditions inside a microchamber in which collagen was perfused at the same time as cells (**B**), showing a better cell seeding in the pre-coated device.

In **Fig. 3.7 A**, almost all cells show a stretched phenotype, as well as the number of cells had increased, indicating a good seeding step due to the fact the collagen was inserted before the cells to coat the substrate of the microfluidic chamber, creating an effective supporting scaffold for cells to adhere and to proliferate. In **Fig. 3.7 B**, cell number also increased, however only a few shows a stretched phenotype, indicating that the seeding step is less efficient when the collagen is perfused in the same suspension as the cells.

After the microfluidic collagen-coating experiments, is was verified that if the collagen is flowed before the cells into the chip, cells tend to attach easier to an already stable supporting scaffold than to a matrix flowed at the same time as them. After optimizing the cell adhesion during the incubation time, the proliferation step must be optimized in order to obtain a viable cell culture after the proliferation step of 48 hours.

3.1.5 Flow Rate for the Proliferation step

After the incubation step, the cells inside the microchamber need to receive a media flow to be kept viable and to proliferate. Controlling the perturbations of the cell environment for the cells used in this work can be achieved by controlling the flow rate through the microchannel. Additionally, not only the culture medium flow transport nutrients but also exerts mechanical and physical stimulus over the adhered cells. The flow rate with that the culture medium is perfused into the biochip have two important roles: (i) to transport essential soluble factors to ensure the viability of the cell culture and (ii) to create concentration gradients that mimic *in vivo* conditions, preserving the adhered state of the cells.[44] An optimal flow is defined through testing several flow (Q) conditions (**Fig. 3.8**) after 4 hours of incubation.

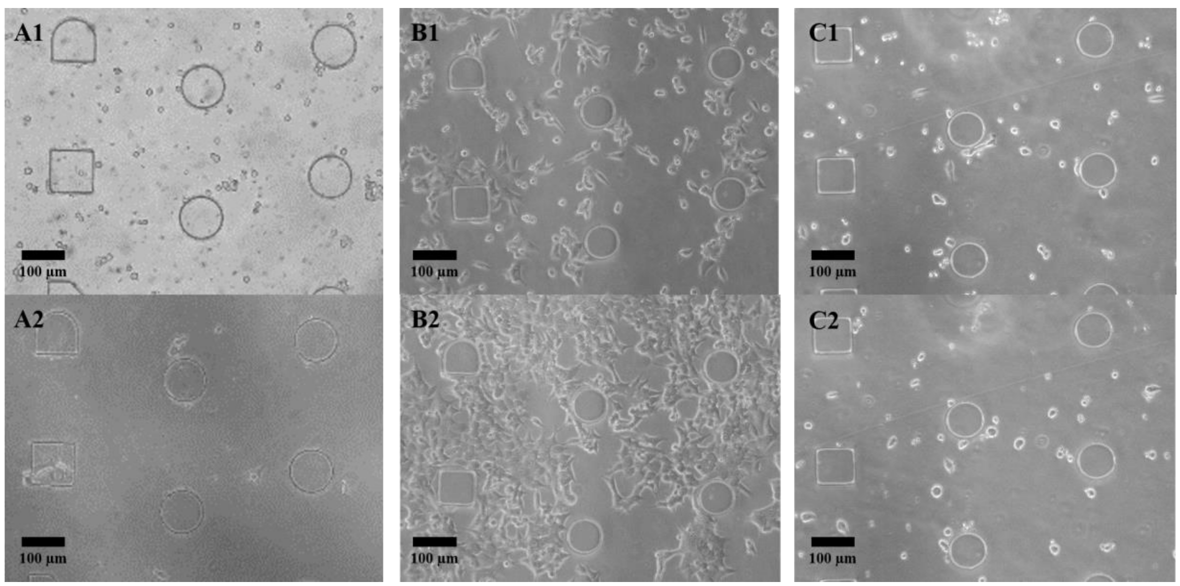

Figure 3.8 – Micrographs taken at two different time points, t = 24 (**Fig. 3.8 A1**, **B1** and **C1**) and 48 h (**Fig. 3.8 A2**, **B2** and **C2**), in the same region of the chip in different microfluidic devices with different flow rates tested, Q = 0 (**Fig. 3.8 C1** and **C2**), 0.1 (**Fig. 3.8 B1** and **B2**) and 0.5 (**Fig. 3.8 A1** and **A2**) µL/min in the proliferation step. The optimal flow rate is Q = 0.1 µL/min as the respective microfluidic device shows an evident proliferation between the two time points as well as the stretched phenotype.

Fig. 3.8 shows the micrographs taken at two different time points, t = 24 (**Fig. 3.8 A1**, **B1** and **C1**) and 48 h (**Fig. 3.8 A2**, **B2** and **C2**), for three different flow rates tested, 0 (**Fig. 3.8 C1** and **C2**), 0.1 (**Fig. 3.8 B1** and **B2**) and 0.5 (**Fig. 3.8 A1** and **A2**) µL/min, during the proliferation step.

In the micrographs regarding to the flow rate Q = 0 µL/min, almost all cells maintained their position between t = 24 h and t = 48 h, as well as the rounded phenotype, indicating that cells aren't adhered to the substrate and are dead due to not receiving culture medium stimulus.

In the micrographs regarding to the flow rate Q = 0.5 μL/min, all cells changed their position between t = 24 h and t = 48 h. At t = 24 h cells showed a rounded shape, indicating that they were under stress due to the excessive flow rate that they were being subject. At t = 48 h cells ended up being washed way due to the continuous and excessive mechanical stress imposed to them.

In the micrographs regarding to the flow rate Q = 0.1 μL/min, all cells remained on their position between t = 24 h and t = 48 h, as well as the stretched shape, indicating an optimal flow rate for the cell culture proliferation. In this condition, between t = 24 h and t = 48 h cells not only kept their adhered phenotype but also increased in number, denoting that Q = 0.1 μL/min is the optimal flow rate for the cell proliferation step.

In summary, after the flow rate optimization for the proliferation step, in which a Q = 0.1 μL/min, condition was verified to be the most appropriate, cell culture state must be verified in order to corroborate that the most part of the cells cultured inside the microfluidic device are viable alive. For this reason, DNA fluorescent dyes are used to determine the cell viability after the cell culturing process inside a biochip.

3.2 Cell Viability Determination using DNA Fluorescent Dyes

After completing the cell culturing of HCT-116 inside a microfluidic device, besides observing the aspect of the cell, cell viability assays were carried out to ensure that the optimized parameters used are trustful.

In this work, two different cell DNA stains were used: Hoechst 33342 (HO342) and 7-Aminoactinomycin D (7-AAD). The first mentioned stains the DNA of both live and dead cells[62] while the latter only intercalates the DNA of apoptotic or necrotic cells, being able to enter to their cytoplasm, while it is excluded by live cells with an intact cell membrane.[65] Despite the bigger use in flow cytometry assays, in this work, fluorescence imaging were used and the observation of cell death suits for an important end-point assay.[64]

Fig. 3.9 shows two similar cell viability assays carried out using a fluorescence microscope, in two different cell chips (**Chip A** and **Chip B**) with a viable cell culture grown with the previously optimized parameters.

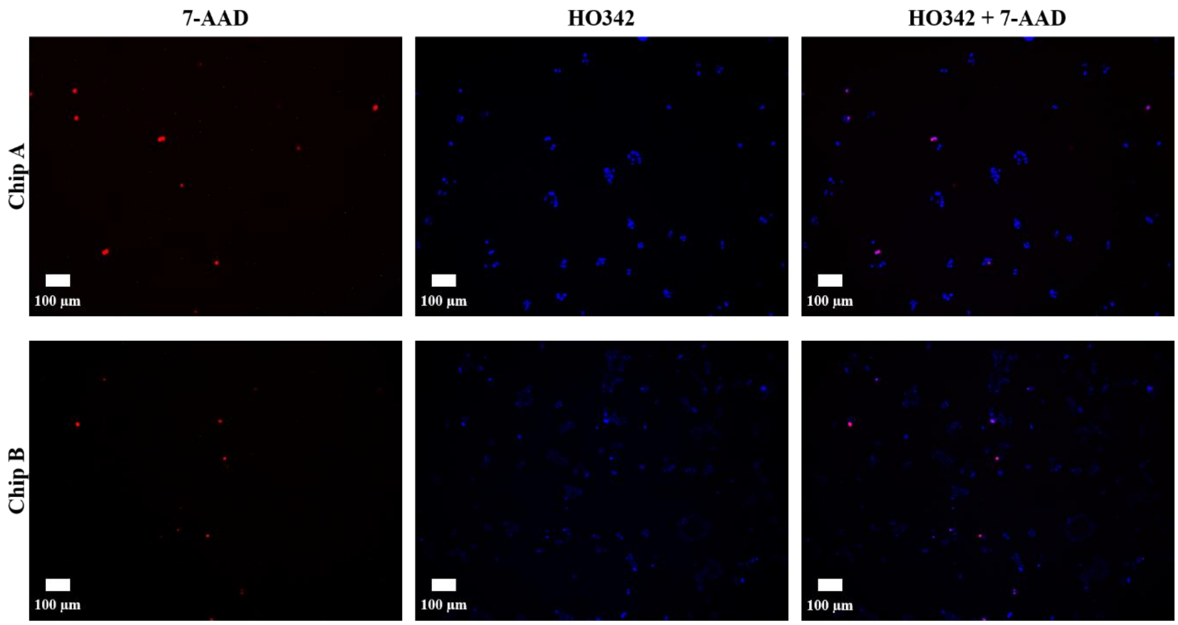

Figure 3.9 – Cell viability assays carried out in two independent chips containing a viable cell culture grown with the optimized parameters. Left images (**7-AAD**) show the micrographs taken using the red filter, middle images (**HO342**) show the micrographs taken using the blue filter and right images (**HO342 + 7-AAD**) show the micrographs taken using both red and blue filters merged. The red dots indicate the presence of dead cells, while the blue dots show both live and dead cells, as it can internalize both. An average cell viability of 90% was determined.

In **Fig. 3.9** are shown for each chip, three different photos of the exact same region of the chip, **7-AAD** of both **Chip A** and **B** show the photos taken with the Rhodamine filter (excitation BP 546/12 nm and emission BP 575-640 nm), showing a few red dots indicating the presence of dead cells in the marked places, **HO342** of both **Chip A** and **B** show the photos taken with the DAPI filter (excitation G 365 nm and emission BP 445/50 nm), showing a high number of blue dots indicating the presence of live and dead cells in the marked places and **HO342 + 7-AAD** of both **Chip A** and **B** show the photos with both DAPI and Rhodamine filters merged, showing a high number of blue dots with overlap of the red ones in the exact same places of those in the left, allowing the distinction between the live and dead cells.

After counting the blue dots in the middle photos, which give the information of the total number of cells in that region of the chip and counting the red dots in the left micrographs, which give the total number of dead cells in that region of the device, admitting that both the same cell distribution and DNA stain occurs in other part of the device, cell viability was determined following **Equation 2**:

$$Cell\ viability\ (\%) = \frac{\#Total\ blue\ dots - \#Total\ red\ dots}{\#Total\ blue\ dots} \quad (2)$$

After calculating the average of both chips, the cell viability determined is 90%. This result is not much far from other values in the literature: 90 to 93%[96] and 95 to 100%.[97]

The determination of cell viability inside a biochip using DNA fluorescent dyes is an end-point assay, which means that this assay is only carried out after culturing the cells for the 48 hours of proliferation required. In order to determine the cell viability in real time, a different approach must be followed. The real-time detection of a specific cell death biomarker release from dead cells was the next approach.

3.3 Adenylate Kinase Detection

In a drug screening assay using tumour cells, cell death through the exposure to anti-cancer drugs must be monitored in order to check on the anti-carcinogenic efficiency of a certain drug. To miniaturize the drug screening process inside a microfluidic device, a specific cell death biomarker, adenylate kinase (AK) – an enzyme released by dead cells – is detected using both luminescent and fluorescent immunoassays approaches.

3.3.1 Luminescent Detection

3.3.1.1 Macroscale Calibration between Adenylate Kinase Solutions and Cell Supernatants

As AK is a cell death biomarker, there is a need to detect its release from cells for applications such as the drug screening. To make a calibration between the amount of AK released by live and dead cells and known AK concentrations, a macroscale assay using a luminometer was developed. **Fig. 3.10** shows a scatter plot with the relative luminescent signal of AK detection using the ToxiLight™ kit.

Fig. 3.10 shows the correlation between several AK dilutions, the amount of AK released by lysed cells and the amount of AK released from live cells.

Regarding the amount of AK released from live cells (red circles), it was expected to below, since AK aren't release from viable cells in huge concentrations, due to its functional plasma membrane that doesn't let that enzyme pass through. The observation of the scatter plot in **Fig. 3.10** shows a basal AK release from viable cells, that is below the detection limit of the assay.

Regarding the amount of AK released from lysed cells (green triangles), respective luminescence was expected to rise in conformity with the cell concentration increase. Through the observation of **Fig. 3.10**, AK release luminescence signal is higher for increased dead cells' concentrations, due to a higher AK release from plasma membrane-damaged cells.[76]

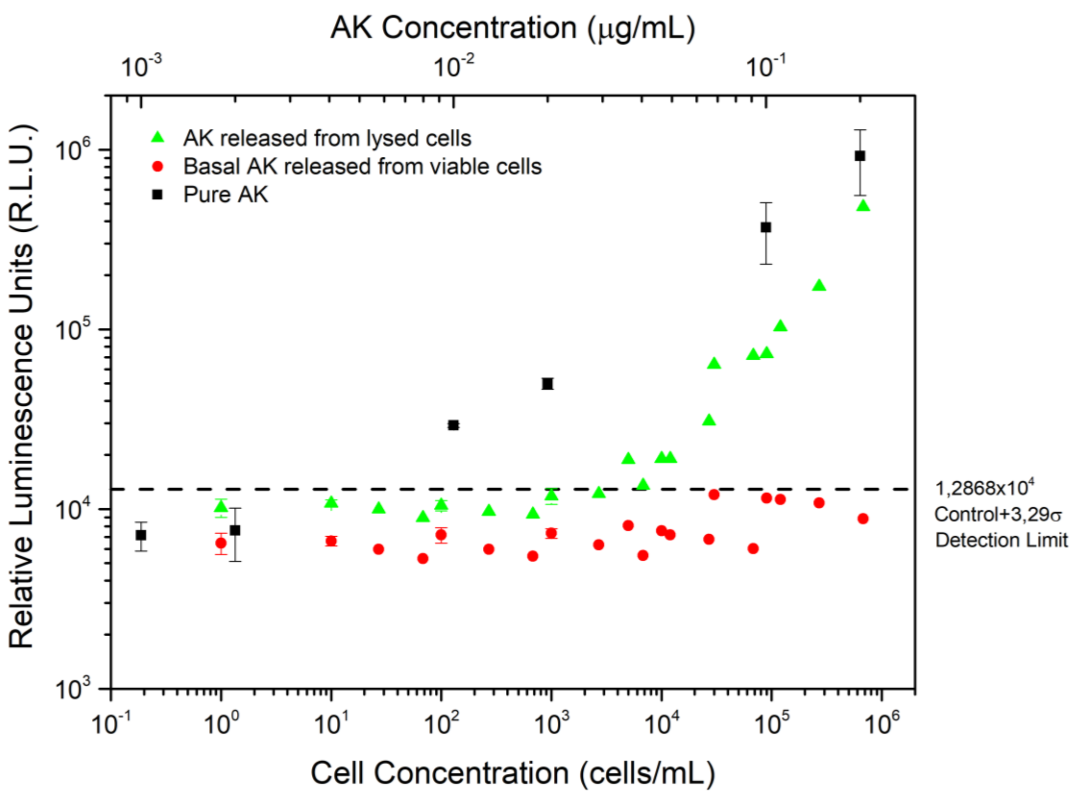

Figure 3.10 – Scatter plot with the relative luminescent signal of AK detection using the ToxiLight™ kit. Live cells (red dots), dead cells (green triangles) and AK dilutions (black squares) were used in various respective concentrations. As expected, the luminescent signal increases for dead cells as cell concentration increases too, due to a higher AK release from the damaged plasma membrane.

These assays can be correlated with the microfluidic cell cultures. As the cell concentration that is perfused inside the microfluidic device is 4×10^6 cells/mL and inside the biochip the volume is approximately 1 μL, only approximately 4000 cells are perfused into the biochip.

Through analysing the scatter plot, a 10x-decrease in the AK concentration approximately corresponds to a 10x-decrease in the luminescence signal, while a 100x-decrease in dead cells' concentration corresponds only to 10x-decrease in the luminescence signal.

Considering that in 4000 cells there are approximately 1000x less AK than in 4×10^6 cells, the luminescence signal is 100x lower. If the concentration of 4×10^6 cells/mL is divided by 1000, a 100x decrease in luminescence signal is verified, and in the cell concentration of 4×10^3 cells/mL the luminescence signal is very close of the detection limit.

These assays were realized using a plate reader in a macroscale dimension. A microscale dimension detection method must be followed due to the use of a microfluidic device for cell culture. After such results, it was assumed that the signal that would be detected at microscale was close to the detection limit of the plate reader. An approach to miniaturize the assay while integrating an optical sensor was then carried out using a PMT for the luminescent detection of AK.

3.3.1.1 Chemiluminescent Detection of Adenylate Kinase using a Photomultiplier

In order to miniaturize the detection of AK, via the integration of a sensor, a photomultiplier (PMT) was used for the detection of adenylate kinase as in another works.[98] In a first instance, an oscilloscope was used for acquiring the output data. To test the sensitivity of the PMT used, the assay was carried out on top of a coverslip and the higher concentration of AK (used for the macroscale assay) was used (**Fig. 3.11**).

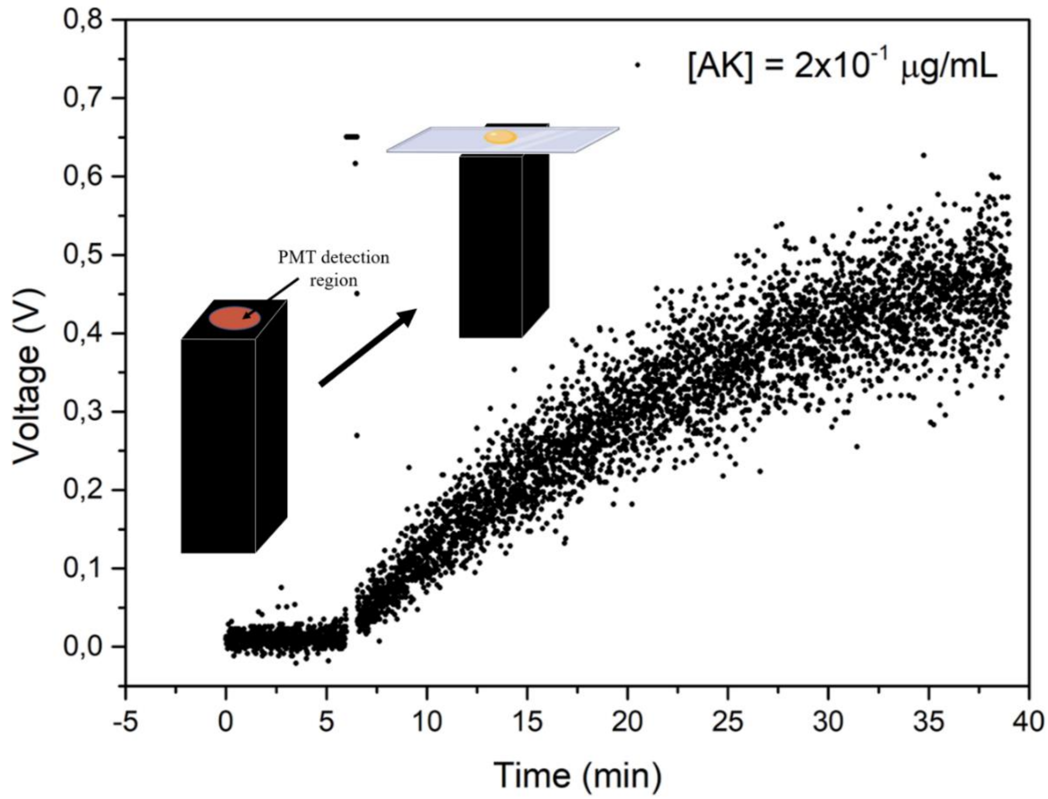

Figure 3.11 – Output voltage increase of a reaction mix on top of a coverslip using an oscilloscope. After positioning the coverslip with a droplet containing the reaction mix, at the AK concentration of 2×10^{-1} µg/mL, the voltage increased approximately 0.5 V.

Using the ToxiLight™™ fabricant specifications, a few microliters droplets containing the reaction mix was poured on top of a coverslip. After putting the coverslip on top of the PMT with the droplet aligned with the light detection region, as observed in **Fig. 3.11**, the signal increase was acquired.

From t = 0 min to t = 6 min, the PMT was acquiring the basal line, without the coverslip on the detection zone. At t = 6 min, a momentaneous increase is verified in moment that the black box is opened for positioning the coverslip on top of the PMT. From t = 6 min until the end of the assay, the voltage increased approximately 0.5 V, stabilising due to reagents run out after approximately 40 minutes.

In order to compare the output voltage of several AK concentrations, an assay comprehending all six different AK concentrations was carried out (**Fig 3.12**).

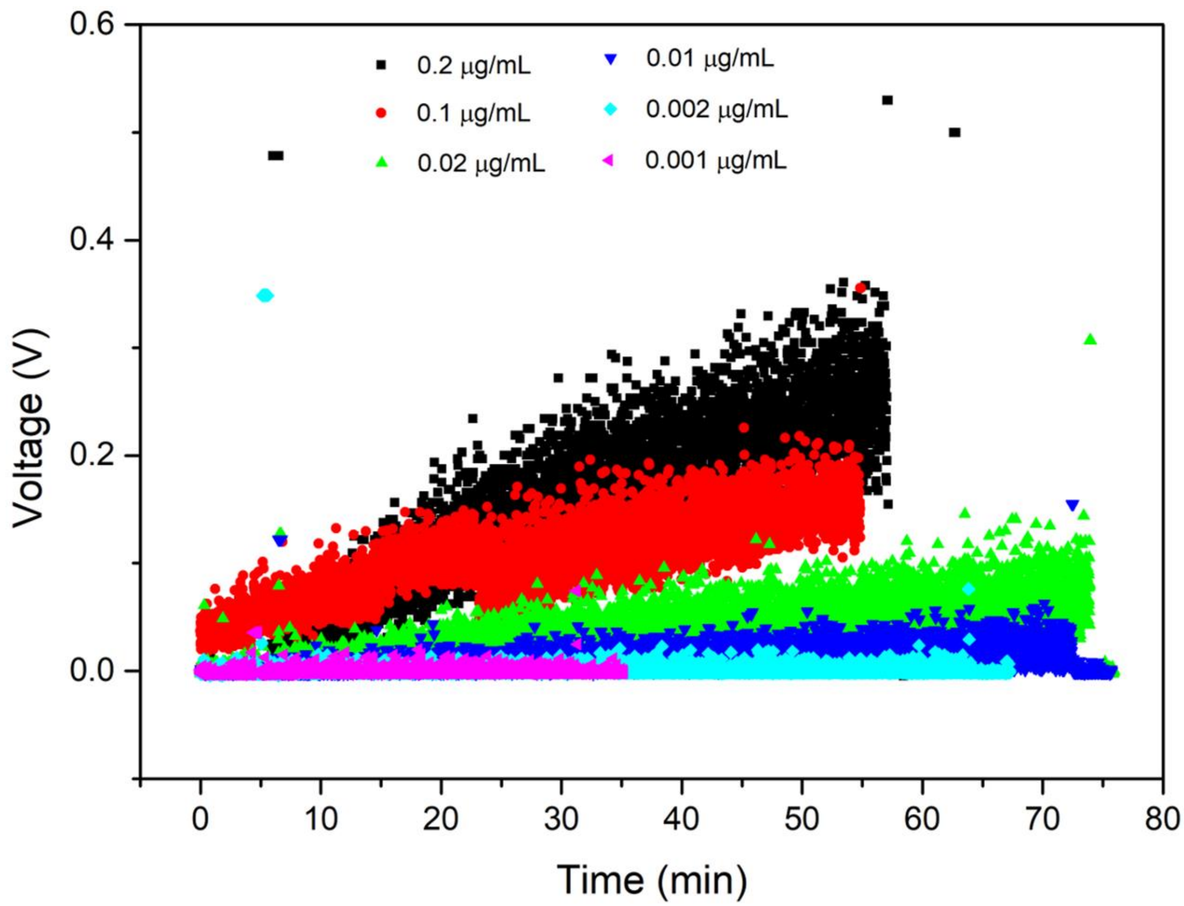

Figure 3.12 – Scatter plot of six different AK concentrations detection on top of a coverslip. The highest concentration tested (0.2 µg/mL) showed an increase in the voltage signal of around 0.3 V. Only the two lowest AK concentrations (0.002 and 0.001 µg/mL) barely didn't lift the voltage signal from 0 V.

After analysing the graphic above, as expected, higher AK concentrations have a greater increase in the output voltage. Only the AK concentrations of 0.2, 0.1, 0.02 and 0.01 µg/mL are detectable, while the concentrations of 0.002 and 0.001 µg/mL aren't, as their values maintained near 0 during the entire assay.

A Fourier transform deconstructs a signal time domain in its frequency domain. When the oscilloscope presents the output data, it is presented in the form of discrete values. Thus, instead of a Fourier transform, a discrete Fourier transform (DFT) is implemented. The fast Fourier transform is just an optimized version of the DFT that requires less computation and simply deconstructs the signal.[99] In order to simplify the viewing of the data, a fast Fourier transform filter was applied, decomposing the signal into frequencies and relative amplitudes of their simple component waves.[100]

Fig. 3.13 shows the decomposed signal verified in **Fig. 3.12** due to the application of a fast Fourier transform (FFT) filter.

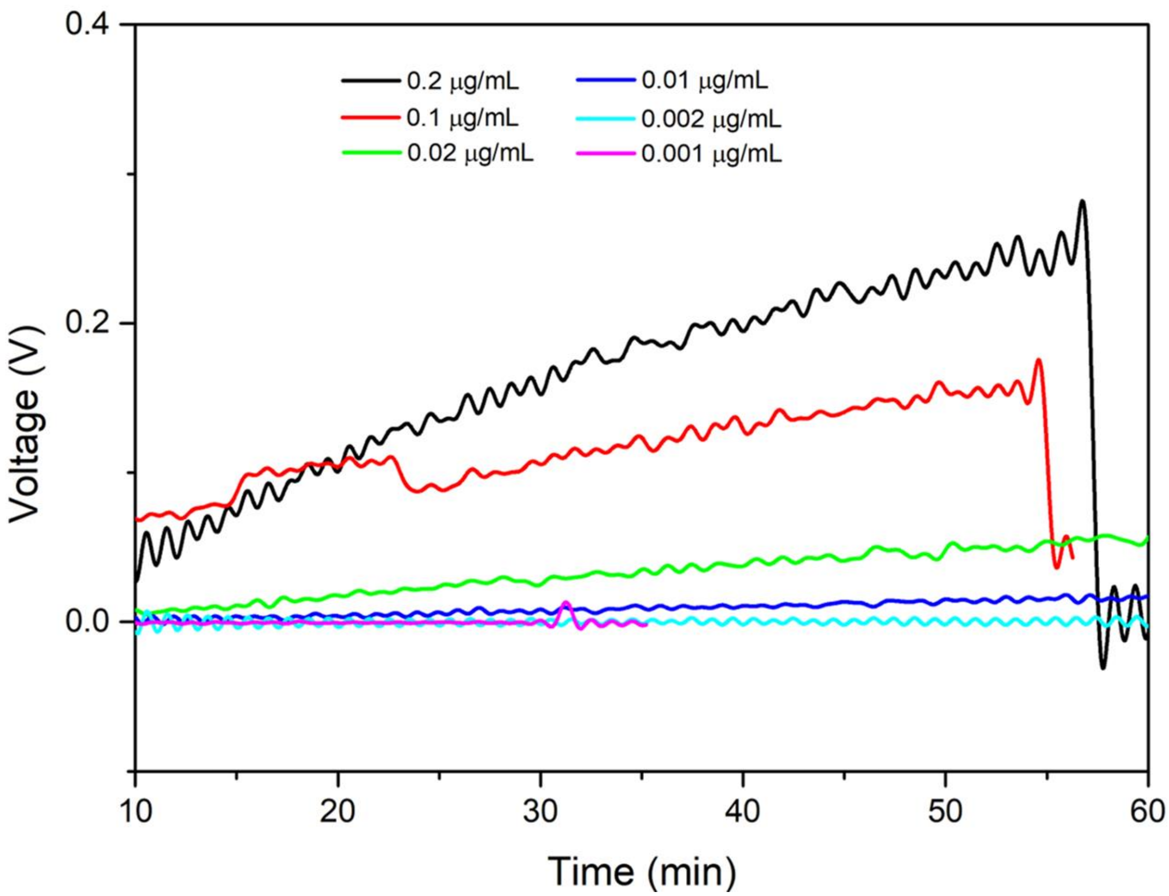

Figure 3.13 – Application of a fast Fourier transform (FFT) filter to the scatter plot of six different AK concentrations detection on top of a coverslip. The cleaned signal corroborated the previous observation that the highest concentration tested (0.2 µg/mL) showed an increase in the voltage signal of around 0.3 V, while the two lowest AK concentrations (0.002 and 0.001 µg/mL) revealed to be undetectable, by showing constant zero voltage values during the assay.

By decomposing the voltage data in their frequencies, a cleaner graphic is obtained. This graphic corroborates the analysis made to the previous one, as the two lowest concentrations are not detectable. The concentration represented by the darker blue line (0.01 µg/mL) seems to have slightly lower values than in the previous graphic, while the three highest AK concentrations maintained the maximum values of voltage verified in **Fig. 3.12**.

As these results revealed promising, an approach using a microfluidic device for AK detection was then carried out.

For the miniaturization of the assay, a microfluidic device was used for the AK detection. **Fig. 3.14** shows the output voltage resulting from the AK luminescent detection inside a microfluidic device, using an AK concentration of 0.2 µg/mL. The microchamber is put on top of the PMT, with the chamber where the reaction mix flows right above the detection region.

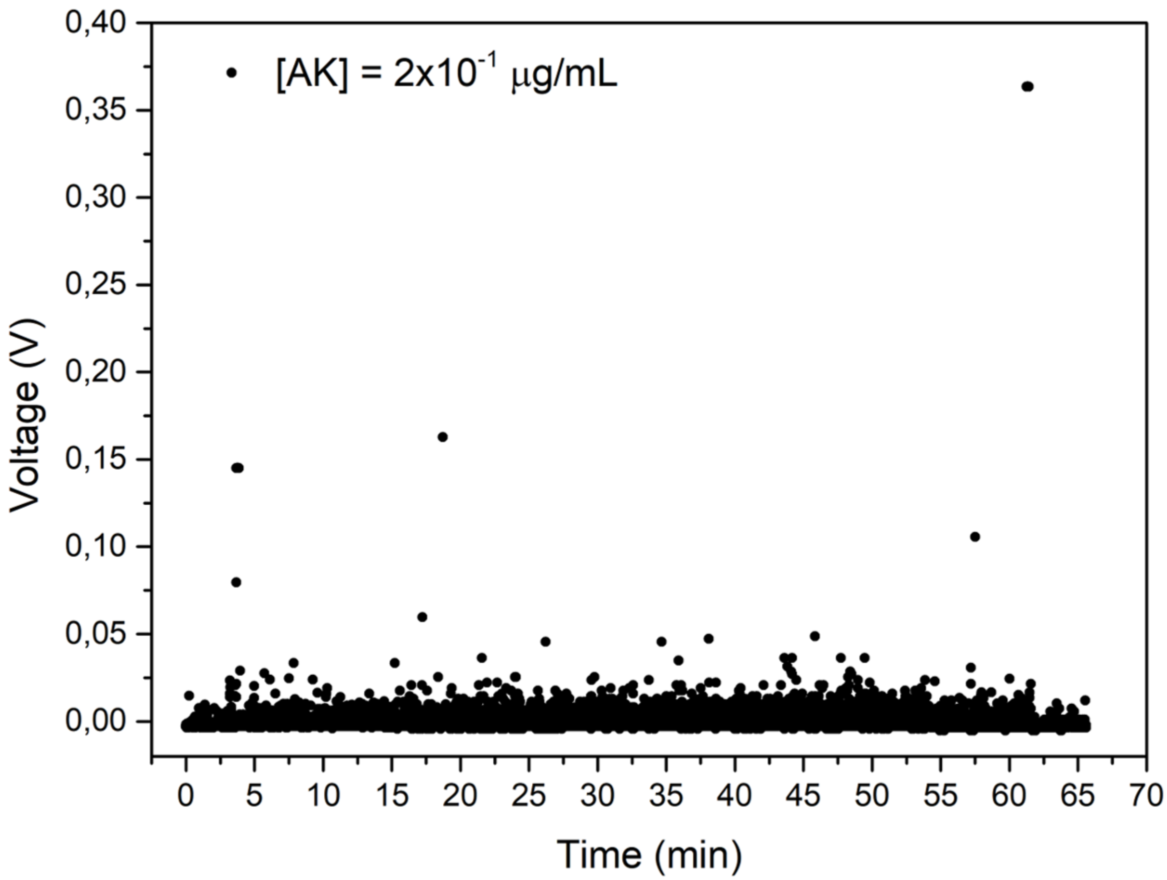

Figure 3.14 – Voltage variation regarding the luminescent detection of AK concentrated to 0.2 µg/mL inside a microfluidic device. Signal increase is very low, reaching approximately 0.025 V. Signal suffers a drop at t = 60 min when the chip is taken off from the top of the PMT.

After analysing the output voltage behaviour during the assay, it is seen that there was almost no increase in signal due to the luminescent activity of ToxiLight™™, only experiencing a little change in the voltage (U = 0.025 V).

The low increase in voltage is observed at t = 60 min. When the black box is opened and the microfluidic device is taken off from the top of the PMT detection region, a small decrease is verified due to the absence of luminescent signal. Although, due to the low uncertainty of the oscilloscope and the low luminescent signal generated in such a small volume, another device, a multimeter, for the acquiring of output voltage was used.

Due to a higher resolution and high-precision checks of voltage, a multimeter imposes several advantages relatively to the oscilloscope, as the latter shows graphically the distortion and noise often present in measured values.

In order to test the multimeter data acquisition capacity, it was measured the voltage increase of the reaction mix on top of a coverslip. **Fig. 3.15** shows the voltage increase regarding the luminescent detection of AK, using a concentration of 0.2 µg/mL with different PMT gain voltage values.

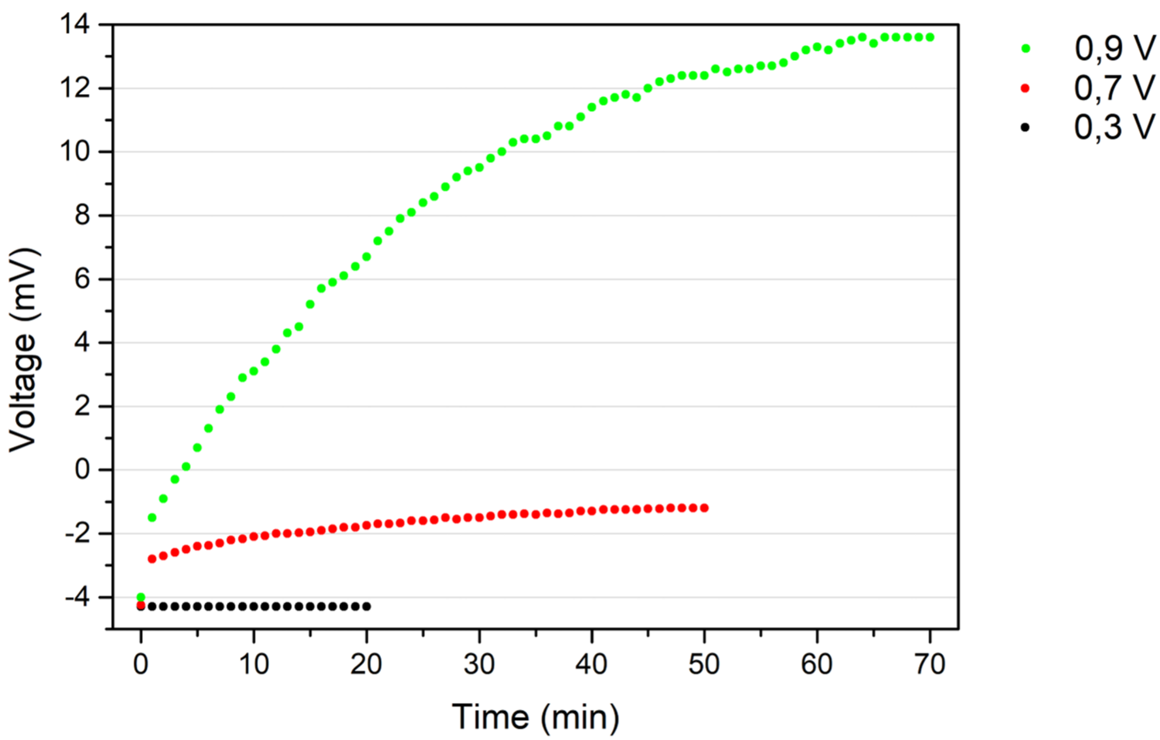

Figure 3.15 – Voltage variation regarding the luminescent detection of AK concentrated to 0.2 µg/mL on top of a coverslip using different voltage gains. For voltage gains of 0.3 and 0.7 V, output voltage suffered small increases, while for the maximum control voltage (U = 0.9 V), the signal suffered an increase of approximately 18 mV.

The gain represents the ability of a circuit to increase the power of a signal from the input (photons in the PMT detection region) to the output (data acquisition). This is made through the connection of a power supply that adds converted energy to the signal.[101] Besides the PMT gain voltage used is always the maximum supported by the photosensor, tests to evaluate the sensitivity of the PMT were carried out. When the lowest voltage gain is used (U = 0.3 V), no signal increase is detected. In the middle voltage gain used (U = 0.7 V), a small increase (ΔU = 2 mV) in the signal is verified while in the maximum control voltage (U = 0.9 V), a high increase in the output voltage is verified (ΔU = 18 mV).

By comparing the output voltage given by the oscilloscope and the multimeter, for the same AK concentration tested, the voltage given by the oscilloscope comprises more noise than the one from the multimeter, that gives exact measurements with a lower uncertainty. Additionally, for the same tested concentration of AK, the ΔU given by the oscilloscope is bigger than the one from the multimeter.

For the miniaturization of the assay, afterwards, the assay was carried out inside a microfluidic chamber (**Fig. 3.16**).

In this assay, that was develop inside a microfluidic device with two inlets for the separate pumping of both components of the luminous reaction, it was verified the smallest increase amongst all other assays in which a PMT was used to detect luminescent signal. For this experiment, in a first pump, a tube was filled with DI water, the AK solution and then DI water again, all separated by a little air gap, while in a second pump, a tube was filled with the same volume of DI water, ToxiLight™ kit solution and DI water again, separating all with a little air gap, in order for the luminescent reaction reagents flow through the chip at the same time. At t = 25 min, pumps were turned off to allow the reaction inside the chip and data acquisition and turned on again at t = 50 min.

From t = 0 min to t = 12 min, only water and air entered the chip. As expected, the signal decrease, as no luminescence signal was being generated. From t = 12 min to the end of the assay, both the luminous reaction reagents and water flowed through the microchamber, as the signal kept increase during this period, which was not expected, because at same point the water entered the chip and washed both AK and ToxiLight™. Signal should have decreased at the moment that water entered the chip. When the liquid containing such reaction is washed away, the signal had to decrease, due to the non-presence of luminous molecules inside the chip.

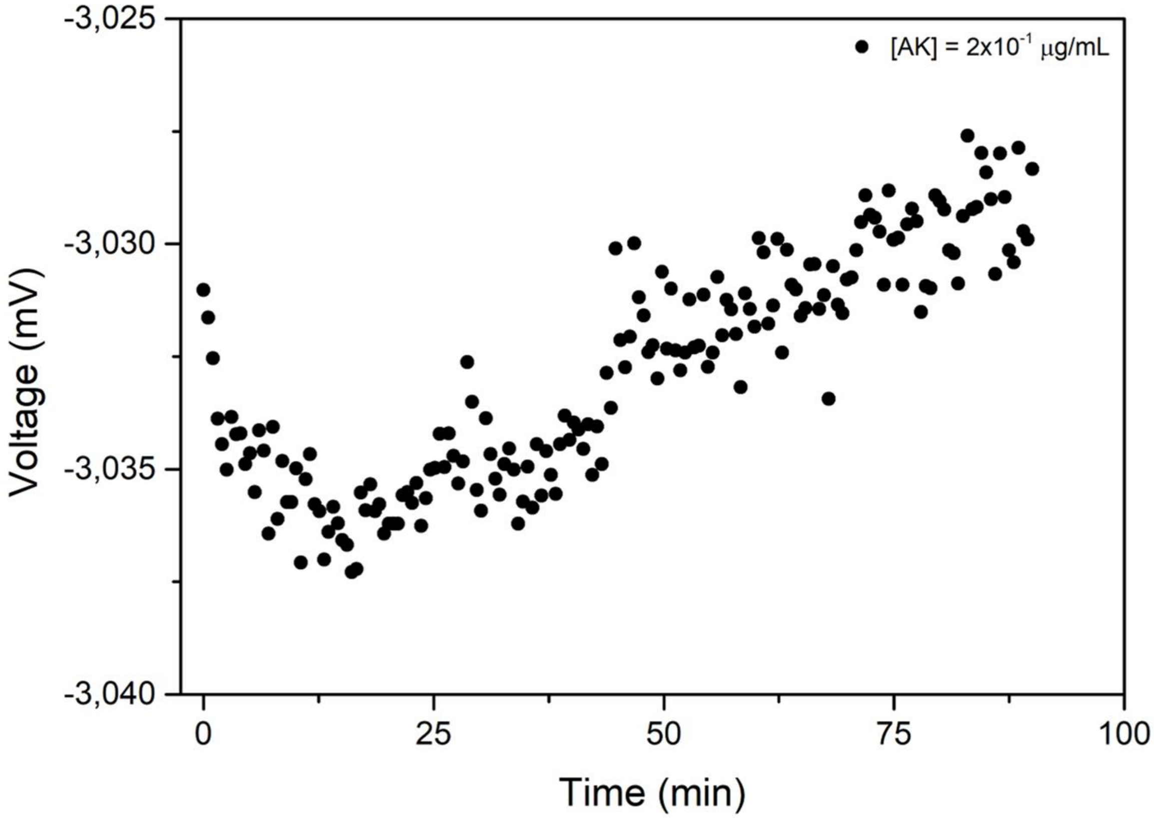

Figure 3.16 – Output voltage variation of the assay regarding the detection of AK in a concentration of 0.2 µg/mL inside a microfluidic device. In this experiment, the output voltage generated is the lowest comparing to the other assays carried out using a photmultiplier. The voltage negative values are related with the multimeter specifications.

Due to the low signal increase verified (ΔU = 10 µV), it was assumed that for lower AK concentrations that needed to be detected in a posterior cell assay, the luminescent detection using a PMT wouldn't be suitable.

After the assays realized using a PMT and two different data acquisition devices, it wasn't possible to detect with precision the highest concentrations of AK used in the macroscale assay. Thus, in order to turn the AK detection in a trustful assay to check on cell viability, another approach was tested, a microfluidic-based immunoassay, in which the signal generated is from antibodies labelled with fluorophores.

3.3.2 Immunoassay Detection

3.3.2.1 Fluorescent Immunoassay Detection using Protein G Sepharose Beads

In order to increase to sensitivity of the assay and to easily obtain a more detectable signal, a new approach for the detection of AK was carried out inside a microcolumn following a sandwich-like assay with the same type of antibody both for AK capturing as for its detection. This type of assay has a limit of detection lower than such assays as nucleic acid tests and PCR amplifications.[102] In this type of assays, due to its high sensitivity, there's a need to avoid non-specific bindings, thus a blocking agent must be used. As stated in other works[103,104], PBS containing BSA in 1% is used as blocking agent in several types of immunoassays.

As PDMS is hydrophobic, proteins tend to bind non-specifically to the polymer surface.[105] **Fig. 3.17** shows a preliminary assay inside a microcolumn without beads to check on the adsorption of the AK to the PDMS surface.

In this assay, no beads were packed inside the microcolumn as well as no capture antibody and several AK concentrations were tested to check their binding affinity to the PDMS surface and to check on the reproducibility of the assay.

By observing the **Fig. 3.17**, it is verified that the left column, where no AK were flowed inside the microchannel shows a higher fluorescent value than the lowest AK concentration tested in this assay, as well as the AK concentration of 0.1 µg/mL showed an higher value than the AK concentration of 0.2 µg/mL. Even with corrections to the micrographs for the control ([AK] = 0 µg/mL) and for the highest fluorescent value ([AK] = 0.1 µg/mL), besides a little dirt present inside the microchannel, almost no fluorescence is observed.

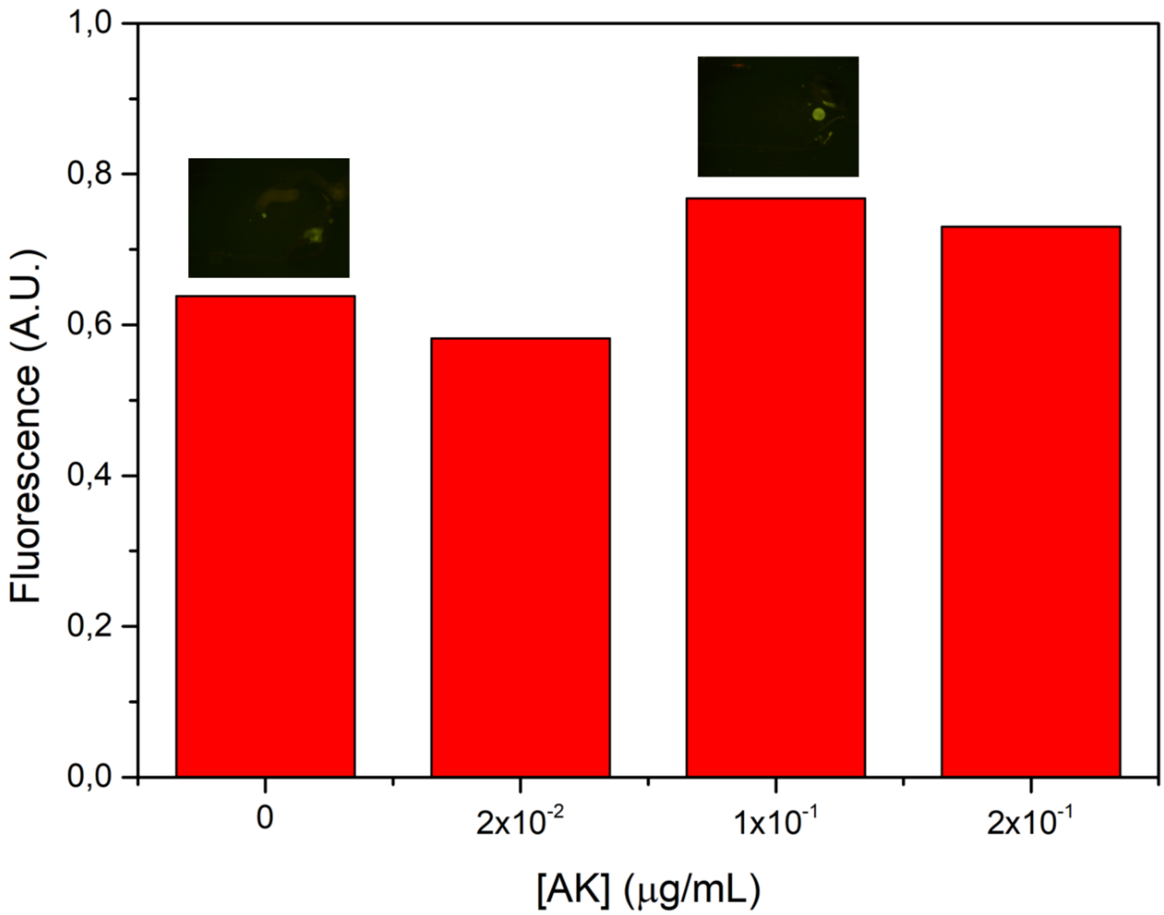

Figure 3.17 – Fluorescent values regarding the AK detection inside a microfluidic device without beads, with the flow of the AK-specific detection antibody labelled with Alexa 430 with a concentration of 10 µg/mL. The fluorescence values from this assay were not expected as the control value ([AK] = 0 µg/mL), that should be the lowest value amongst the others, shows a higher fluorescent signal than the AK concentration of 0.02 g/mL, while for [AK] = 0.1 µg/mL, the fluorescent result is higher than the highest AK concentration tested.

These results were not expected and several reasons for these fluorescent values could be (i) the low concentration (10 µg/mL) of the detection AK-specific antibody labelled with Alexa 430 (α-AK-430) or the low time of exposure in the moment of the micrograph acquisition under the fluorescence microscope.

Afterwards, another assay based in the same concept was tested, however with a higher α-AK-430 concentration (100 µg/mL). **Fig. 3.18** shows the same assay tested before, regarding the adsorption of AK to PDMS and the binding of the α-AK-430 to AK for its fluorescence detection, using two different exposure times.

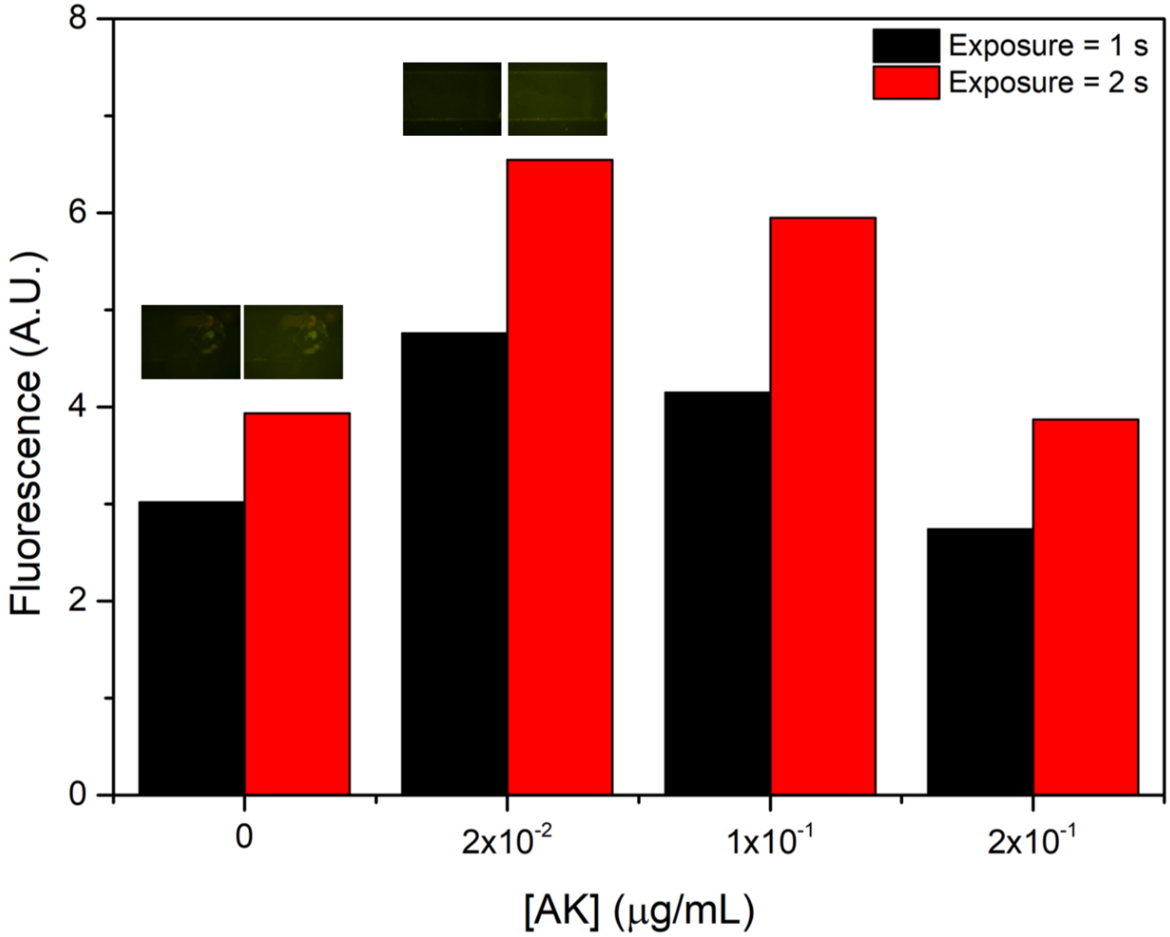

Figure 3.18 – Fluorescent values regarding the AK detection inside a microfluidic device without beads, with the flow of the AK-specific detection antibody labelled with Alexa 430 with a concentration of 100 µg/mL. For the AK concentrations of 0 and 0.2 µg/mL, the fluorescent signal is very similar, being the first mentioned slightly higher. Regarding the AK concentrations of 0.02, 0.1 and 0.2, the signal decreases as the AK concentration increases. For the exposure time of 2 seconds, the difference between each AK concentration is higher and consistent to what is verified for the 1 second exposure time.

By following the same concept of the previous assay, through observing the bar chart in **Fig. 3.18**, by increasing the work concentration of α-AK-430 from 10 to 100 µg/mL, the fluorescence signal increased for all AK concentrations tested comparing to the previous assay.

Regarding the control value in this assay, its signal increased comparing to the previous assay and even surpassed the value of the AK concentration of 0.2 µg/mL. For [AK] = 0.1 and 0.02 µg/mL, the values are higher than the control and the highest concentration of AK, 0.2 µg/mL, which was not expected but corroborates the previous observations with a more diluted α-AK-430. In this assay, the lowest AK concentration showed the higher fluorescence value.

By increasing the time of exposure, the signal increase is clear between the micrographs with 1 and 2 seconds of time exposure. Additionally, by increasing the time of exposure, the fluorescence signal difference between the conditions tested is higher, allowing a clearer distinction.

When flowing the AK solution through the microchannel, the AK binding to the PDMS might not be that strong and the blocking agent may compete for the binding sites when it is flowed after the AK. In order to test this hypothesis, a sandwich-like assay with the flow of α-AK before the AK for the enzyme capture was carried out.

Fig. 3.19 shows the fluorescence signal detected for 1 and 2 seconds of exposure time, after a sandwich-like assay, by flowing the AK-capturing α-AK.

The control, [AK] = 0 µg/mL, shows the lowest fluorescent value amongst all concentrations tested. [AK] = 0.1 µg/mL shows the highest signal, even higher than the maximum AK concentration tested, 0.2 µg/mL. Additionally, the AK concentration of 0.02 µg/mL shows a very similar signal to the highest AK concentration tested.

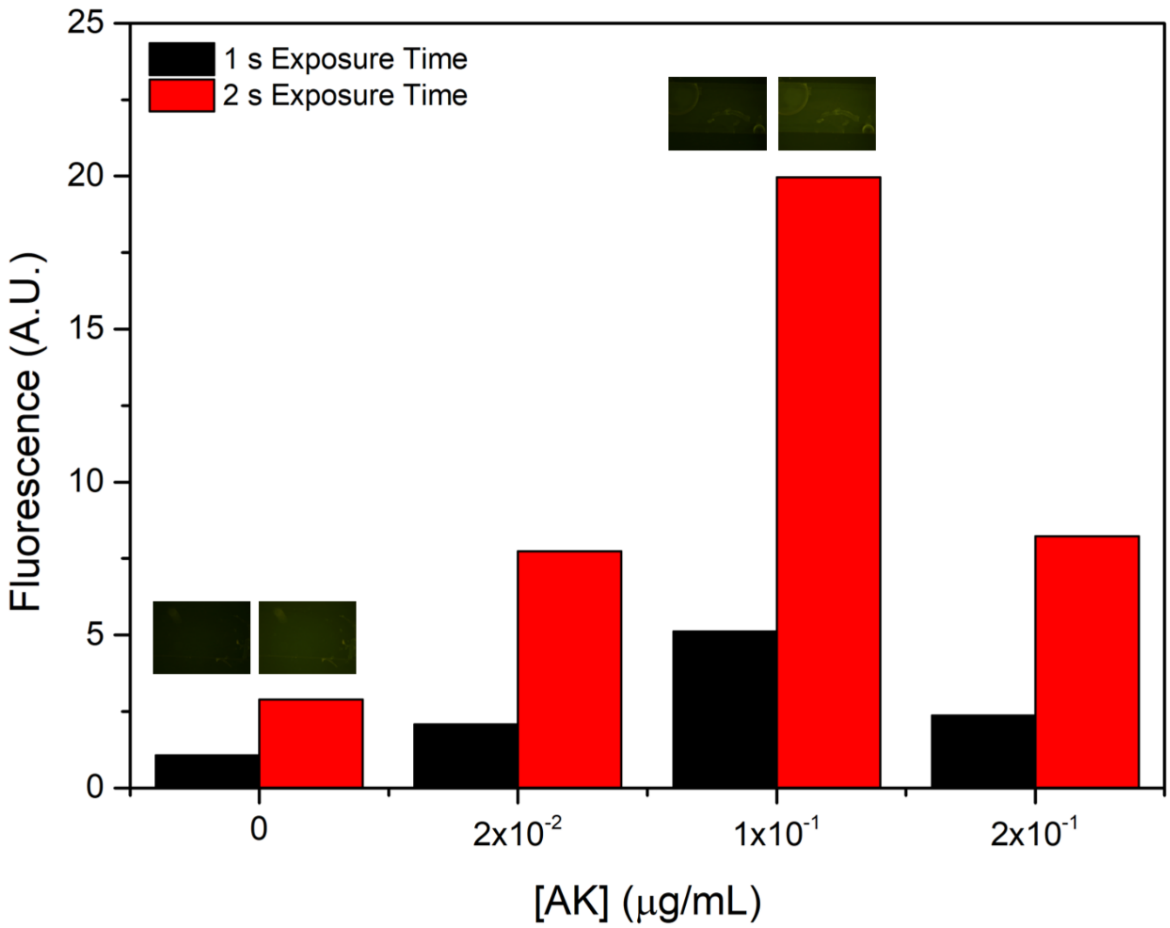

Figure 3.19 – Fluorescent values regarding the AK detection inside a microfluidic device without beads, AK specific antibody for the capture of AK and with the flow of the AK-specific detection antibody labelled with Alexa 430. The AK concentrations of 0.02 and 0.2 µg/mL show very similar values of fluorescence while the middle concentration of 0.1 µg/mL shows the highest signal. In the other way, the condition where no AK was flowed shows the lowest fluorescence value.

At this point, the hypothesis regarding the competitivity between AK and BSA loses strength, as only the signal does not increase only for the highest AK concentration. Comparing to the previous assay, the concentration of α-AK-430 is the same, 100 µg/mL, and the only value that increased is the one for [AK] = 0.1 µg/mL. The α-AK-430 might not bind with a high affinity only to AK but also to BSA or even PDMS or the α-AK.

In order to concentrate the immunoassay inside the microcolumn in a more restricted region, α-AK was adsorbed to previously packed Sepharose beads functionalized with Protein G. Immunoassays using packed beads inside a microfluidic device increase the sensitivity of the assay. Protein G have a high reactivity for human IgGs, binding specifically to the constant Fc region of the immunoglobulin, leaving the variable Fab region available to bind the antigen.[105]

Fig. 3.20 shows the fluorescence signal detected for 1 and 2 seconds of exposure time, after a sandwich-like assay with packed Protein G Sepharose beads for the surface adsorption of the AK-capturing α-AK and the α-AK-430 for the detection of AK.

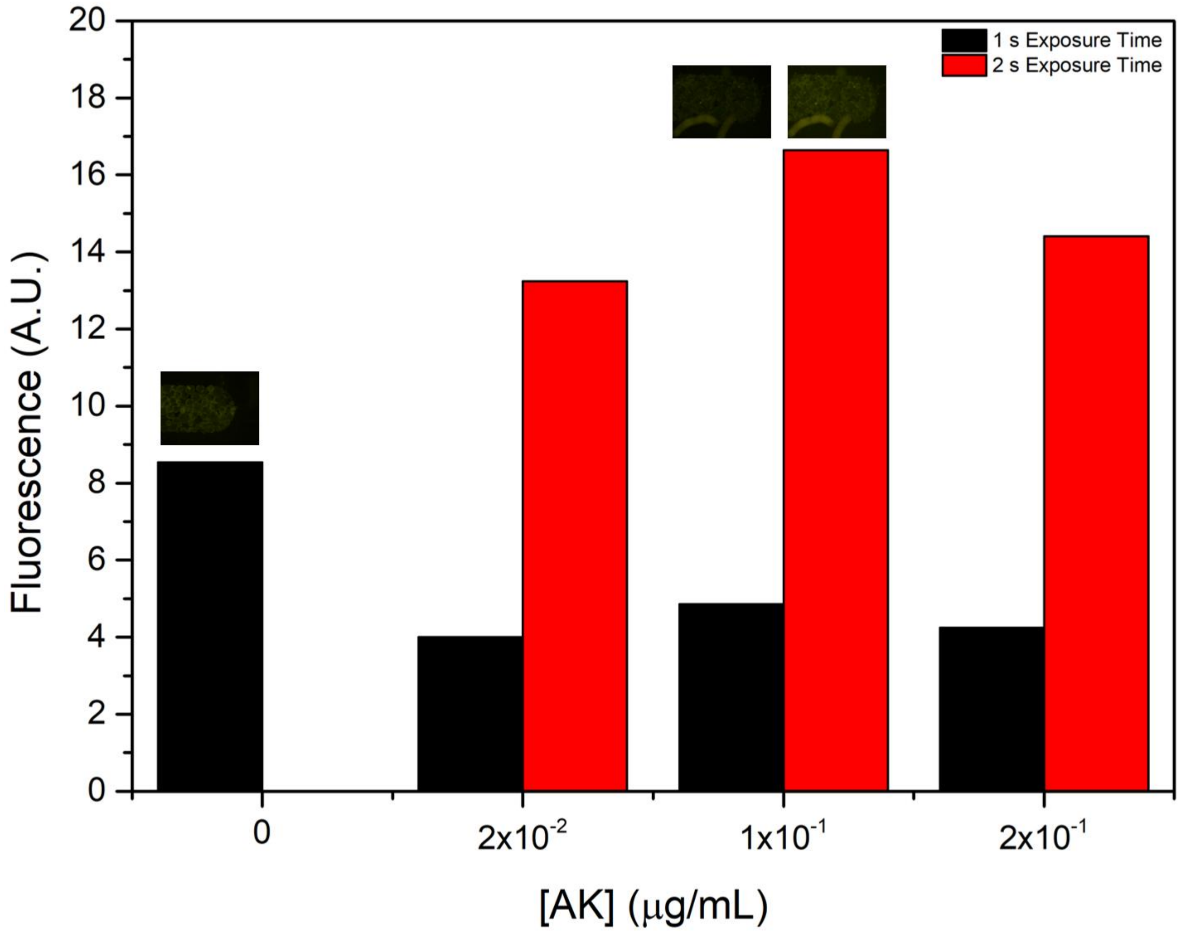

Figure 3.20 – Fluorescent values regarding the AK detection inside a microfluidic device with Protein G Sepharose beads functionalized with Protein G, AK specific antibody for the capture of AK and with the flow of the AK-specific detection antibody labelled with Alexa 430. The control, [AK] = 0 µg/mL, shows the highest fluorescence value for 1 second of exposure time. The AK concentrations of 0.02, 0.1 and 0.2 µg/mL, for the same time of exposure show similar values between each other, being consistent with the highest concentration presenting a lower signal than the concentration of 0.1 µg/mL.

The control value, [AK] = 0 µg/mL, for the exposure time of 1 second shows the higher value of fluorescence. Regarding the other concentrations, the behaviour of the signal variation is very similar to the first assays, where for [AK] = 0.2 µg/mL the fluorescence signal is lower than for [AK] = 0.1 µg/mL.

At this point, due to not expected results, the reason for these results could be the labelling of α-AK with Alexa 430. Its fluorescence might be too low to present significant differences between tested conditions. Another reason could be the fact that the fluorophore binds in the amine groups present in the antibody, which might be the same binding sites to the AK, not being able to bind strongly to the AK and being washed away during the washing step.

To test the validity of the hypothesis mentioned above, a final assay was carried out by flowing only α-AK-430 in a channel without beads and in a channel with only Protein G Sepharose beads. **Fig. 3.21** shows a bar chart with assays realized in a microcolumn with and without Protein G Sepharose beads, flowing only the α-AK-430. This graphic also comprises the sandwich-like assays results for comparison reasons.

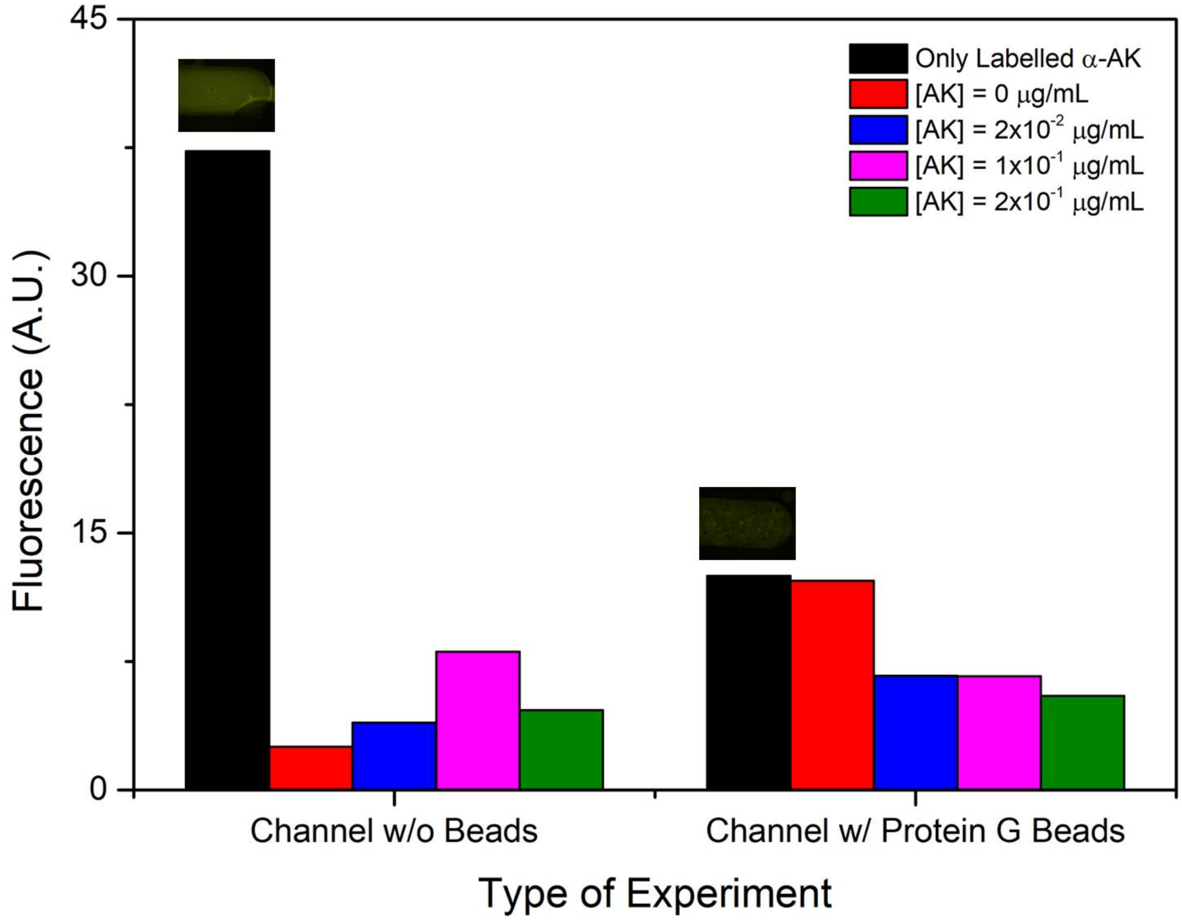

Figure 3.21 – Fluorescent values regarding the adenylate kinase detection inside a microcolumn performing a sandwich-like assay in two different conditions: (i) a channel with packed beads and a channel without any beads inside. For each condition, it was tested the adsorption of the AK-specific antibody labelled with Alexa 430 (α-AK-430) and four different AK concentrations in a sandwich-like immunoassay. The high level of the solo α-AK-430 indicates high adsorption rates to the PDMS and normal fluorescent conditions of the fluorophore.

Regarding the assays using a microcolumn without beads, the value for the flow of α-AK-430 per se is the highest among those type of assays. Among the assays using a microcolumn with

Protein G Sepharose, the values for experiment with only the α-AK-430 flow and the control value are very similar and the highest among other AK concentrations tested for that condition.

As soon as the α-AK-430 highly fluoresces inside the device without packed beads, it can be stated that the α-AK-430 can adsorb to the PDMS surface. Due to the high difference in the fluorescent signal comparing to the other assays realized inside the channel without Protein G Sepharose beads, no problem with the fluorophore fluorescence signal exists.

In the microcolumn with Protein G Sepharose beads, the assay with only the flow of α-AK-430 through the channel, by showing a very similar signal to the control value ([AK] = 0 μg/mL), indicates that Protein G Sepharose beads are not the most suitable for the detection of AK.

By observing the values in both conditions for the AK concentrations of 0.02, 0.1 and 0.2 μg/mL, they revealed to be very low and inconstant in what concerns the expected result: for a higher AK concentration, a higher fluorescence signal. Instead of that, the AK concentration of 0.2 μg/mL showed in all experiments lower fluorescence signals than the 0.1 μg/mL. These results might show that the labelling of α-AK binds the fluorophore directly on the binding sites to the antigen, making it not accurate for the AK detection.

Additionally, the BSA has showed in other works that in the presence of some types of human antibodies, they bind non-specifically to this blocking agent.[106] These cross-reactions of BSA might be another reason for the results showed in this section.

By a sandwich-based immunoassay using Protein G Sepharose beads to adsorb the α-AK and BSA to block the non-specific binding sites, this approach revealed not efficient in distinguishing the signal generated by different AK concentrations. A final approach for the detection of AK in a microfluidic-based immunoassay was carried out using another type of beads, other type of approach in what concerns to what is adsorbed first in the beads, another blocking agent and another detection antibody.

3.3.2.2 Fluorescent Immunoassay Detection using Agarose Beads

Following the previous approach, agarose beads-based microfluidic immunoassays were realized for the AK detection. The agarose beads (Ag – MMC) are functionalized with a phenyl group and six methylene groups for hydrophobic interactions, a carboxyl group for ionic interactions and two hydroxyl groups for hydrogen bonding.[107] In other works, due to its whole structure, Capto-MMC shows multiple modes of interaction for protein binding applications.[108] For the new approach, the blocking agent was also changed and Gammanorm® (γ-norm), a polyclonal human IgG solution containing 59% of IgG1, 36% of IgG2, 4.9% of IgG3 and 0.5% of IgG4[109] was used as described in a previous work.[84]

In these immunoassays, the AK was directly adsorbed on the Ag – MMC and then 2 different antibodies were flowed: (i) the α-AK (from mouse) to bind specifically to the AK and then (ii) a detection antibody specific to mouse IgGs that is labelled with FITC (α-IgG-FITC).

Fig. 3.22 shows the first assay using Ag – MMC for the detection of AK inside a microcolumn, in which was tested the washing conditions.

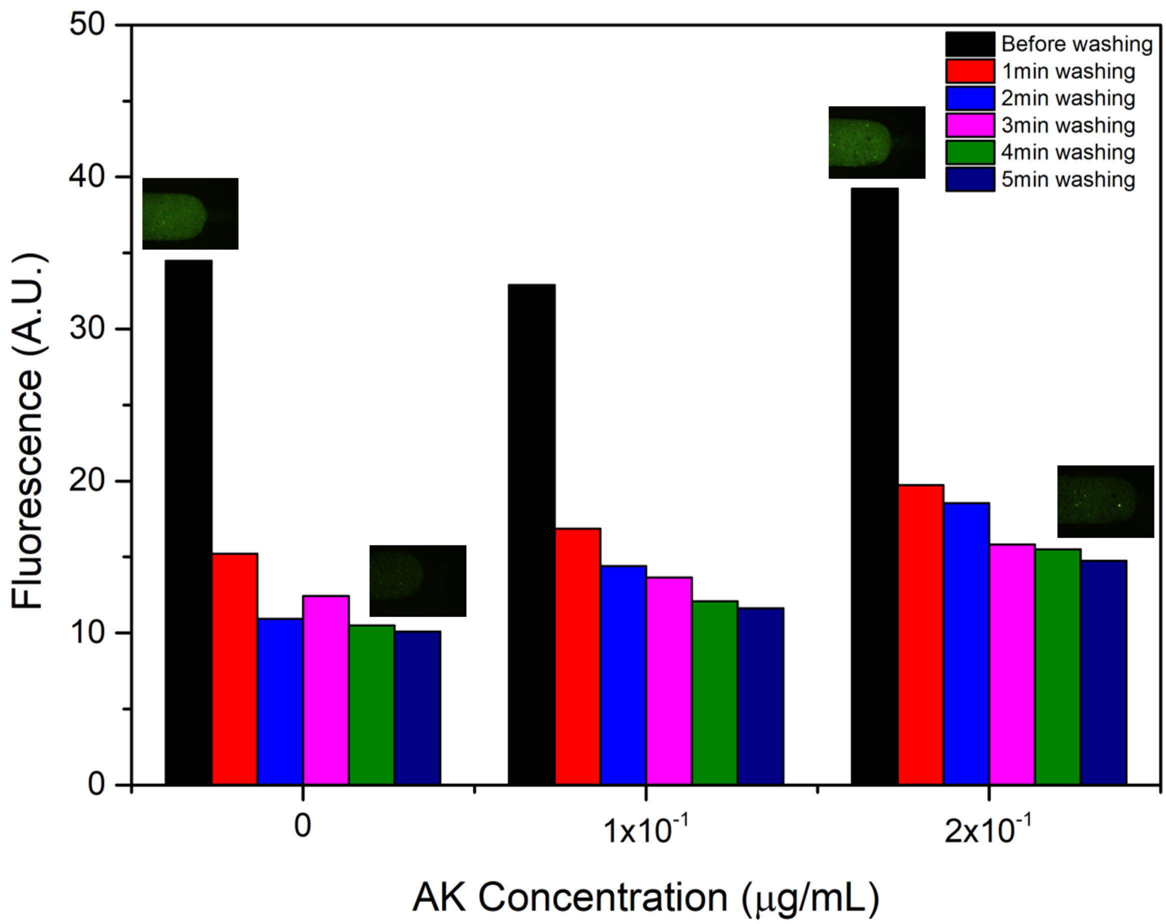

Figure 3.22 – Fluorescent values regarding the test of several times of the washing step. The values correspondent to the 'before washing' condition are clearly higher than the others tested conditions. Without the exception of [AK] = 0 µg/mL, the signal decreased proportionally to the time of washing.

For all the concentrations tested, the value given before the washing is by far higher than the values for each washing time. For [AK] = 0 µg/mL, values didn't decrease proportionally to the time of washing as for the other tested AK concentrations, suffering a sudden increase in the washing time of 3 minutes.

This assay was carried in order to verify if the washing step would highly affect the fluorescence values given, through the possible washing out of α-IgG-FITC that was already attached to the α-AK. If that happened, a huge drop would be verified in the signal from certain step to the next on in the bar chart. Thus, the washing step condition remained for 2 minutes.

In order to test the affinity of the α-IgG-FITC to AK and the affinity of AK to the PDMS in a different type of assay (different from the sandwich-like immunoassay), in one condition (i) the α-AK wasn't flowed through the column and (ii) the AK was directly flow through the non-packed Ag – MMC column. **Fig. 3.23** shows the fluorescence values resulted from this immunoassay.

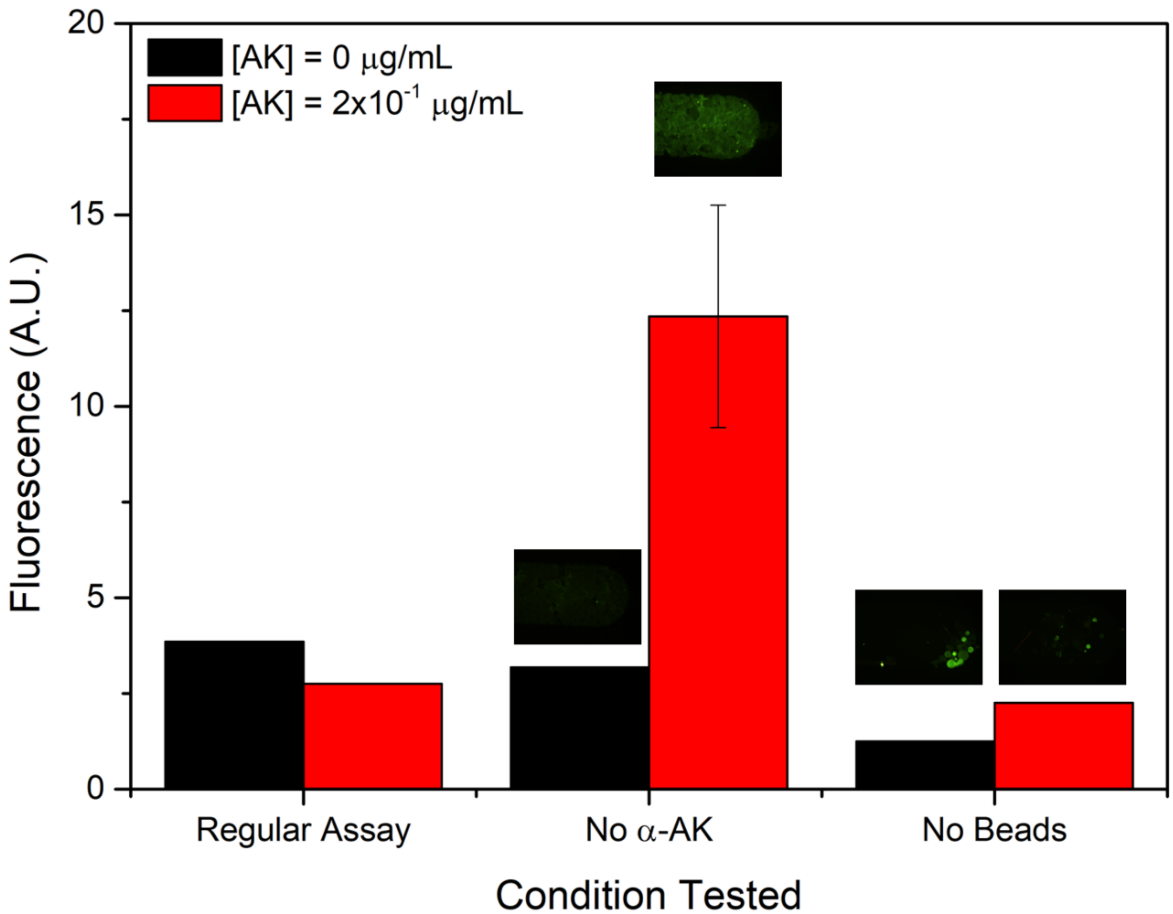

Figure 3.23 – Relative fluorescence signal for [AK] = 0 and 0.2 μg/mL at three tested conditions: (i) the regular assay (AK – γ-norm – α-AK – α-IgG-FITC, through this order), (ii) the immuneassy without the flowing of α-AK and (iii) the immunoassay without Ag – MMC inside the microcolumn. The condition (ii) shows that the α-IgG-FITC has affinity to AK, due to its high value for [AK] = 0.2 μg/mL.

This assay was carried out after the box containing the stock solutions of AK and α-AK has been left out of the freezer overnight. Through kinetic assays carried out using these same stock solutions, it was verified a variation in the enzyme kinetics by 10-15%, which may have caused slight changes in the results.

Regarding the regular assay (AK – γ-norm – α-AK – α-IgG-FITC, through this order), the control value ([AK] = 0 μg/mL) shows a higher fluorescent value than in [AK] = 0.2 μg/mL. This result may indicate that the slight change in the kinetics of AK may have affected its binding-capacity to the α-AK or the α-AK and the α-IgG-FITC compete for the binding to AK, generating a lower fluorescent value for [AK] = 0.2 μg/mL.

In what concerns to the condition without the flow of α-AK, the value correspondent to the AK-containing condition is by far higher than the control. Through the observation of the results for this condition, exists a competition between α-AK and α-IgG-FITC for binding the AK, and it can be confirmed by the higher value of fluorescence shown for [AK] = 0.2 μg/mL when α-AK is not flowed inside the channel, existing a clear affinity by the α-IgG-FITC for the AK.

Finally, for the no packed beads condition and comparing to the one shown in **Fig. 3.17**, in the same concentrations tested the difference between AK concentrations is similar, being the values in **Fig. 3.23** a little higher. These results confirm that AK binds weakly to the PDMS surface, being that surface almost covered by the γ-norm, generating a low fluorescence signal due to the washing of almost all α-IgG-FITC.

In order to test two more conditions: (i) the immunoassay without the blocking agent and without α-AK to check on the role of γ-norm in this assay and (ii) the adsorption of the α-IgG-FITC to the Ag – MMC. **Fig. 3.24** shows the results in fluorescence for these tested conditions.

For the assay without the flow of α-AK and the one without packed beads inside the column, the fluorescence values were accordant the ones verified in the **Fig. 3.23**, being slight similar, as well their distribution in what concerns to the concentrations of AK.

Regarding the condition without the flow of either the γ-norm and the α-AK, as expected, the signal was the highest amongst all the other conditions for [AK] = 0.2 μg/mL. The condition tested in which the α-IgG-FITC is flowed and adsorbed to the Ag – MMC inside the microcolumn is similar to the previous condition for [AK] = 0 μg/mL, which in fact have the same assay reagents, and to the condition where the α-AK was not flowed for [AK] = 0 μg/mL.

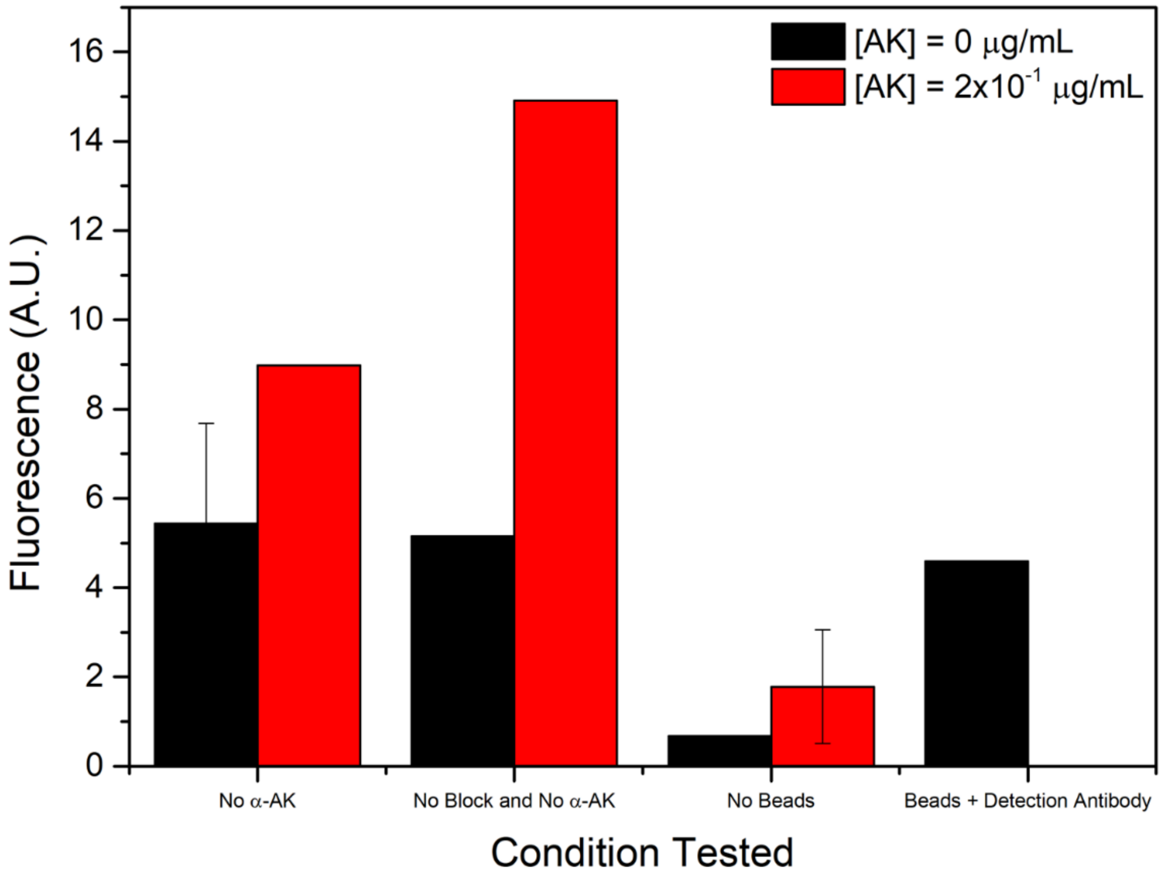

Figure 3.24 – Fluorescence signals for the AK detection using two different conditions to the ones tested before: for [AK] = 0 and 0.2 μg/mL, (i) the immunoassay realized without the flow of the blocking agent and the α-AK, and (ii) the flow of the detection antibody to check on the normal fluorescence signal without the AK binding. When neither α-AK nor the blocking agent are flowed inside the column for [AK] = 0.2 μg/mL, the number of non-specific bindings increase, increasing the signal due to the binding of α-IgG-FITC to AK and weakly to the Ag – MMC.

The α-IgG-FITC adheres to the Ag – MMC, as it is confirmed by the high signal fluorescence given for the condition without the flow of either the γ-norm and the α-AK for [AK] = 0.2 μg/mL. Without the blocking, the number of non-specific bindings increases, as the α-IgG-FITC binds not only to the AK adsorbed on the beads but also to the beads, not as strongly as the AK, as the last condition (Ag – MMC + α-IgG-FITC) corroborates.

In order to test the condition seen in the previous assay to have the highest fluorescent value, several AK concentrations were tested inside a microcolumn with the AK being adsorbed on the packed Ag – MMC and the flow of the detection antibody. **Fig 3.25** shows the fluorescent signals generated with this immunoassay.

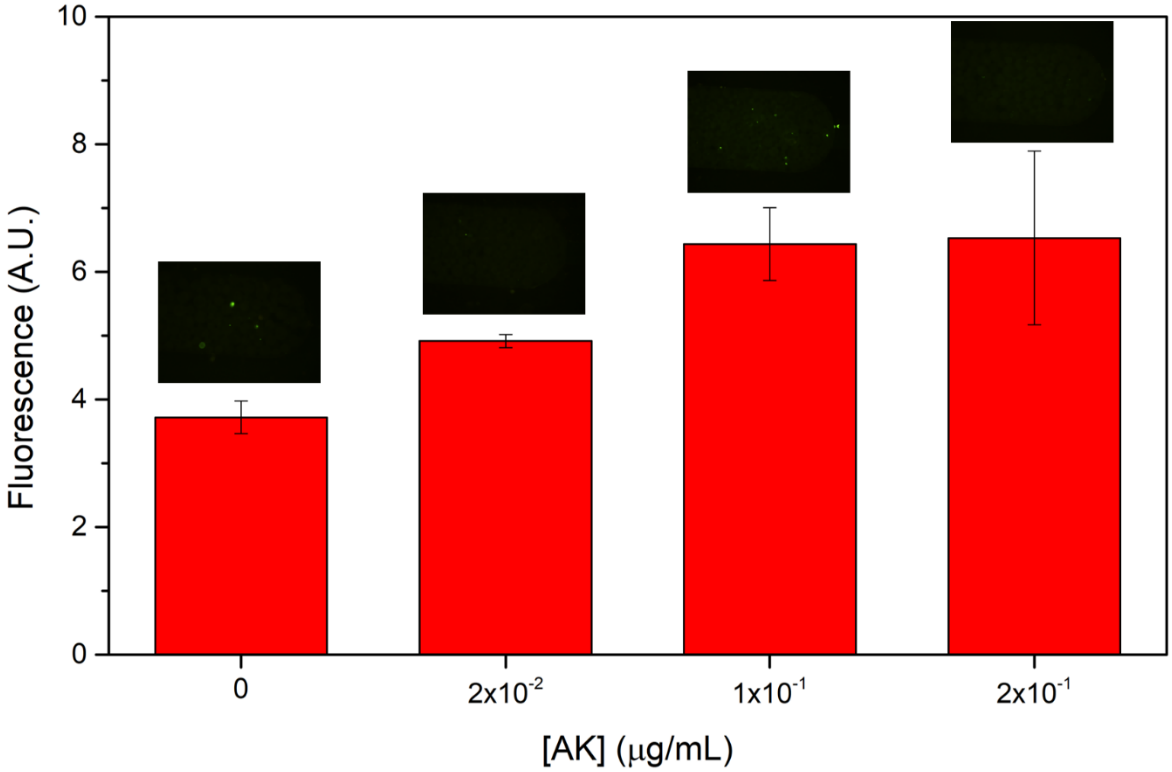

Figure 3.25 – Fluorescence signals for the AK detection in an immunoassay with the AK adsorbed in the packed Ag – MMC inside the microchannel and the flow of the detection antibody, α-IgG-FITC. It is verified an increase in the signal that follows the increase in the AK concentration. Besides the control value ([AK] = 0 μg/mL) having the lower signal, the difference between the conditions tested is not clear in terms of relative fluorescent units.

The fluorescent signal increased with the increase of the AK concentration. The control value ([AK] = 0 μg/mL) shows the lower value amongst other AK concentrations, although, a difference of only 3 relative fluorescence units doesn't give the certainty required to continue with this type of assay. Additionally, the fact that neither α-AK nor γ-norm were flowed inside the microchannel doesn't assure that the α-IgG-FITC is binding specifically to the AK, as the increase in signal verified in the graphic might not be assertive.

After shipping the new reagents (AK and α-AK), a final assay was developed, flowing all the components of the immunoassay inside the microfluidic device using the reagents diluted for reagents-saving and the reagents in the concentrations previously described in another work.[84] **Fig. 3.26** shows this experiment with several AK concentrations.

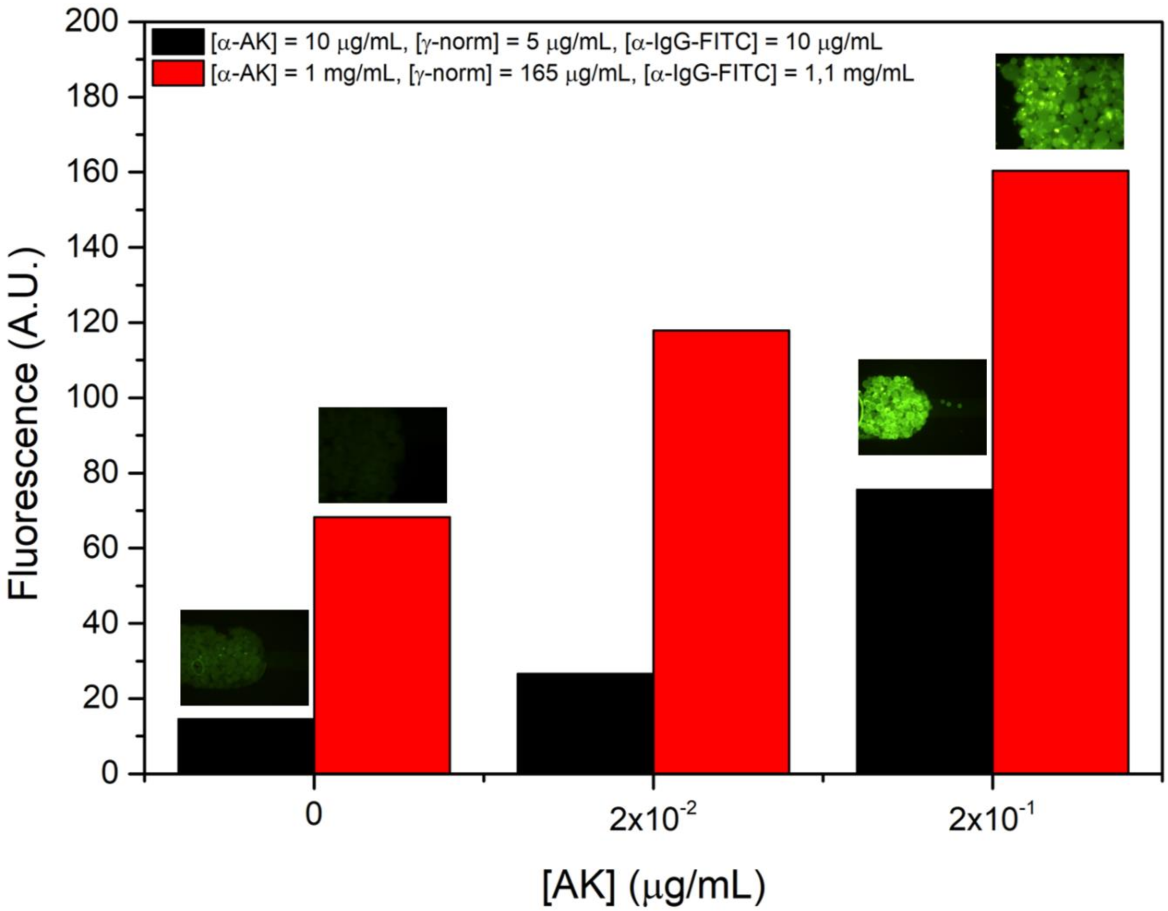

Figure 3.26 – Relative fluorescence signals regarding the AK detection using new reagents in the concentrations described in this work for economizing the reagents and in the concentrations explained in another work.[84] The red bars show an increase in 2 to 4-fold relatively to the verified in the black bars. The increase in the fluorescence signal shows that it follows the AK concentration increase, as expected for these immunoassays.

The black bars in **Fig. 3.26** show the immunoassay signals using the concentrations used previously described in **Chapter 2** while the red bars show the signals resulting from the same immunoassay using higher concentrations of the blocking agent, the α-AK and the α-IgG-FITC. By observing the bar plot, in both conditions, the increase in the fluorescence signal follows the increase in the AK concentration.

By comparing between the AK concentrations tested, with a 2 to 4-fold increase in the signal for each AK concentration, the increase in signal due to the more concentrated reagents may not only be due to the higher concentration of α-IgG-FITC but also due to the higher concentration of γ-norm and α-AK. The more concentrated α-IgG-FITC means a higher number of fluorescence molecules, resulting a in higher fluorescence signal, if a high concentrated blocking agent is flowed in the column, a more effective blocking of the non-specific bindings is realized, not letting the α-AK directly bind to the beads non-specifically.

With these new reagents that hadn't their kinetics affected, along with the previously mentioned agarose beads functionalization on their surface, the immunoassay for the detection of the antibody shows the expected increase. If a comparison is made between these results and the signal values given for the regular assay in Fig. 3.23, it might be confirmed that with these new reagents, the immunoassay shows results according to the previously expected: higher relative fluorescence values in the order of the 100's and control values with the lowest signal comparing to the other AK concentrations.

This final approach revealed more promising than the ones where a PMT was used and the previous type of microfluidic-based immunoassay. Using these type of beads and more concentrated antibodies (α-AK and α-IgG-FITC) and blocking agent (γ-norm), the difference between the different AK concentrations tested is higher, enabling the detection of a lower concentration of AK inside a microfluidic device.

However, several optimizations to the experiment must be made in order to integrate it in a drug screening platform for the detection of cell death due to the AK adsorption in the packed Ag – MMC, that was released by dead cells.

4. Conclusions

Cell cultures inside microfluidic devices allow the miniaturization of the commonly used complex and time-wasting processes, decreasing the reagents consumption, the generated waste per experiment and consequently the costs associated. The focus of this work is to perfuse and proliferate HCT-116 cells inside a microfluidic device for posterior application regarding the development of a drug screening platform.

In this project, several crucial parameters in a microfluidic cell culture were optimized: (i) collagen concentration, important in the adherence of cells to the inside walls of the microfluidic structure, (ii) cell concentration, the parameter that influences the amount of cells perfused into the chip as well as the confluence in the end of the assay, (iii) the incubation time, a parameter that highly influences cells adherence, (iv) collagen adsorption method, a parameter that was found to weigh on cells capacity to adhere or not to the support scaffolding and (v) the flow rate of the proliferation step, a parameter that directly affects the number of viable cells inside the microfluidic cell chamber after 48 hours. All these parameters were optimized during this project and a viable and reproducible cell culture was obtained.

After the microfluidic cell culture optimization, a way to monitor the cell viability was addressed. An end-point approach using the DNA-specific fluorophores Hoechst 33342 and 7-Aminoactinomycin D revealed successfully and to not cause any cytotoxicity effect, revealing an average cell viability of 90%.

In order to monitor the cell death for the drug screening platform, a cell death biomarker release from dead cells was addressed. Adenylate kinase (AK) is released from dead cells when their membrane is damaged through cell lysis or drugs cytotoxicity effect.

For the comparison between dead cells AK release and known AK concentrations in solution, a plate-reader assay using a commercial ToxiLight™ kit for the luminescent AK detection was carried out. The AK concentration that needs to be detected comparing with the cell concentration and number of cells inside the cell chip revealed to be near the limit of detection.

In order to miniaturize the assay in a microfluidic device, a photomultiplier (PMT) was used for the luminescence detection of AK using known concentrations of the enzyme. Due to the low sensitivity of the PMT, another approach using immunoassays in a microcolumn was developed. These assays were carried using known AK concentrations in order to develop a sensitive assay able to detect different AK concentrations near the limit of detection of the first plate reader assay. This approach revealed the most promising, due to the higher sensitivity of the fluorescence detection, as it was possible to detect an AK concentration very close to the detection limit previously stated.

Although all the limitations existent during the experiments, the achieved objectives defined at the beginning of the project were: (i) familiarization with microfabrication processes and microfluidic structures fabrication, (ii) microfluidic chip handling for the perfusion, incubation and proliferation of a cell culture, (iii) the use of a photosensor for the detection of a cell death biomarker, (iv) development of an enzymatic biosensor immunoassay for the detection of a cell death biomarker

4.1 Future Work

As not all objectives could be addressed due to material or time constraints, as prospects for the future, since it is possible to detect the AK near the detection limit required for the assay using cell cultures, cell cultures might be cultured inside a microfluidic device to induce their death with anti-cancer drugs and check on the release of AK using an immunoassay.

Other approach that could be addressed is the integration of cell culture parameters (oxygen content and pH) sensors in the microfluidic device and connected to a data acquisition device for the automatic data saving, in order to monitor the state of the cell culture in real-time during the proliferation step.

5. References

1. World Health Organization. *Latest global cancer data: Cancer burden rises to 18.1 million new cases and 9.6 million cancer deaths in 2018*. PRESS RELEASE Nº 263 (2018).

2. Torre, L. A. *et al.* Global Cancer Statistics, 2012. *CA. Cancer J. Clin.* **65**, 87–108 (2015).

3. World Health Organization. *Colorectal cancer*. Retrieved from: http://gco.iarc.fr/today/data/factsheets/cancers/10_8_9-Colorectum-fact-sheet.pdf (2019).

4. Carvalho, M. R. *et al.* Colorectal tumor-on-a-chip system: A 3D tool for precision onco-nanomedicine. *Sci. Adv.* **5**, eaaw1317 (2019).

5. Ragnhammar, P., Hafström, L., Nygren, P. & Glimelius, B. A systematic overview of chemotherapy effects in colorectal cancer. *Acta Oncol. (Madr).* **40**, 282–308 (2001).

6. Tsai, H. F., Trubelja, A., Shen, A. Q. & Bao, G. Tumour-on-a-chip: Microfluidic models of tumour morphology, growth and microenvironment. *J. R. Soc. Interface* **14**, 17-37 (2017).

7. Pandey, C. M. *et al.* Microfluidics Based Point-of-Care Diagnostics. *Biotechnol. J.* **13**, 1–11 (2018).

8. Mancera-Andrade, E. I., Parsaeimehr, A., Arevalo-Gallegos, A., Ascencio-Favela, G. & Parra-Saldivar, R. Microfluidics technology for drug delivery: A review. *Front. Biosci. - Elit.* **10**, 74–91 (2018).

9. Streets, A. M. & Huang, Y. Chip in a lab: Microfluidics for next generation life science research. *Biomicrofluidics* **7**, 1–23 (2013).

10. Sia, S. K. & Whitesides, G. M. Microfluidic devices fabricated in poly(dimethylsiloxane) for biological studies. *Electrophoresis* **24**, 3563–3576 (2003).

11. Boyd-Moss, M., Baratchi, S., Di Venere, M. & Khoshmanesh, K. Self-contained microfluidic systems: A review. *Lab Chip* **16**, 3177–3192 (2016).

12. Halldorsson, S., Lucumi, E., Gómez-Sjöberg, R. & Fleming, R. M. T. Advantages and challenges of microfluidic cell culture in polydimethylsiloxane devices. *Biosens. Bioelectron.* **63**, 218–231 (2015).

13. Lavoie, E., Wangdi, T. & Kazmierczak, B. Advances in Microfluidic Materials, Functions, Integration and Applications. *Chem. Rev.* **13**, 1133–1145 (2012).

14. Kumar, S. *et al.* Microfluidic-integrated biosensors: Prospects for point-of-care diagnostics. *Biotechnol. J.* **8**, 1267–1279 (2013).

15. Hammond, J. L., Formisano, N., Estrela, P., Carrara, S. & Tkac, J. Electrochemical biosensors and nanobiosensors. *Essays Biochem.* **60**, 69–80 (2016).

16. Bhatia, S. N., Balis, U. J., Yarmush, M. L. & Toner, M. Effect of cell-cell interactions in preservation of cellular phenotype: Cocultivation of hepatocytes and nonparenchymal cells. *FASEB J.* **13**, 1883–1900 (1999).

17. Folch, A. & Toner, M. Microengineering of Cellular Interactions. *Annu. Rev. Biomed. Eng.* **2**, 227–256 (2000).

18. Julich, S. *et al.* Evaluation of a microfluidic chip system for preparation of bacterial DNA from swabs, air, and surface water samples. *Biologicals* **44**, 574–580 (2016).

19. Reinholt, S. J. & Baeumner, A. J. Microfluidic isolation of nucleic acids. *Angew. Chemie - Int. Ed.* **53**, 13988–14001 (2014).

20. Regnault, C., Dheeman, D. & Hochstetter, A. Microfluidic Devices for Drug Assays. *High-Throughput* **7**, 18 (2018).

21. Ma, J., Wang, Y. & Liu, J. Biomaterials meet microfluidics: from synthesis technologies to biological applications. *Micromachines* **8**, 255 (2017).

22. Ward, K. & Fan, Z. H. Mixing in microfluidic devices and enhancement methods. *J. Micromechanics Microengineering* **25**, 094001 (17pp) (2015).

23. Weibel, D. B. & Whitesides, G. M. Applications of microfluidics in chemical biology. *Curr. Opin. Chem. Biol.* **10**, 584–591 (2006).

24. Nayak, S. *et al.* Microfluidics-based point-of-care test for serodiagnosis of Lyme Disease. *Sci. Rep.* **6**, (2016).

25. Smith, S. *et al.* Microfluidic Cartridges for Automated, Point-of-Care Blood Cell Counting. *SLAS Technol.* **22**, 176–185 (2017).

26. Pandya, H. J. *et al.* A microfluidic platform for drug screening in a 3D cancer microenvironment. *Biosens. Bioelectron.* **94**, 632–642 (2017).

27. Phan, D. T. T. *et al.* A vascularized and perfused organ-on-a-chip platform for large-scale drug screening applications. *Lab Chip* **17**, 511–520 (2017).

28. Viravaidya, K., Sin, A. & Shuler, M. L. Development of a Microscale Cell Culture Analog to Probe Naphthalene Toxicity. *Biotechnol. Prog.* **20**, 316–323 (2004).

29. Chung, B. G. *et al.* Human neural stem cell growth and differentiation in a gradient-generating microfluidic device. *Lab Chip* **5**, 401–406 (2005).

30. Irimia, D. *et al.* Microfluidic system for measuring neutrophil migratory responses to fast switches of chemical gradients. *Lab Chip* **6**, 191–198 (2006).

31. Li Jeon, N. *et al.* Neutrophil chemotaxis in linear and complex gradients of interleukin-8 formed in a microfabricated device. *Nat. Biotechnol.* **20**, 826–830 (2002).

32. Gau, V. & Wong, D. Oral Fluid Nanosensor Test (OFNASET) with advanced electrochemical-based molecular analysis platform. *Ann. N. Y. Acad. Sci.* **1098**, 401–410 (2007).

33. Christodoulides, N. *et al.* Lab-on-a-chip methods for point-of-care measurements of salivary biomarkers of periodontitis. *Ann. N. Y. Acad. Sci.* **1098**, 411–428 (2007).

34. Weltin, A. *et al.* Cell culture monitoring for drug screening and cancer research: A transparent, microfluidic, multi-sensor microsystem. *Lab Chip* **14**, 138–146 (2014).

35. Wong, A. H. H. *et al.* Drug screening of cancer cell lines and human primary tumors using droplet microfluidics. *Sci. Rep.* **7**, 1–15 (2017).

36. Zhang, Y. S. *et al.* Multisensor-integrated organs-on-chips platform for automated and continual in situ monitoring of organoid behaviors. *Proc. Natl. Acad. Sci.* **114**, E2293–E2302 (2017).

37. Lee, K. S., Boccazzi, P., Sinskey, A. J. & Ram, R. J. Microfluidic chemostat and turbidostat with flow rate, oxygen, and temperature control for dynamic continuous culture. *Lab Chip* **11**, 1730–1739 (2011).

38. Son, K. J., Gheibi, P., Stybayeva, G., Rahimian, A. & Revzin, A. Detecting cell-secreted growth factors in microfluidic devices using bead-based biosensors. *Microsystems Nanoeng.* **3**, 17025 (2017).

39. Yamagishi, A. *et al.* Microfluidic device coupled with a microfabricated oxygen electrode for the measurement of bactericidal activity of neutrophil-like cells. *Anal. Chim. Acta* **985**, 1–6 (2017).

40. Gruber, P. *et al.* Real-time pH monitoring of industrially relevant enzymatic reactions in a microfluidic side-entry reactor (μSER) shows potential for pH control. *Biotechnology Journal* **12**, 1600475 (2017).

41. Kim, S. H., Lee, G. H., Park, J. Y. & Lee, S. H. Microplatforms for Gradient Field Generation of Various Properties and Biological Applications. *J. Lab. Autom.* **20**, 82–95 (2015).

42. Voldman, J., Gray, M. L. & Schmidt, M. A. Microfabrication in Biology and Medicine. *Annu. Rev. Biomed. Eng.* **1**, 401–425 (1999).

43. Kimura, H., Sakai, Y. & Fujii, T. Organ/body-on-a-chip based on microfluidic technology for drug discovery. *Drug Metab. Pharmacokinet.* **33**, 43–48 (2018).

44. El-Ali, J., Sorger, P. K. & Jensen, K. F. Cells on chips. *Nature* **442**, 403–411 (2006).

45. Li, C. W. & Wang, G. J. MEMS manufacturing techniques for tissue scaffolding devices. in *MEMS for Biomedical Applications* 192–217 (2012). doi:10.1016/B978-0-85709-129-1.50008-0

46. Tabeling, P. *Introduction to Microfluidics*. Oxford University Press, USA (2005).

47. Onanuga, T., Rumler, M. & Erdmann, A. A physical model for innovative laser direct write lithography. *Opt. Microlithogr. XXX* **10147**, (2017).

48. Dietzel, A. Microsystems for pharmatechnology: Manipulation of fluids, particles, droplets, and cells. in *Fabrication of Microfluidic Devices* 1–348 (2016). doi:10.1007/978-3-319-26920-7

49. Saito, M., Touno, I., Omiya, K., Homma, T. & Nagatomo, T. A Process for Photoresist Removal after Aluminum Etching Using Plasma Treatment in a Gas Containing Hydrogen. *J. Electrochem. Soc.* **149**, 451–454 (2002).

50. Martinez-Duarte, R. & Madou, M. SU-8 Photolithography and Its Impact on Microfluidics. in *Microfluidics and Nanofluidics Handbook* 231–268 (2011). doi:10.1201/b11188-11

51. Qin, D., Xia, Y. & Whitesides, G. M. Soft lithography for micro- and nanoscale patterning. *Nat. Protoc.* **5**, 491–502 (2010).

52. Smith, K. H., Tejeda-Montes, E., Poch, M. & Mata, A. Integrating top-down and self-assembly in the fabrication of peptide and protein-based biomedical materials. *Chem. Soc. Rev.* **40**, 4563–4577 (2011).

53. Silverio, V. & Freitas, S. C. de. Microfabrication Techniques for Microfluidic Devices. in *Complex Fluid-Flows in Microfluidics* 22–51 (2017). doi:10.1007/978-3-319-59593-1

54. Weibel, D. B., DiLuzio, W. R. & Whitesides, G. M. Microfabrication meets microbiology. *Nat. Rev. Microbiol.* **5**, 209–218 (2007).

55. Derkus, B. Applying The Miniaturization Technologies for Biosensor Design. *Biosens. Bioelectron.* **79**, 901–913 (2016).

56. Rothbauer, M., Zirath, H. & Ertl, P. Recent advances in microfluidic technologies for cell-to-cell interaction studies. *Lab Chip* **18**, 249–270 (2018).

57. Coluccio, M. L. *et al.* Microfluidic platforms for cell cultures and investigations. *Microelectron. Eng.* **208**, 14–28 (2019).

58. Joshi, P. N. Cells and Organs on Chip—A Revolutionary Platform for Biomedicine. in *Lab-on-a-Chip Fabrication and Application* 49 (2016). doi:http://dx.doi.org/10.5772/57353

59. Eribol, P., Uguz, A. K. & Ulgen, K. O. Screening applications in drug discovery based on microfluidic technology. *Biomicrofluidics* **10**, 1–27 (2016).

60. Liu, X., Zheng, W. & Jiang, X. Cell-Based Assays on Microfluidics for Drug Screening. *ACS Sensors* **4**, 1465–1475 (2019).

61. Eduati, F. *et al.* A microfluidics platform for combinatorial drug screening on cancer biopsies. *Nat. Commun.* **9**, 1-13(2018).

62. Purschke, M., Rubio, N., Held, K. D. & Redmond, R. W. Phototoxicity of Hoechst 33342 in time-lapse fluorescence microscopy. *Photochem. Photobiol. Sci.* **9**, 1634–1639 (2010).

63. Schmid, I., Uittenbogaart, C. & Jamieson, B. D. Live-cell assay for detection of apoptosis by dual-laser flow cytometry using Hoechst 33342 and 7-amino-actinomycin D. *Nat. Protoc.* **2**, 187–190 (2007).

64. Wlodkowic, D. *et al.* Chip-Based Dynamic Real-Time Quantification of Drug-Induced Cytotoxicity in Human Tumor Cells. *Anal. Chem.* **81**, 6952–6959 (2009).

65. Kim, G., Donnenberg, V., Donnenberg, A., Gooding, W. & Whiteside, T. A novel multiparametric flow cytometry based cytotoxicity assay simultaneously immunophenotypes effector cells: Comparisons to a 4 h 51Cr-release assay. *J. Immunol. Methods* **325**, 51–66 (2007).

66. Goossens, N., Nakagawa, S., Sun, X. & Hoshida, Y. Cancer biomarker discovery and validation. *Transl. Cancer Res.* **4**, 256–269 (2015).

67. Dumbrava, E. I., Meric-Bernstam, F. & Yap, T. A. Challenges with biomarkers in cancer drug discovery and development. *Expert Opin. Drug Discov.* **13**, 685–690 (2018).

68. Dhandapani, M. & Goldman, A. Preclinical Cancer Models and Biomarkers for Drug Development: New Technologies and Emerging Tools. *J. Mol. Biomark. Diagn.* **8**, 1–8 (2017).

69. Liu, Y. & Schanze, K. S. Conjugated Polyelectrolyte Based Real-Time Fluorescence Assay for Adenylate Kinase. *Anal. Chem.* **81**, 231–239 (2009).

70. Biology, C., Panayiotou, C., Solaroli, N. & Karlsson, A. The many isoforms of human adenylate kinases. *Int. J. Biochem. Cell Biol.* **49**, 75–83 (2014).

71. Waldmann, R. Investigations on the Molecular Biology of Human Adenylate Kinase 2 Deficiency (Reticular Dysgenesis) and the Establishment and Characterisation of an

Adenylate Kinase 2-deficient Mouse Model. (Ulm University, 2017). doi:10.18725/OPARU-6585

72. Klepinin, A. *et al.* Simple oxygraphic analysis for the presence of adenylate kinase 1 and 2 in normal and tumor cells. *J. Bioenerg. Biomembr.* **48**, 531–548 (2016).

73. Choo, H., Kim, B., Kwon, O. & Lee, C. S. Secretion of adenylate kinase 1 is required for extracellular ATP synthesis in C2C12 myotubes. *Exp. Mol. Med.* **40**, 220–228 (2008).

74. Köhler, C. *et al.* Release of adenylate kinase 2 from the mitochondrial intermembrane space during apoptosis. *FEBS Lett.* **447**, 10–12 (1999).

75. Marshall, K. D., Edwards, M. A., Krenz, M., Davis, J. W. & Baines, C. P. Proteomic mapping of proteins released during necrosis and apoptosis from cultured neonatal cardiac myocytes. *Am. J. Physiol. Physiol.* **306**, 639–647 (2014).

76. Pereira, D. M., Gomes, S. E., Borralho, P. M. & Rodrigues, C. M. P. MEK5/ERK5 activation regulates colon cancer stem-like cell properties. *Cell Death Discov.* **5**, 1–13 (2019).

77. Lyons, S. K., Patrick, P. S. & Brindle, K. M. Imaging mouse cancer models in vivo using reporter transgenes. *Cold Spring Harb. Protoc.* **2013**, 685–699 (2013).

78. Ahmed, D. *et al.* Epigenetic and genetic features of 24 colon cancer cell lines. *Oncogenesis* **2**, e71 (2013).

79. Rajput, A. *et al.* Characterization of HCT116 Human Colon Cancer Cells in an Orthotopic Model. *J. Surg. Res.* **147**, 276–281 (2008).

80. Ulery, B. D., Nair, L. S. & Laurencin, C. T. Biomedical applications of biodegradable polymers. *J. Polym. Sci. Part B Polym. Phys.* **49**, 832–864 (2011).

81. Woodcock, S. E., Johnson, W. C. & Chen, Z. Collagen adsorption and structure on polymer surfaces observed by atomic force microscopy. *J. Colloid Interface Sci.* **292**, 99–107 (2005).

82. Chumbimuni-torres, K. Y. *et al.* Adsorption of Proteins to Thin-Films of PDMS and Its Effect on the Adhesion of Human Endothelial Cells. *RSC Adv.* **1**, 706–714 (2011).

83. Qian, Z., Ross, D., Jia, W., Xing, Q. & Zhao, F. Bioactive polydimethylsiloxane surface for optimal human mesenchymal stem cell sheet culture. *Bioact. Mater.* **3**, 167–173 (2018).

84. Pinto, I. F. *et al.* The application of microbeads to microfluidic systems for enhanced detection and purification of biomolecules. *Methods* **116**, 112–124 (2017).

85. MicroChem. SU-8 2000 Permanent Epoxy Negative Photoresist. (2014).

86. Sunkara, V. *et al.* Simple room temperature bonding of thermoplastics and poly(dimethylsiloxane). *R. Soc. Chem.* **11**, 962–965 (2011).

87. Somaiah, C. *et al.* Collagen promotes higher adhesion, survival and proliferation of mesenchymal stem cells. *PLoS One* **10**, 1–15 (2015).

88. ATCC. *Protocol for Thawing, Propagation and Cryopreservation of NCI-PBCF-CCL247 (HCT 116) (ATCC®CCL-247 ™) colorectal carcinoma*. **1.6**, (2012).

89. Frantz, C., Stewart, K. M. & Weaver, V. M. The extracellular matrix at a glance. *J. Cell Sci.* **123**, 4195–4200 (2010).

90. Tapia, F., Vázquez-Ramírez, D., Genzel, Y. & Reichl, U. Bioreactors for high cell density and continuous multi-stage cultivations: options for process intensification in cell culture-based viral vaccine production. *Appl. Microbiol. Biotechnol.* **100**, 2121–2132 (2016).

91. Nunes, P. S., Kjaerulff, S., Dufva, M. & Mogensen, K. B. Real-time direct cell concentration and viability determination using a fully automated microfluidic platform for standalone process monitoring. *Analyst* **140**, 4007–4020 (2015).

92. Hemmingsen, M. Usability and Applicability of Microfluidic Cell Culture Systems. (2012).

93. Gao, D., Jin, F., Zhou, M. & Jiang, Y. Recent advances in single cell manipulation and biochemical analysis on microfluidics. *Analyst* **144**, 766–781 (2019).

94. Kim, L., Toh, Y. C., Voldman, J. & Yu, H. A practical guide to microfluidic perfusion culture of adherent mammalian cells. *Lab Chip* **7**, 681–694 (2007).

95. Wei, C. *et al.* On-chip culture of osteocytes. *18th Int. Conf. Miniaturized Syst. Chem. Life Sci. MicroTAS 2014* 554–557 (2014).

96. Virumbrales-Muñoz, M. *et al.* Enabling cell recovery from 3D cell culture microfluidic devices for tumour microenvironment biomarker profiling. *Sci. Rep.* **9**, 1–14 (2019).

97. Goral, V. N., Zhou, C., Lai, F. & Yuen, P. K. A continuous perfusion microplate for cell culture. *Lab Chip* **13**, 1039–1043 (2013).

98. Ruan, Q., Chen, Y., Gratton, E., Glaser, M. & Mantulin, W. W. Cellular characterization of adenylate kinase and its isoform: Two-photon excitation fluorescence imaging and fluorescence correlation spectroscopy. *Biophys. J.* **83**, 3177–3187 (2002).

99. Rockmore, D. N. The FFT: An Algorithm the Whole Family Can Use. *Inst. Electr. Electron. Eng.* **2**, 60–64 (2000).

100. Gallagher, T. A., Nemeth, A. J. & Hacein-Bey, L. An introduction to the Fourier transform: Relationship to MRI. *Am. J. Roentgenol.* **190**, 1396–1405 (2008).

101. Graf, R. F. *Modern Dictionary of Electronics*. (1999). doi:10.1192/bjp.112.483.211-a

102. Juncker, D., Bergeron, S., Laforte, V. & Li, H. Cross-reactivity in antibody microarrays and multiplexed sandwich assays: Shedding light on the dark side of multiplexing. *Curr. Opin. Chem. Biol.* **18**, 29–37 (2014).

103. Hamzehlou, S., Albert, P. R. & Farajollahi, M. M. Requirement of a Blocking Step in Affinity Purification of Polyclonal Antibodies. *Int. J. Mol. Cell. Med.* **4**, 196–198 (2015).

104. Ji, Y. *et al.* Adenylate kinase hCINAP determines self-renewal of colorectal cancer stem cells by facilitating LDHA phosphorylation. *Nat. Commun.* **8**, 1-16 (2017).

105. Kim, D. & Herr, A. E. Protein immobilization techniques for microfluidic assays. *Biomicrofluidics* **7**, 1–47 (2013).

106. Xiao, Y. & Isaacs, S. N. Enzyme-Linked Immunosorbent Assay (ELISA) and Blocking with Bovine Serum Albumin (BSA) - Not all BSAs are alike. *J. Immunol. Methods* **384**, 148–151 (2012).

107. Arakawa, T. *et al.* Capto MMC mixed-mode chromatography of murine and rabbit antibodies. *Protein Expr. Purif.* **127**, 105–110 (2016).

108. Hirano, A., Arakawa, T. & Kameda, T. Interaction of arginine with Capto MMC in

multimodal chromatography. *J. Chromatogr. A* **1338**, 58–66 (2014).

109. Lalli, E., Sarti, G. C. & Boi, C. Effect of the spacer arm on non-specific binding in membrane affinity chromatography. *MRS Commun.* **8**, 65–70 (2018).

6. Appendix

Appendix A – Python language script for the multimeter automatic acquisition of voltage values

```
import matplotlib.pyplot as plt # DATA PLOT

import numpy as np

import visa

import time

import sys

import pandas as pd


# Change this variable to the address of your instrument

VISA_ADDRESS = 'USB0::2391::2567::MY48004154::INSTR'

try:

    # Create a connection (session) to the instrument

    resourceManager = visa.ResourceManager()

    session = resourceManager.open_resource(VISA_ADDRESS)

    session.write('*RST')

    session.write('*CLS')

except visa.Error as ex:

    print('Couldn\'t connect to \'%s\', exiting now...' % VISA_ADDRESS)

    sys.exit()


# For Serial and TCP/IP socket connections enable the read Termination Character, or read's will timeout

if session.resource_name.startswith('ASRL') or session.resource_name.endswith('SOCKET'):

    session.read_termination = '\n'


#PARAMETROS DE AQUISIÇÃO

session.write('VOLT:DC:APER 200E-3') # RESOLUCAO

intervalo_aquisicao = 5400 # IN SECONDS
```

```
start = time.time()
tempo = 0

x, y = [], []

while tempo <= intervalo_aquisicao:

    # Create a Pandas Excel writer using XlsxWriter as the engine.
    writer = pd.ExcelWriter('test_check_3.xlsx', engine='xlsxwriter')

    session.write('MEAS:VOLT:DC?')
    dados = session.read();
    dados = dados.strip()
    dados = dados.split(",")

    tempo = time.time() - start;
    print(dados);
    print(tempo);
    x.append(tempo)
    y.append(float(dados[0]))
    time.sleep(30)

    # Create a Pandas dataframe from the data.
    df = pd.DataFrame({'Time': x, 'Voltage': y})
    # Convert the dataframe to an XlsxWriter Excel object.
    df.to_excel(writer, sheet_name='Sheet1')
    # Close the Pandas Excel writer and output the Excel file.
    writer.save()

plt.scatter( x, y)
```

Appendix B – Accepted Abstract and Extended Abstract for the µTAS Conference in October 2019

Appendix B.1 – Accepted Abstract

Topic No. 6.07 Abstract Reference No: 0000

Oral (Obtained through Website)

Development of a microfluidic platform for targeted phage selection: in pursuit of personalized colorectal cancer treatments

Eduardo J.S. Brás[*1,4], Pedro G.M. Condelipes[*1], Pedro M. Fontes[*1,2], Ricardo F. Serrão[1], Vanda Marques[2], Marta B. Afonso[2], Cecília M.P. Rodrigues[2], Virginia Chu[1], João Gonçalves[2], João Pedro Conde[1,3]

[1]Instituto de Engenharia de Sistemas e Computadores – Microsistemas e Nanotecnologias (INESC MN) and IN – Institute of Nanoscience and Nanotechnology, Lisbon, Portugal

[2]iMed.ULisboa - Research Institute for Medicines, Faculty of Pharmacy, University of Lisbon, Lisbon, Portugal.

[3]Department of Bioengineering, Instituto Superior Técnico, Universidade de Lisboa, Lisbon, Portugal

[4]IBB – Institute for Bioengineering and Biosciences, Instituto Superior Técnico, Universidade de Lisboa, Lisbon, Portugal

*- Authors with equal contribution

The World Cancer Research Fund puts colorectal cancer as the third and second most common occurring cancer in men and woman respectively, with 1.8M new cases around the globe in 2018 alone.[1] These staggering numbers make it a high priority for the development of new, and ideally personalized forms of treatment. Phage display technology applications include the development of therapeutic agents, which can be further enhanced if the patient's own tumor cells are used as targets for screening.[2] In this work, we present a microfluidic system that allows the culturing of human tumor cells, the capture of specific binding phages and the retrieval of these captured phages for replication.

The microfluidic device is comprised of a 1x1cm chamber of 20 µm height made of polydimethylsiloxane, chemically bonded to a polystyrene (PS) dish (Figure 1-A) *via* silanization. Cells from human colon adenocarcinoma cell-line, HCT116, are injected into the microfluidic chip after it has been sterilized and coated with a layer of collagen Type I and left to adhere to the PS for 4h at 37ºC, 5%CO_2. Once cells have begun to adhere (4h post seeding), the cell culture phase is initiated, by injecting McCoy's 5a modified complete growth medium at an appropriate flow rate that avoids wash-out of the cells while allowing for sufficient medium renewal, as seen in Figure 1-B.

Once 70-80% of cell confluence is reached (ca. 48h), a suspension of fluorescently labeled phages are injected into the microfluidic chip. As a model, a M13 bacteriophage genetically engineered to display a VHH-based antibody, anti-CXCR4, was used, due to its binding to the CXCR4 chemokine receptor expressed by the tumor cells. As a negative control, a VCSM13-helper phage was used since it is not genetically engineered to display any protein that confers specificity for this cell line and no fluorescence was registered for this control. By monitoring the fluorescence over time it is possible to calculate the flux of phages captured by the cells in these conditions and estimate the total number of phages captured as seen in Figure 2. In these fluidic conditions, for the duration of the experiment it is safe to assume that all phages were captured.

After the phages were injected into the chip, bound to the cells, and any non-specific binding phages were washed away, the phages that successfully attached to the cells were retrieved by applying a negative pressure to the microfluidic chip using a syringe pump. This results in the physical collapse of the structure leading to mechanical cell lysis and phage retrieval as seen in Figure 3. Through phage titration [2], it was confirmed that approximately 30% of the phages captured by the cells were retrieved.

The results presented here demonstrate a microfluidic methodology to screen potential therapeutic targets for specific types of cancer.

Word Count: 462

References

1- https://www.wcrf.org/dietandcancer/cancer-trends/colorectal-cancer-statistics;

2- Bazan, Justyna, Ireneusz Całkosiński, and Andrzej Gamian. "Phage display—A powerful technique for immunotherapy: 1. Introduction and potential of therapeutic applications." *Human vaccines & immunotherapeutics* 8.12 (2012): 1817-1828.

3- Squires, Todd M., Robert J. Messinger, and Scott R. Manalis. "Making it stick: convection, reaction and diffusion in surface based biosensors." *Nature biotechnology* 26.4 (2008): 417.

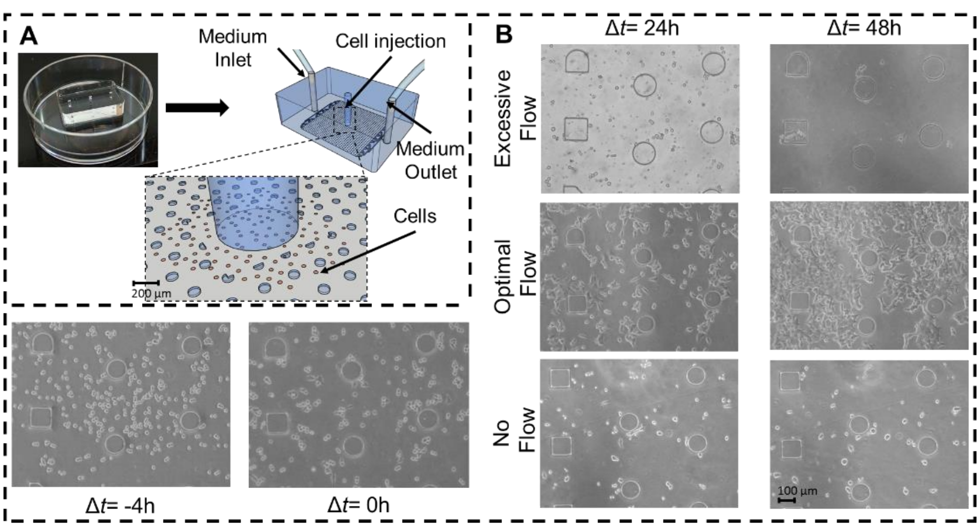

Figure 1 – Representation of the microfluidic platform used for the cell culture (A). The microfluidic device is comprised by a 1x1 cm chamber which is 20 µm in height. The circular posts serve as structural support for the PDMS layer of the device. The micrographs reflect the progression of the cell culture due to different fluidic conditions, with the optimal flow rate being 0.1µL/min (B).

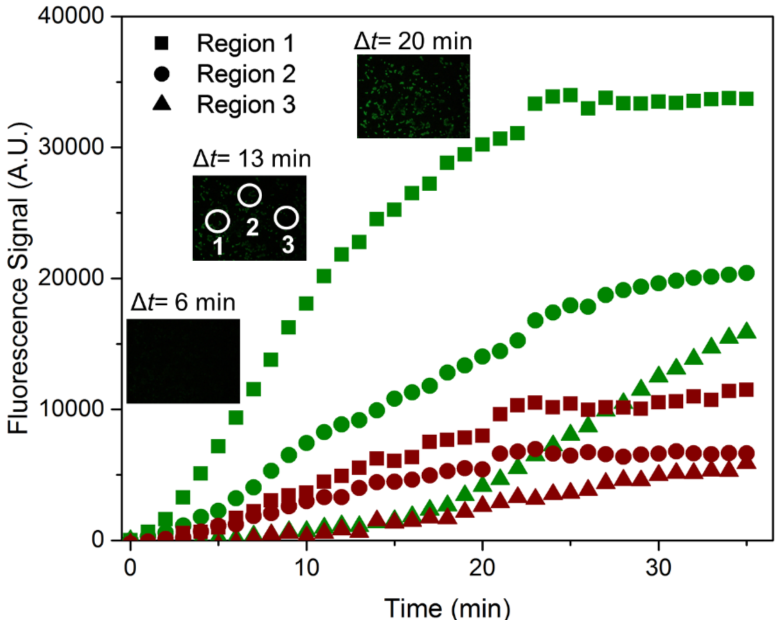

Figure 2 – Progression of phage capture for both the BODIPY FL labelled M13 anti-CXCR4 phage (green) and the PHRODO RED M13 anti-CXCR4 (red). The first phages attach to the surface of the tumor cells, while the second luminesce when they are internalized by these cells. By calculating the phage flux to the cells, according to the same principles presented in Squires et. al. [3], we can estimate a phage capture rate of approximately 100%, within the current time frame of the experiment, which translates to the capture of approximately 3.8x10^{8} phages. Each micrograph represents a section of the channel with 780 µm in length.

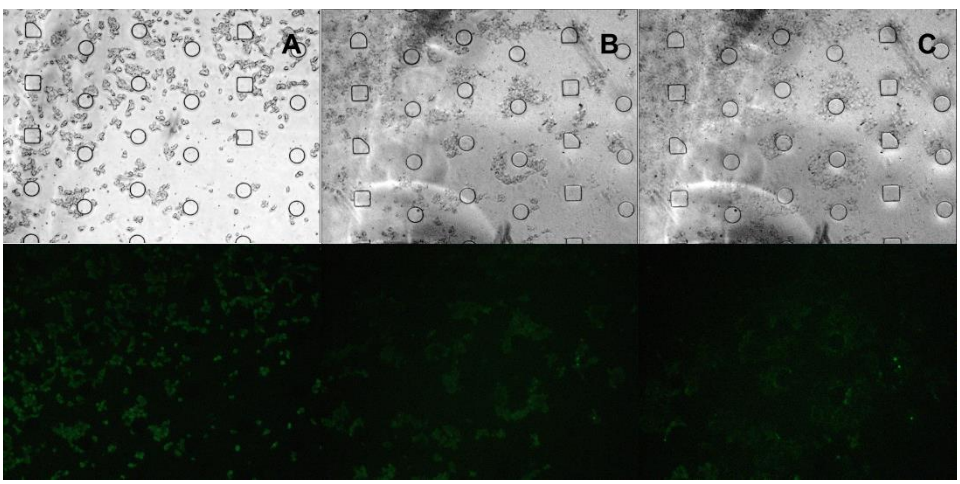

Figure 3 – Mechanical cell lysis, by collapse of the microfluidic chip. Initially the cells are in their normal conformation (A), when pressure is applied the cells are seen to flatten out (B) and eventually rupture and release the attached fluorescent phages (C). The fluorescent micrographs demonstrate the captured phages dispersing and eventually being washed away in the process. Through titration, the phage

Appendix B.2 – Extended Abstract

DEVELOPMENT OF A MICROFLUIDIC PLATFORM FOR TARGETED PHAGE SELECTION: IN PURSUIT OF PERSONALIZED COLORECTAL CANCER TREATMENTS

Eduardo J.S. Brás*[1,4], Pedro G.M. Condelipes*[1], Pedro M. Fontes*[1,2], Ricardo F. Serrão[1], Vanda Marques[2], Marta B. Afonso[2], Cecília M.P. Rodrigues[2], Virginia Chu[1], João Gonçalves[2] and João Pedro Conde+[1,3]

[1]*Instituto de Engenharia de Sistemas e Computadores – Microsistemas e Nanotecnologias (INESC MN) and IN – Institute of Nanoscience and Nanotechnology, Lisbon, Portugal*

[2]*iMed.ULisboa - Research Institute for Medicines, Faculty of Pharmacy, Universidade de Lisboa, Lisbon, Portugal*

[3]*Department of Bioengineering, Instituto Superior Técnico, Universidade de Lisboa, Lisbon, Portugal*

[4]*IBB – Institute for Bioengineering and Biosciences, Instituto Superior Técnico, Universidade de Lisboa, Lisbon, Portugal*

*- Authors with equal contribution

ABSTRACT

In this work, we present a microfluidic system that allows the culturing of cells from human colon cancer for a minimum of 48h. The cell culture is then used to capture specific binding phages which can be retrieved for replication and analysis. This system represents a stepping stone towards a simple phage selection system.

KEYWORDS: Microfluidics, M13 phage, Colon cancer, HCT116, Personalized medicine

INTRODUCTION

The World Cancer Research Fund puts colorectal cancer as the third and second most common occurring cancer in men and women respectively, with 1.8M new cases around the globe in 2018 alone [1]. These very high numbers make it a high priority for the development of new, and ideally personalized, forms of treatment. Phage display technology applications include the development of therapeutic agents, which can be further enhanced if the patient's own tumor cells are used as targets for screening [2].

EXPERIMENTAL

The microfluidic device is composed of a 1x1 cm chamber of 20 µm height made of polydimethylsiloxane (PDMS), chemically bonded to a polystyrene (PS) dish (Figure 1-A) *via*

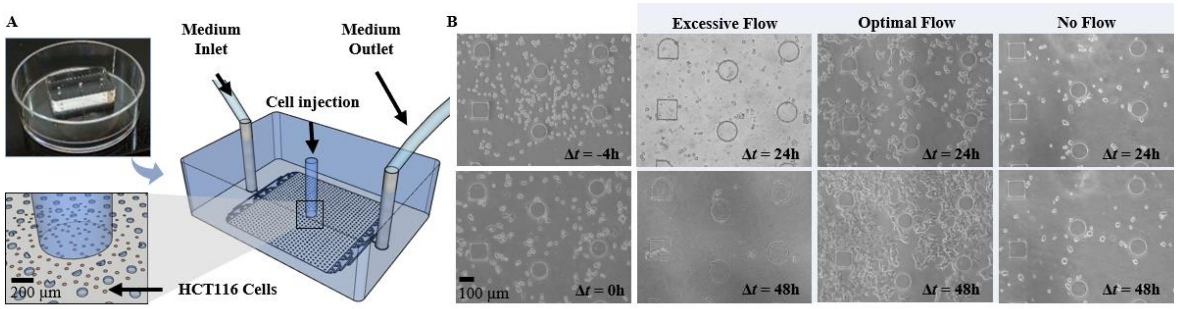

silanization. *Figure 1: (A) Representation of the microfluidic platform used for the cell culture. The circular posts serve as structural support for the PDMS layer of the device. (B) The micrographs reflect the progression of the cell culture under different fluidic conditions, with the optimal flow rate being 0.1 μL/min.*

Cells from human colon adenocarcinoma cell-line, HCT116, are inserted into the microfluidic chip after the chip has been sterilized and coated with a layer of collagen Type I, then left to adhere to the PS for 4 h at 37 ºC, 5% CO_2.

Once cells have begun to adhere (4 h post seeding), the cell culture phase is initiated, by injecting McCoy's 5a modified complete growth medium at an appropriate flow rate that avoids wash-out of the cells while allowing for enough medium renewal, as seen in Figure 1-B. Once 70-80% of cell confluence is reached (ca. 48h), a suspension of fluorescently labeled phages is injected into the microfluidic chip. As a model, a M13 bacteriophage, genetically engineered to display a VHH-based antibody - anti-CXCR4, was used due to its binding to the CXCR4 chemokine receptor expressed by tumor cells. As a negative control, a VCSM13-helper phage was used since it is not genetically engineered to display any protein that confers specificity for this cell line and no fluorescence was registered for this control.

RESULTS AND DISCUSSION

By monitoring the fluorescence over time, it is possible to calculate the flux of phages captured by the cells in these conditions and estimate the total number of phages captured, as seen in Figure 2-A. In these fluidic conditions, for the duration of the experiment it is safe to assume that all phages were captured.

Figure 2: (A) Capture progression of both BODIPY FL (green) and the pHrodo Red (red) labelled M13 anti-CXCR4 phages. While the green phages are always fluorescent, the red phages only fluoresce when they are internalized by these cells. By calculating the phage flux to the cells, according to the principles presented in Squires et. al. [3], a capture rate of approximately 100% is estimated, within the current time frame of the experiment, which translates to the capture of approximately $3.8x10^8$ phages. (B) Mechanical cell lysis, by collapse of the microfluidic chip. (I) Initially cells are adhered, (II) when pressure is applied cells flatten out and (III) eventually rupture releasing the bound phages.

After the phages were injected into the chip, bound to the cells, and any non-specific binding phages were washed away, the phages that successfully attached to the cells were retrieved by applying a negative pressure to the microfluidic chip using a syringe pump, as seen in Figure 2-B.

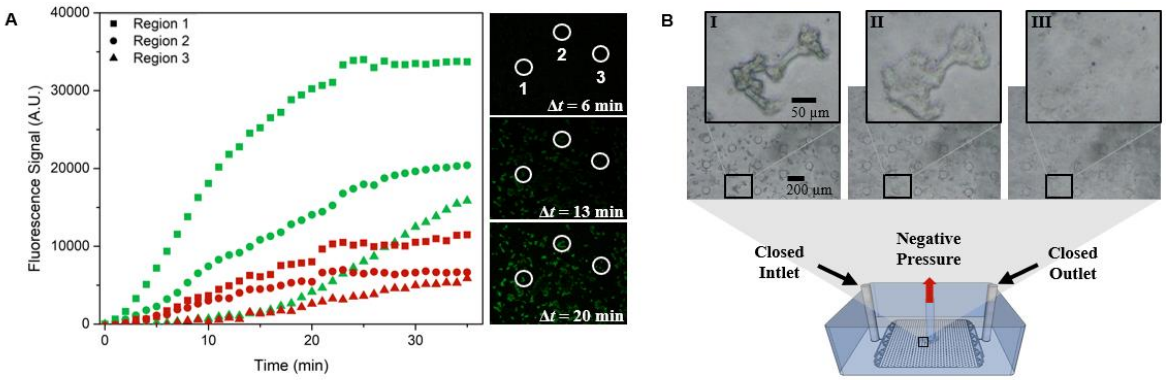

Through phage titration [2], it was confirmed that approximately 30% of the phages captured by the cells were retrieved.

The results presented here demonstrate a microfluidic methodology to screen potential therapeutic targets for specific types of cancer.

ACKOWLEDGEMENTS

The authors thank the funding from the European Structural & Investment Funds through the COMPETE Program under the Program grant LISBOA-01-0145-FEDER-016405 and from National Funds through FCT – Fundação para a Ciência e a Tecnologia under the Program grant SAICTPAC/0019/2015, three PhD grants for E.J.S. Brás (PD/BD/128167/2016), P.M. Fontes (PD/BD/135275/2017) and V. Marques (PD/BD/135467/2017), and also to the Research Units (UID/DTP/04138/2019, UID/NAN/50024 and UID/Multi/04046/2013).

REFERENCES

[1] https://www.wcrf.org/dietandcancer/cancer-trends/colorectal-cancer-statistics.

[2] Bazan, Justyna, *et al*. "Phage display—A powerful technique for immunotherapy: 1. Introduction and potential of therapeutic applications." Human vaccines & immunotherapeutics 8.12 (2012): 1817-1828.

[3] Squires, Todd *et al*. "Making it stick: convection, reaction and diffusion in surface-based biosensors." Nature biotechnology 26.4 (2008): 417.

CONTACT

+ João Pedro Conde - joao.conde@tecnico.ulisboa.pt